2012

Examining Intracellular Phosphorylation Gradients During Cell Division

Lei Tan

EXAMINING INTRACELLULAR PHOSPHORYLATION GRADIENTS DURING CELL DIVISION

A Thesis Presented to the Faculty of

The Rockefeller University

in Partial Fulfillment of the Requirements for

the degree of Doctor of Philosophy

by

Lei Tan

June 2012

EXAMINING INTRACELLULAR PHOSPHORYLATION GRADIENTS DURING CELL DIVISION

Lei Tan, Ph.D.

The Rockefeller University 2012

The dynamic cellular reorganization needed for successful mitosis requires spatial regulatory cues. I examine this problem at two different levels.

First, I analyze a phosphorylation gradient for substrates of the chromosomal passenger complex (CPC). CPC is a conserved regulator involved in key mitotic events such as chromosome-microtubule attachment and spindle midzone formation. Previously, spatial phosphorylation gradients have been reported for CPC substrates, raising the possibility that CPC-dependent signaling establishes order on the micron-length scale in dividing cells. However, this hypothesis has not been tested, largely because of incomplete characterization of the CPC-dependent phosphorylation dynamics. Here I examine the spatiotemporal dynamics of CPC-dependent phosphorylation along

microtubules throughout mitosis using a Förster resonance energy transfer-based sensor. I find that a CPC-substrate phosphorylation gradient, with highest phosphorylation levels between the two spindle poles, emerges when a cell enters mitosis. After anaphase onset, the gradient emerges and persists until cell cleavage. Selective mislocalization of the CPC during anaphase suppresses gradient formation, but overall substrate phosphorylation levels remain unchanged. Under these conditions, the spindle midzone fails to organize and function properly. My findings suggest a model in which the CPC establishes phosphorylation gradients to coordinate the spatiotemporal dynamics needed for error-free cell division.

Second, I examine the contribution of a microtubule crosslinking protein PRC1 to microtubule organization during cytokinesis. I find that PRC1 depletion leads to abnormal elongation of anaphase spindle, which depends on microtubules. I also find that the dynamics of growing microtubule plus-ends imaged by EB1-GFP is not significantly altered. Based on these findings, I propose a model for how PRC1 contributes to the length control of the anaphase spindle.

ACKNOWLEDGEMENTS

I would like to express my deepest gratitude to Dr. Tarun Kapoor, my mentor, for his guidance and constructive advice on my projects. I have learnt a lot from him about giving presentations and writing scientific papers.

I thank Dr. Emily Foley, Dr. Radhika Subramanian, Dr. Yuta Shimamoto, Dr. Josh Weinger, and Dr. Ben Houghtaling, for sharing reagents, teaching me laboratory techniques and helpful discussions. I also want to thank Maria Maldonado and Dr. Sarah Wacker for editing my manuscripts. All other former and current Kapoor lab members have helped me from time to time, and I greatly appreciate it.

During the past five years, I also got a lot of help from scientists in other labs. I thank Dr. Hiro Funabiki and the Funabiki lab members (Dr. Boo Shan Tseng, John Xue, Adriana Garzon, Dr. Christian Zierhut, and all others) for giving me frequent help, from sharing lab reagents to discuss unpublished data. I also want to thank Dr. Mike Lampson from Upenn and his lab members for sharing reagents and unpublished data. At late stage of my graduate study, I got help from Dr. Ge Yang and his graduate student Minhua Qiu, on speckle tracking analysis. I am grateful to their time and effort on helping me.

I am also appreciative to my committee members, Dr. Fred Cross, Dr. Hiro Funabiki and Dr. Tim Ryan, for their highly valuable comments and suggestions during my graduate study, as well as Dr. Duane Compton from Dartmouth for taking the time to act as the external member of my thesis committee.

At last, I would like to thank my family Miaoquan Tan, Jie Liu and Qi Wang for their tremendous support over the past years.

TABLE OF CONTENTS

LIST OF FIGURES

PAGE

Chapter 1

Chapter 3

Chapter 4

Appendix

LIST OF TABLES

CHAPTER 1: INTRODUCTION

1.1 Gradients and spatial signaling in biological systems

To achieve various goals, cells respond to internal and external cues using signaling networks. Over the years, extensive lists of the components of these signaling networks have been built, thanks in part to genetics and RNA interference (RNAi) technology (Kholodenko et al.). Researchers also have a relatively good understanding of the structures of these networks, and have already begun to engineer and redesign networks to give desired outputs (Ma et al., 2009; Peisajovich et al.). However, our understanding of the spatial aspect of signaling networks has lagged behind (Kholodenko et al.). Currently, known mechanisms for spatial control of signaling include scaffolding proteins, organelle positioning, signaling domain assembly (e.g. lipid rafts), and gradient formation (Kholodenko et al.). Among these, gradients aroused great research interest, likely due to two reasons. First, compared with other mechanisms, gradients have the potential for encoding rich information to allow fine-tuning of spatial signals, rather than acting as an ON/OFF switch. Second, gradients are evolutionarily conserved: this mechanism is utilized by various organisms, from

bacteria to human cells, and is involved in key processes such as development and cell division.

Gradients can be generated by reaction-diffusion mechanisms. Two general models have been proposed to explain gradient formation. The first one requires an activator and an inhibitor of a protein or a process, with different diffusivities. The activator autocatalytically reproduces itself and stimulates the inhibitor, which renders spatially uniform distribution unstable and drives gradient formation. For this model to work, the inhibition kinetics must be faster and the inhibitor diffusion coefficient must be larger than that of the activator to prevent autocatalytic explosion. This model has been applied to explain how morphogen gradients could be generated within initially near-uniform embryos and subsequently direct cell responses that give rise to patterns during development (Gierer, 1982). The second model exploits pre-existing heterogeneity in a cell. Similar to the first model, it requires two antagonistic reactions catalyzed by an activator and suppressor, such as phosphorylation and dephosphorylation catalyzed by a kinase and phosphatase, respectively. However, owing to the presence of pre-existing cellular structures, such as membranes and chromosomes, opposing activator and

suppressor are often spatially separated in their localization. Therefore, the environment for reactions and diffusion is initially non-homogeneous and does not resemble the uniform media described in the first model. In this model, a gradient pattern is generated through the high concentration of activated substrate close to the activator and low concentrations farther away (where the suppressor localizes). Provided that the suppressor is far from saturation, the range of the gradient depends on the diffusion coefficients and the reaction rates. Gradients that could be explained by this model include the yeast MAPK Fus3 (Maeder et al., 2007), the yeast Pom1 (Martin and Berthelot-Grosjean, 2009; Moseley et al., 2009), protein Tyr phosphatase 1B (Yudushkin et al., 2007) and the small GTPase Ran gradient (Clarke and Zhang, 2008). While reaction-diffusion models are simple and follow similar assumptions, the situation in vivo is more complex and will be discussed in detail for several systems later in this chapter.

Gradients have been observed in a variety of biological processes where they extend across a wide range of length scales. Morphogen gradients in embryos are believed to provide positional information for cells to guide cell fate determination during development (Ashe and

Briscoe, 2006) (e.g. BMP and Dpp in drosophila). In wound healing, a tissue-scale hydrogen peroxide gradient is observed in zebrafish larvae and is proposed to mediate rapid wound detection by recruiting leukocytes in tissues (Niethammer et al., 2009). During cell division, a couple of gradients have been discovered (Caudron et al., 2005; Fuller et al., 2008; Kalab et al., 2006; Niethammer et al., 2004). Bacteria cell division utilizes Min protein gradients to position their division plane (Loose et al., 2011). Yeast cells generate polar gradients of Pom1 kinase to coordinate cell size and mitotic entry (Martin and Berthelot-Grosjean, 2009; Moseley et al., 2009). In plants, ion gradients (e.g. calcium) guide pollen tube growth (Holdaway-Clarke and Hepler, 2003). These gradients, despite their variety, are all important for relating spatial information to signaling.

1.2 Intracellular gradients and cell growth in size or in number

Thanks to the advancement of molecular probes and imaging techniques, a number of micron-scale intracellular gradients have been visualized. These gradients are often related to cell growth, either in size or in number. In

this chapter I will review intracellular gradients involved in cell growth in various biological systems, with a focus on how gradients are generated and how they deliver positional information.

1.2.1 Pom1 in yeast cell growth

Rod-shaped fission yeast cells elongate until they divide in the middle. Polar gradients of the dual specificity tyrosine kinase Pom1 have been described and are involved in this process (Martin and Berthelot-Grosjean, 2009; Moseley et al., 2009). The intracellular gradient of active Pom1 kinase reaches its maximum at the two cell ends and its minimum at the midcell, the future site of cytokinetic furrowing (Figure 1.1A). The gradient of active Pom1 maintains a relatively constant size throughout the cell cycle (at all times Pom1 activity is low ~8 μm from the cell tip). As fission yeast cells grow and become more elongated, there is a larger region of decreased Pom1 levels at the cell equator (Figure 1.1B).

The Pom1 gradient is proposed to spatially couple cell length with mitotic entry so that cells divide at a defined and reproducible size (Martin and Berthelot-Grosjean, 2009; Moseley et al., 2009). It has been discovered that Pom1 is a does-dependent G2-M inhibitor that negatively regulates

Cdr2, the Wee1 inhibitor (Figure 1.1C). It is known that Cdr2 localizes to the midcell. Therefore, in short cells, active Pom1 overlaps with Cdr2, preventing its inhibition of Wee1 that in turn suppresses Cdk1 activity to block mitotic entry. As cells elongate, Pom1 is cleared from the cell equator and releases the inhibition of Cdr1 and Cdr2. This model proposes that the Pom1 gradient generates information about cell size and coordinates this with mitotic entry by regulating Cdk1 through Cdr1, Cdr2, and Wee1 (Martin and Berthelot-Grosjean, 2009; Moseley et al., 2009).

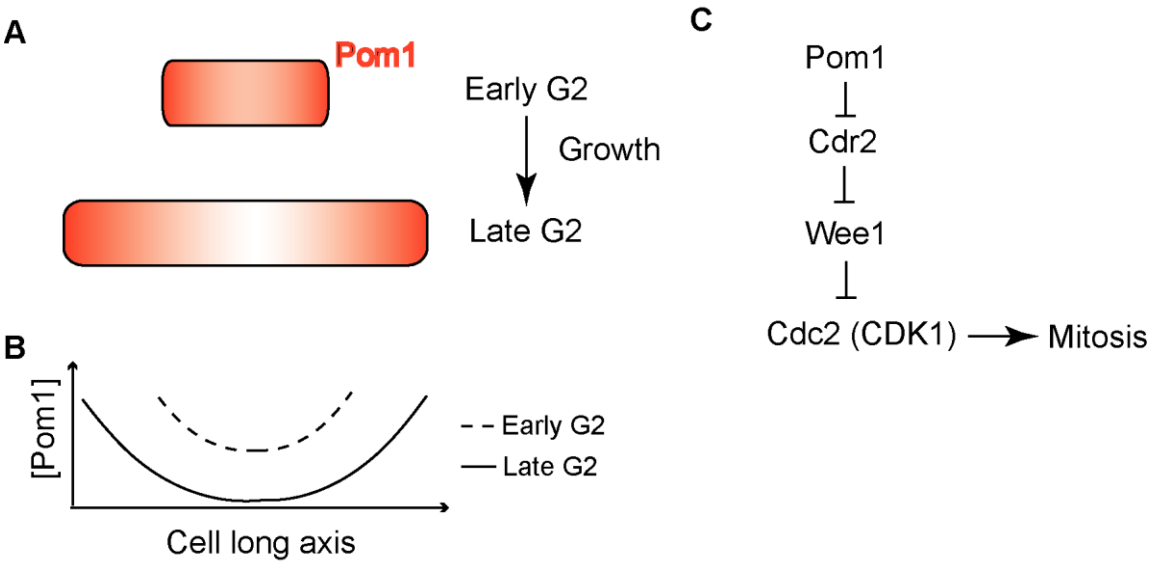

Figure 1.1 The Pom1 concentration gradient in fission yeast cell growth. (A) A schematic for Pom1 concentration gradient in yeast cells, at early and late G2 (red shading represents Pom1 concentration). (B) Pom1 concentration profile along the cell growth axis, during early and late

G2. (C) Pom1 suppresses mitotic entry by inhibiting Cdr2, which downregulates Wee1, a Cdc2 (CDK1) inhibitor.

Based on cell biological and biochemical analysis, reaction-diffusion mechanisms have been proposed to explain the formation of the Pom1 gradient. The two antagonistic reactions that control Pom1 membrane association are Pom1 dephosphorylation and phosphorylation. Membrane association of Pom1 is promoted through dephosphorylation, which exposes a positively charged basic region that increases its membrane association. The dephosphorylation reaction is thought to be spatially regulated by Tea4, which is deposited by microtubules to the cell tips and facilitates interactions between Pom1 and its phosphatase Dis2 (Hachet et al., 2011). On the other hand, Pom1 autophosphorylation lowers its affinity for the membrane and promotes its detachment, limiting the lateral spreading of Pom1 along the membrane. Diffusion of Pom1 in cytoplasm allows its encounter with Tea4 to initiate a new cycle of membrane association. Therefore, this phosphorylation-dephosphorylation reaction cycle, coupled with diffusion, is thought to shape the Pom1 polar gradients.

1.2.2 Calcium gradients in plant pollen tube growth

As sperm cells in flowering plants are not motile, a highly specialized cell type called the pollen tube is essential to carry sperm cells to the ovule for fertilization. The pollen tube germinates from the pollen grain and grows the entire length through the stigma, style, ovary, and ovules to reach the egg cells (Figure 1.2A). Pollen tube growth is very rapid. For example, a pollen tube from maize can attain growth rates of 3 µm/s, which is one of the fastest-growing cell types known (Wilsen and Hepler, 2007). The growth is highly confined to the tip of the tube, and ions (e.g. calcium, protons, potassium and chloride) have been found to be necessary for this process (Holdaway-Clarke and Hepler, 2003). Here we address the role of a calcium gradient in pollen tube growth, as it is well-studied in this system.

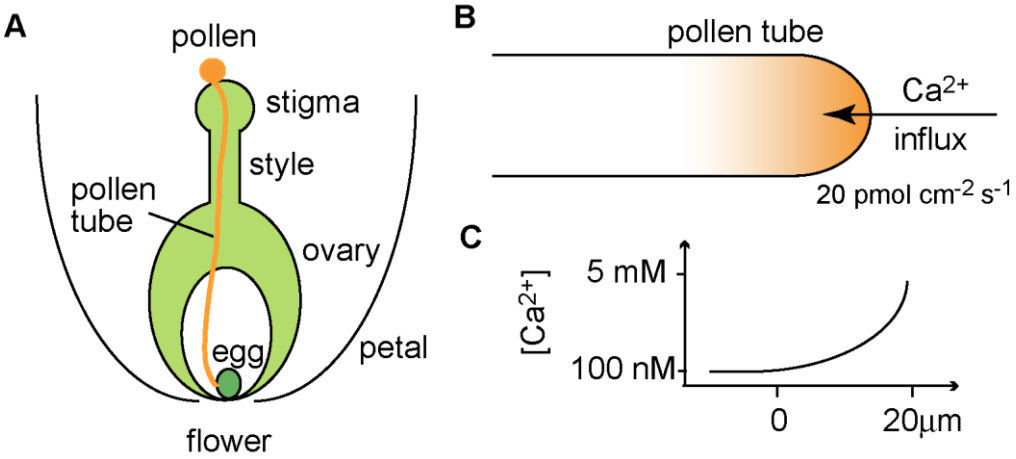

Figure 1.2 Calcium gradients in pollen tube growth. (A) A cartoon illustrating pollen tube growth after pollination.

(B) Cytoplasmic calcium concentration is elevated at the tip of the growing pollen tube (orange shading represents calcium concentration). (C) A graph showing the calcium concentration along the central axis of the pollen tube.

Ratiometric calcium imaging has revealed that there is a calcium gradient with the highest concentrations of calcium at the apical plasma membrane of the growing pollen tube. The gradient extends from 1-5 μM Ca++ at the apex of a growing tube to a basal concentration of 150-300 nM Ca++ 20 μm from the growing tube (Figure 1.2B, (Rathore et al., 1991)). The formation of the calcium gradient depends on two antagonistic processes: calcium entry into pollen tubes and sequestration of the elevated calcium in cytoplasm. Calcium enters into pollen tubes mainly through extracellular calcium influx (Wilsen and Hepler, 2007). Studies with a calcium-selective vibrating electrode reveal an extracellular influx of calcium that is spatially focused toward the tip of the tube and is of substantial magnitude (20 pmol cm^{-2} s^{-1}) (Holdaway-Clarke et al., 1997). In current models, such localized influx mainly depends on calcium channels. Stretch-activated calcium channels have been identified on the plasma membrane of both the grain and the tip of pollen tubes (Dutta and Robinson, 2004). It is speculated that deformation of the plasma membrane at

the tip during turgor-dependent cell elongation, would be sufficient to open stretch-activated calcium channels, which would then allow the rapid calcium influx into only the tip of the pollen tube. Besides the mechanosensitive calcium channel, other calcium selective channels are activated by hyperpolarization of the membrane potential and glutamate receptors that conduct calcium have also been identified (Shang et al., 2005; Wu et al., 2011; Wu et al., 2010a; Wu et al., 2007). Additionally, calcium could be sequestered by efflux pumps or intracellular membrane systems (i.e. ER, mitochondria and secretory vesicles)(Hepler et al., 2012). Efflux pumps such as ACA9 have been shown to distribute along the tip and shank of the pollen tube (Schiøtt et al., 2004), and thus would be poised to pump calcium out of these regions. Besides efflux pumps, it is known that ER lumen sequesters high levels of calcium (100-500 μM), possiblythrough an ER lumen protein calreticulin, which is capable of binding 25 moles of calcium per mole of protein (Iwano et al., 2009). As cellular imaging reveals that elements of the ER continuously move toward the apex of the pollen tube and then turn rearward through the core of the pollen tube (Lovy-Wheeler et al., 2007), this streaming pattern is suggested to sequester calcium as the fresh supply of ER

sweeps through the tip region. Besides ER, a calcium pump (ECA3) is found on post Golgi endomembranes, which suggests that secretary vesicles may sequester calcium as well (Sze et al., 2006). It seems likely that different calcium sequestration pathways work together to maintain the gradient and restrict its spread into the pollen tube.

Targets for calcium action at the apex of pollen tubes include the actin cytoskeleton, cell motility, and exocytosis of apically accumulated vesicles (e.g. those that contain cell wall precursors needed for cell elongation) (Holdaway-Clarke and Hepler, 2003). Several lines of evidence show that localized changes in calcium concentration at the tip control the direction of pollen tube growth. Experimentally imposing localized external gradients of an ionophore to facilitate ion transport, or an inhibitor of the calcium channel, induces predictable reorientation of pollen tube growth (i.e. bending towards the highest concentration of ionophore and away from the source of the inhibitor)(Malhó et al., 1995). Furthermore, localized photoactivation of caged Ca++ (nitr-5) in different pollen tube domains has revealed that increasing calcium concentration on one side of the pollen tube apex induced reorientation of the growth axis toward that side. A decrease in calcium concentration, through

photoactivating diazo-2 (a caged Ca++ chelator), promotes bending toward the opposite side (Malhó et al., 1995). These experiments suggest that calcium gradients at the tip of the pollen tube provide spatial cues for determining growth direction.

1.2.3 Min gradient in bacteria cell division

Rod-shaped bacteria generally divide with high precision along the midcell (deviation ~3%) so that a mother cell can produce two equally sized daughters (Guberman et al., 2008; Trueba, 1982). In current models, the mechanical force needed for constriction is provided by the tubulin homolog FtsZ, a GTPase protein, which localizes to the midcell and forms a ring-like structure (Adams and Errington, 2009). How FtsZ is spatially restricted to the division plane, well before constriction, is relatively well-understood in E. coli and this process involves formation of a Min protein gradient.

The Min gradient involves three proteins: MinC, MinD and MinE. Initial analyses suggested that MinC and MinD localize to the two cell ends and block FtsZ assembly, whereas MinE forms a static ring at the midcell to clear MinC and MinD (de Boer et al., 1991; de Boer et al., 1989). More recently live cell imaging revealed that localization

of these protein are dynamic rather than static: MinC and MinD oscillate rapidly between the two cell ends (1-2 min cycle time) (Raskin and de Boer, 1999b). During these oscillations, MinD levels grow from one pole toward the midcell and then shrink toward the same pole; as MinD disappears at one pole, it reappears at the opposite pole, finishing the other half of the cycle (Raskin and de Boer, 1999b) (Figure 1.3A). MinE, instead of being static at the midcell, also oscillates and is tightly coupled to the edges of MinD (Fu et al., 2001; Hale et al., 2001) (Figure 1.3A). As the oscillations occur on a timescale much shorter than cell division, it leads to a spatial gradient of MinD on time average, with the maximal protein concentration at the cell poles and minimal concentration at the midcell (Loose et al., 2011)(Figure 1.3B). This time-averaged gradient of MinC-MinD which peaks at the poles prevents lateral interactions between FtsZ filaments and weakens the longitudinal bonds between FtsZ molecules (Dajkovic et al., 2008; Hu and Lutkenhaus, 2000). This confines the FtsZ ring and subsequent constriction to the midcell.

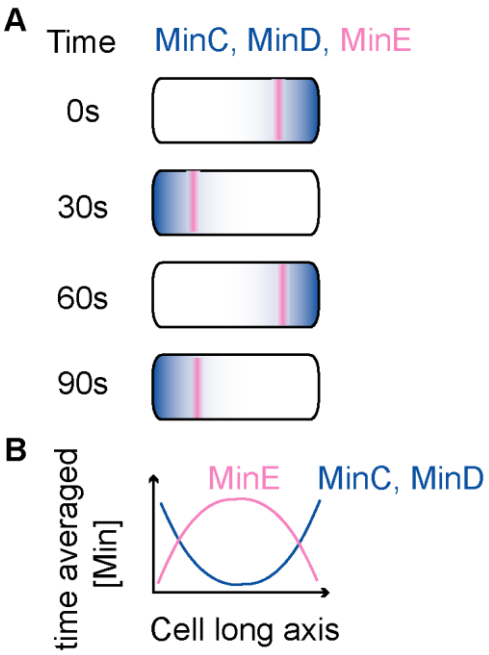

Figure 1.3 Min protein gradients in bacteria cell division. (A) A schematic illustrating MinC, MinD and MinE protein localization. MinC and MinD oscillate between two cell ends and MinE forms a band coupling to the edge of MinC and MinD. (B) A time average Min protein concentration profile along the long axis of the cell.

The mechanism for Min protein oscillation and the subsequent gradient is not completely understood. Biochemical analysis showed that MinD is a membrane-bound ATPase and it could recruit MinC, an inhibitor of FtsZ ring formation (Bi and Lutkenhaus, 1991; Hu et al., 1999). MinD also recruits MinE, which stimulates MinD's ATPase activity and subsequently displaces MinD from the membrane (Ma et al., 2003; Ma et al., 2004; Pichoff et al., 1995; Raskin and de Boer, 1997). MinE and MinC share the same binding

site on MinD and they compete with each other for MinD binding (Hu and Lutkenhaus, 2003; Lackner et al., 2003; Wu et al., 2010b). MinD and MinE are essential for the oscillation and MinC is dispensable (Hu and Lutkenhaus, 1999; Raskin and de Boer, 1999a). Current model that explain the Min oscillations is based on reaction-diffusion mechanism. The model consists of two antagonistic reactions: cooperative MinD binding to the membrane and MinE displacing MinD from the membrane (Loose et al., 2008; Meinhardt and de Boer, 2001). Because MinE can remain attached to the membrane only in the presence of MinD, a MinE maximum causes its own local destabilization and shifts from local MinD depression into a neighboring region with higher MinD concentration. This results in a wave of MinE that sweeps MinD off the membrane. As the membrane-bound MinD and freely diffusible MinE at one pole have diminished, a new MinD activation at the opposite pole is triggered and completes the cycle (Meinhardt and de Boer, 2001). This model is supported by computational simulation and by in vitro reconstitution of the MinD-MinE wave formation on the membrane sheet (Loose et al., 2008). The mechanism of averaging the periodic variation (i.e. oscillation) in the protein localization to generate a gradient and define cellular position is interesting and

has not yet been widely explored in other biological systems.

1.2.4 Ran gradient in animal cell division

Accurate chromosome segregation in animal cells depends on proper assembly of the mitotic spindle, a bipolar array of microtubules that emanate from centrosomes at the two poles. Among the many pathways that contribute to the robustness of spindle assembly is the small GTPase Ran gradient (Clarke and Zhang, 2008; Kalab and Heald, 2008). Ran GTPase cycles between GTP- and GDP-bound forms, and this is controlled by regulators with distinct localizations: Ran's guanine nucleotide exchange factor (GEF) regulator of chromatin condensation 1 (RCC1), which binds to chromatin, promotes GDP exchange with GTP; Ran's GTPase-activating protein RanGAP which accelerates Ran's GTP hydrolysis is cytoplasmic (Clarke and Zhang, 2008). It has been observed that GTP-bound Ran forms a concentration gradient that peaks around chromatin (Figure 1.4A)(Kalab et al., 2006; Kalab et al., 2002). This gradient is thought to provide spatial cues for microtubules to assemble into a bipolar shape (Kalab and Heald, 2008).

The role of Ran GTPase in regulating microtubule dynamics and spindle assembly was revealed in Xenopus extracts (Kalab et al., 1999). Addition of Ran GTPase activating protein (GAP) RanBP1 to the extracts reduced microtubule growth, while addition of a constitutively

active mutant of Ran promotes microtubule formation (Kalab et al., 1999). These effects have been shown to be mediated by cytoplasmic factors that promote microtubule polymerization and bundling. For example, RanGTP releases spindle assembly factors (SAF) such as TPX2 from importin β nuclear transport receptors, so that SAFs could bind to microtubules and properly function (Gruss et al., 2001). There are dozens of regulators of mitotic spindle assembly that are bound and inhibited by importin β, and are under regulation of RanGTP (Gruss et al., 2001; Nachury et al., 2001; Wiese et al., 2001). In current models, the RanGTP gradient provides spatial cues to activate downstream SAFs around chromatin, so the spindle can properly assemble (Clarke and Zhang, 2008; Kalab and Heald, 2008).

Imaging of a RanGTP binding probe has revealed the distribution of RanGTP to be anisotropic during cell division and it is most abundant around the chromatin (Kalab et al., 2006; Kalab et al., 2002). The generation of the gradient is thought to be driven by two opposing reactions: diffusion and a positive feedback loop. On one hand, GDP is exchanged for GTP in a molecule of Ran, by the chromatin-associated RanGEF RCC1 (Clarke and Zhang, 2008). On the other hand, the GTP hydrolysis reaction is promoted by both Ran GTPase enzymatic activity and RanGAP proteins

such as RanBP1 (Clarke and Zhang, 2008). As RCC1 is also a cargo that is released by importin β upon RanGTP binding, the increase in RanGTP around chromatin promotes delivery of additional RCC1 to chromatin, resulting in a positive feedback loop (Kalab and Heald, 2008). Likely due to the self-reinforcing feedback loop, the free RanGTP gradient has been shown to be very steep and does not extend over the full length of a spindle (Caudron et al., 2005). Therefore another mechanism must propagate the spatial information in addition to the RanGTP gradient.

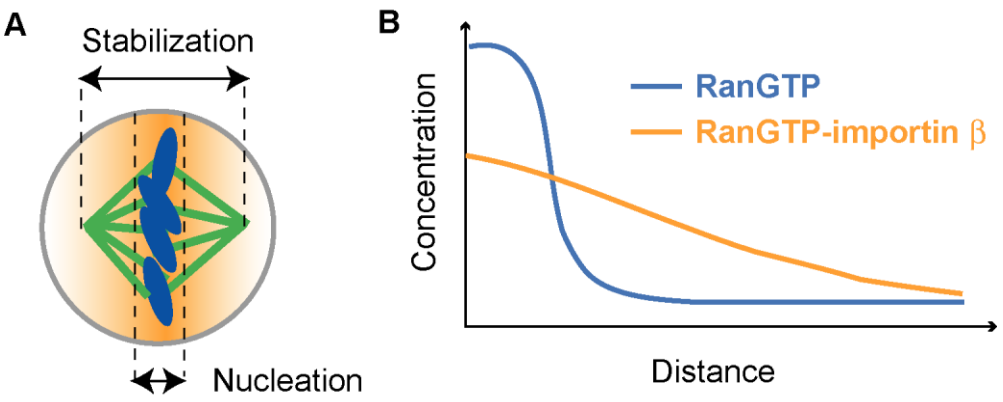

Figure 1.4 RanGTP gradients in spindle assembly. (A) A model for how the RanGTP gradient coordinates spindle assembly during mitosis (orange shading represents RanGTP concentration). As microtubule nucleation and stabilization is promoted at different RanGTP concentration thresholds, microtubule nucleation is promoted around chromosomes only. (B) A graph of the RanGTP gradient and the RanGTP-importin β interaction gradient. The distance is from chromosomes. The

RanGTP gradient sets up the RanGTP-importin β gradient, which could extend over the spindle length.

Interestingly, as RanGTP regulates microtubule dynamics via importin β, a shallower interaction gradient of RanGTP-importin β that extends over the length of the spindle was discovered to be built upon the RanGTP gradient (Figure 1.4B). This interaction gradient has been observed in both Xenopus extracts and human cells (Caudron et al., 2005; Kalab et al., 2006; Kalab et al., 2002). Although spindle length in Xenopus egg extracts is ~4-fold longer than in human cells, the RanGTP-importin β interaction gradient extends over the full length of the spindle in both systems, revealing the robustness of the gradient across species. In current models, by activating the release of SAFs, RanGTP-importin β can promote two different processes: microtubule nucleation and stabilization of growing microtubules (Caudron et al., 2005). Titration experiments in Xenopus egg extracts suggest that microtubule nucleation and stabilization are activated at two different threshold concentrations of RanGTP-importin β, with a higher concentration needed for nucleation (Caudron et al., 2005). As the RanGTP-importin β interaction gradient peaks around mitotic chromosomes and declines

further away, it has been proposed that such a gradient shape promotes microtubule nucleation only around the chromosomes while stabilizing microtubules over the entire spindle (Figure 1.4A). This threshold model of promoting different processes at different levels could explain how the RanGTP-importin β interaction gradient achieves fine-tuning in spatial organization of spindle assembly (Caudron et al., 2005). The threshold model also has been used to explain the mechanism of action for morphogen gradients during development (Ashe and Briscoe, 2006).

1.2.5 Substrate phosphorylation gradient of the Chromosomal Passenger Complex (CPC) in animal cell division

Another gradient found during animal cell division is the substrate phosphorylation gradient of the Chromosomal Passenger Complex (CPC, comprised of Aurora B kinase, INCENP, Survivin and Borealin, Figure 1.5A). The CPC is required for chromosome condensation and cohesion, kinetochore-microtubule attachments, the spindle checkpoint, and cytokinesis (Ruchaud et al., 2007). Its functions are known to be tightly coupled to its dynamic localizations: the CPC localizes on condensing chromosomes in prophase and then concentrates at the inner centromeres until anaphase onset (Figure 1.5B,C, upper panels) (Ruchaud et al., 2007). The CPC then disembarks from inner centromeres to the

spindle midzone (Figure 1.5B,C, lower panels). The CPC phosphorylates a wide range of proteins, including condensins, centromere/kinetochore proteins (e.g. CENP-A, KNL1, Ndc80), proteins that modulate microtubule dynamics (e.g. MCAK, OP18, MKLP1), and proteins that regulate membrane contractility (e.g. Myosin II regulatory light chain) (Ruchaud et al., 2007). The CPC-substrate phosphorylation gradient has been proposed to provide spatial cues for these downstream effecter proteins (Fuller et al., 2008).

Interestingly, the CPC-substrate phosphorylation gradient has been suggested to be present at two different stages of cell division, extending over dramatically different length scales. Imaging of the chromosome- and centromere-targeted FRET sensors for CPC activity, together with immunofluorescence of CPC endogenous substrates, revealed that a substrate phosphorylation gradient appears after anaphase onset (Fuller et al., 2008). The shape of the anaphase gradient is such that maximum phosphorylation is at the middle of the separating chromosomes, and the phosphorylation level is lower towards the two cell ends (Fuller et al., 2008). Besides the anaphase gradient, prior to anaphase, a putative CPC-substrate phosphorylation gradient that extends over ~1 μm at the

centromere/kinetochore region, has been implicated by imaging of kinetochore-targeted FRET sensors (Lampson and Cheeseman, 2010).

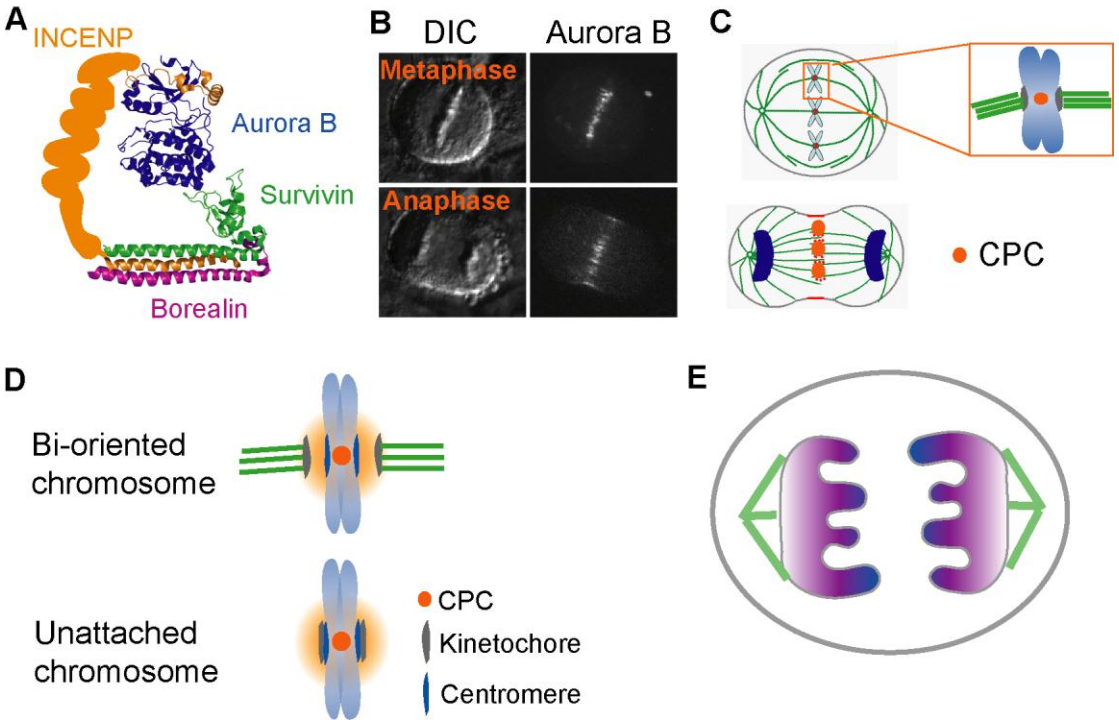

Figure 1.5 CPC-substrate phosphorylation gradients in mitosis. (A) A schematic of the CPC complex. Note that the structure of the coiled-coil region of INCENP is not solved yet. (B) Dynamic CPC localization. HeLa cells expressing mCherry-Aurora B are imaged live. DIC and mCherry-Aurora B images of a representative metaphase and anaphase cell are shown. (C) A schematic for CPC localization at metaphase and anaphase. (D) A schematic for a putative CPC-substrate phosphorylation gradient prior to anaphase onset. With bi-oriented chromosomes, kinetochores are stretched and CPC-substrates at the kinetochores are less phosphorylated, while in unattached chromosomes, CPC-substrates at kinetochores are highly phosphorylated. The orange shading represents CPC substrate phosphorylation. (E) A schematic for CPC-substrate phosphorylation gradient at anaphase. CPC substrates on chromosomes are more phosphorylated near the

middle of the cell and less phosphorylated towards two cell ends. The purple shading represents phosphorylation.

1.2.5.1 A putative CPC-substrate phosphorylation gradient centered at inner centromeres prior to anaphase

A phosphorylation gradient centered at inner centromeres and extended over kinetochores has not been directly visualized, partially due to its length scale being close to the diffraction limit of light. However, its existence has been suggested by two approaches. First, phosphorylation levels of FRET-based sensors targeted to kinetochores vs. centromeres were compared in cells treated with small molecules that alter the relative positioning of kinetochores to centromeres (Liu et al., 2009). Phosphorylation of a CPC substrate at the kinetochore was found to depend on its distance from the kinase at the inner centromere. Second, phosphorylation levels of FRET-based sensors that were targeted to different sites of the kinetochore were compared. Results from this experiment showed that the phosphorylation levels anti-correlate with the predicted distance from the sensor location to the inner centromere (Welburn et al., 2010). A reaction-diffusion mechanism could explain this gradient: the CPC is activated by being locally concentrated at inner

centromeres, with active CPC being released to diffuse away from the centromere and subsequently inactivated by phosphatases.

This inner centromere-centered gradient has been proposed to be the mechanism for how tension is sensed at centromeres/kinetochores to selectively stabilize correct microtubule attachments (Lampson and Cheeseman, 2010). As the CPC has multiple microtubule-binding substrates at kinetochores, the gradient is proposed to allow for the combinatorial phosphorylation of these substrates to generate graded levels of microtubule-binding activity, with high phosphorylation abolishing microtubule binding. The spatial distribution of the substrates along the kinetochore axis leads to their differential phosphorylation in response to changes in tension and attachment state. Therefore, the gradient in this system might promote a tension-dependent fine-tuning of kinetochore-microtubule interactions (Figure 1.5D). A key concern for this model is that differences in substrate positions at kinetochores are smaller than 100 nm (Wan et al., 2009; Welburn et al., 2010). Whether the gradient is steep enough to act on these length scales, is currently unclear and worth further examination.

1.2.5.2 A CPC-substrate phosphorylation gradient centered at the spindle midzone during anaphase

The anaphase phosphorylation gradient of CPC-substrates has been visualized by both FRET sensor imaging and immunofluorescence of endogenous CPC substrates (Fuller et al., 2008). The shape of the gradient is such that the highest phosphorylation levels are in the middle of the cell (Figure 1.5E). The mechanism for how this gradient is generated is likely to be a reaction-diffusion mechanism that is similar to the pre-anaphase gradient (Fuller et al., 2008). According to theoretical models for phosphorylation gradient formation (Brown and Kholodenko, 1999), the difference in length scale for these two gradients could be due to the difference in local CPC concentration and the half-life of the CPC at centromeres vs. the spindle midzone.

This anaphase gradient has been proposed to transmit signal over micron length scales, from the spindle midzone to the cell cortex, to specify furrow location (Fuller et al., 2008). However, the CPC is dispensable for cleavage furrow ingression. Whether and how the anaphase gradient of CPC-substrate phosphorylation contributes to cleavage furrow specification has not been functionally tested. To answer these questions, the shape of the gradient needs to

be perturbed and subsequent phenotypes should be examined in detail.

1.3 Unresolved issues

Here I have reviewed several intracellular gradients relevant in cell growth (either in size or in number), where spatial cues are essential in the signaling process. In most cases, the key components needed for generating the gradient have been identified by perturbation experiments. The generation of these gradients are frequently explained through reaction-diffusion mechanisms. However, pre-existing cellular structures that could change diffusion rates and local protein concentrations, along with layered regulatory networks that could change reaction dynamics, often make the generation of gradients more complex than modeled by simple reaction-diffusion mechanisms. An outstanding question for most gradient systems is how the gradient functions in providing spatial cues. This question remains difficult to answer due to the challenges of separating the role of individual proteins from that of the gradient pattern.

This thesis includes two parts. In the first part, I examined spatio-temporal dynamics of CPC-substrate

phosphorylation throughout mitosis, and analyzed the contribution of the anaphase CPC-substrate phosphorylation gradient to cytokinesis. In the second part, I described my efforts towards examining the microtubule crosslinking protein PRC1's role in cytokinesis.

CHAPTER 2: MATERIALS AND METHODS

2.1 Constructs used

For microtubule-targeted sensor and phosphorylation site mutated sensor, first DNA encoding amino acid 590-964 in hMAP4 was amplied from hMAP4 cDNA (Openbiosystem) and cloned into the cytosolic FRET sensor plasmid (a gift from Dr. E.A. Foley) (Fuller et al., 2008). Then CFP in the sensor was substituted by a CFP codon variant (a gift from E. Wang at Dr. M.A.Lampson's lab). For chromosome-targeted FRET sensors, a CFP codon variant was also cloned into the construct to substitute the CFP in previous plasmids (Fuller et al., 2008). mCherry-INCENP wild type was constructed by cloning human INCENP construct that is resistant to RNAi (a gift from S.M.A. Lens) into pMSCV N-terminal mCherry destination vector by gateway cloning according to Invitrogen gateway cloning manual. mCherry-INCENP T59E mutant was generated by quick-change method. GFP-anillin was constructed by cloning anillin cDNA (a gift from M. Glotzer) into pMSCV N-terminal GFP destination vector by gateway cloning. GFP-PRC1 was constructed by cloning GFP-PRC1 (a gift from Dr. R. Subramanian) into pMSCV destination vector by gateway cloning. GFP-PRC1 wildtype that is resistant to RNAi (a gift from Dr. R.

Subramanian), and GFP-PRC1 floppy linker mutant (a gift from Dr. R. Subramanian) was cloned into pMSCV destination vector by gateway cloning. GFP-EB1 was a gift from Dr. B. Houghtaling. For FKBP-FRB dimerizer plasmids, pMSCV H2B-mCherry-FRB was used (a gift from Dr. E.A. Foley). FKBP-GFP-Aurora B plasmid was constructed by gateway recombination of Aurora B entry clone and pMSCV FKBP-GFP destination vector (a gift from Dr. E.A. Foley).

2.2 FRET sensor substrate sequence

The Aurora sensor uses 'KVNKIVKNRRTVAI' as its substrate sequence(Fuller et al., 2008). The Plk sensor uses 'LLLDSTLSINWD' as its substrate sequence(Fuller et al., 2008).

2.3 Cell culture

Cells were cultured in DMEM (Invitrogen, for 293-Ampho cells) or DMEM/F12 1:1 nutrient mix (Invitrogen, for hTERT-RPE1 cells) supplemented with 10% FBS (Atlanta Biologicals) and penicillin-streptomycin (100 U/ml and 100 µg/ml respectively, Invitrogen), at 37°C in a humidified atmosphere with 5% CO_2. Cell lines used for imaging are retroviral stable cell lines. Retroviruses were generated by transfecting 293-Ampho cells by calcium phosphate

precipitation. hTERT-RPE1 cells were then infected by retrovirus with 4 µg/ml polybrene (Sigma) and selected by puromycin (Sigma), G418 (Sigma), or blasticidin (Sigma).

RNAi transfections were carried out by using Invitrogen RNAi Max reagent following the manufacturer's instructions. Cells were then either plated in 6-well plates (for immunoblots) or on No. 1.5 12 mm circular coverslips (for immunofluorescence, Fisher Scientific). For Aurora B RNAi experiments, hTERT-RPE1 cell lines expressing the Aurora FRET sensor were transfected with Aurora B siRNA oligos (5'- AACGCGGCACUUCACAAUUGA-3') (Fuller et al., 2008). For INCENP RNAi experiments, hTERT-RPE1 cell lines expressing either mCherry-INCENP wildtype or T59E mutant were transfected with INCENP siRNA oligos (5'-UGACACGGAGAUUGCCAAC-3') (Vader et al., 2006). For PRC1 RNAi experiments, hTERT-RPE1 cell lines expressing the siRNA-resistant PRC1 wildtype or floppy linker mutants were transfected with PRC1 siRNA oligos (5'-GGCUUCUAGGCGUGAGGAG-3')(Neef et al., 2007).

For monopolar cytokinesis, coverslips were incubated in medium with kinesin-5 inhibitor STLC (2 µM, Sigma, dissolved in DMSO) and ethanol (0.1%, pharmco, solvent for purvanol A) for 5 hours and then exchanged into medium with

both STLC (2 μM, Sigma) and Cdk1 inhibitor purvanol A (30 μM, Tocris bioscience, dissolved in ethanol)(Hu et al., 2008).

2.4 Live Cell Imaging

hTERT-RPE1 cells were grown on poly-D-lysine (Sigma)-coated No. 1.5 22x22mm coverslips (Fisher Scientific) and mounted in a Rose chamber in L-15 media without phenol-red (Invitrogen, imaging media). The media was supplemented with 10% FBS. The imaging chamber was maintained at 35 °C to 37 °C by an air stream stage incubator (Nevtek). The FRET sensor was imaged and the data was processed as published(Fuller et al., 2008). For linescan projections of the emission ratio images, custom software was written in Matlab (Mathworks). Briefly, emission ratios were calculated for intensities above background. The spindle axis was determined by connecting the two centrosomes of the cell and the position of the midpoint between the two centrosomes was set to be zero. Emission ratios of pixels with the same position along the spindle elongation axis were averaged and the standard deviation was calculated. The linescan projection was generated by plotting the averaged emission ratio against position, with standard deviation for the emission ratio at all positions.

For imaging the FRET sensors, cells that have both spindle poles within 2 μm distances in the z-direction were imaged, so as to reduce errors from stack averaging. For imaging sensors in Aurora kinase inhibition experiment in Fig. 2, rose chambers with cells expressing FRET sensors were assembled with 0.1% DMSO (solvent for ZM447439) in imaging media. Metaphase cells were found and tracked until anaphase onset and then media was exchanged to imaging media with ZM447439 (10 μM, Chemietek, dissolved in DMSO). Cells were then imaged every 2 min for 12 min.

For imaging FRET sensors in other small molecule inhibitors (i.e. ZM447439 (chemietek), latrunculin B (Sigma) and BI2536 (Steegmaier et al., 2007)), rose chambers with cells expressing FRET sensors were assembled with 0.1% DMSO (solvent for ZM447439, latrunculin B and BI2536) in imaging media. In the case of ZM447439, cells were incubated with 0.3 μM inhibitor for 30 min and then subjected to imaging. Metaphase cells that show a clear metaphase plate and have both spindle poles within 2 μm distances in z-direction were imaged. For latrunculin B and BI2536 experiments, metaphase cells were located and media was exchanged to imaging media containing 2 μM latrunculin B or 250 nM BI2536. Anaphase cells were tracked for >20 min post anaphase onset.

For near-simultaneous imaging of FRET sensors and mCherry-INCENP in live cells (Fig. 2, Fig. 4), FRET sensors were imaged as above, using a camera (Photometrics 512B) mounted on the microscope's sideport. mCherry-INCENP images for the same cells were collected near simultaneously using epi-fluorescence on a separate camera (Photometrics HQ), mounted on the microscope's baseport.

For GFP-anillin analysis in Fig. 4, hTERT-RPE1 cell lines stably expressing GFP-anillin, GFP-PRC1 and mCherry-INCENP wild type or T59E were used. Confocal fluorescence images were acquired every 10s using a Nikon TE2000 microscope (Morrell Instruments) with a PlanApo 100× NA 1.40 objective. Anaphase onset (time zero) was determined based on centromere separation in the mCherry-INCENP channel. The equatorial plane was determined by averaging the GFP-PRC1 localization from images at 330s, 340s and 350s. Linescans (width = 10 pixels) were generated for images from all timepoints. For each linescan profile, there are two peaks for GFP-anillin signal, corresponding to the two edges of the cell. The maximum GFP-anillin signal intensity **Ip** (for the equatorial GFP-anillin signal at each timepoint) was calculated by averaging three pixels, with the maximum intensity pixel at the center, for each cell edge (i.e. averaging signal for a total of 6 pixels).

The relative enrichment factor was calculated using the following equation: (**Ip**(t) - **Ip** (t=0)) / (**Ip**(t=0)), and was plotted against time. These analyses were carried out using MATLAB.

For micromanipulation experiments with microneedles, REP1 cell lines expressing GFP-PRC1 and GFP-anillin were plated on collagen-coated coverslips and the coverslips were assembled in an open rose chamber. The micromanipulation was performed following published set-up (Shimamoto et al., 2011).

For FKBP-FRB dimerizer imaging, Hela cells co-expressing FKBP-GFP-Aurora B and H2B-mCherry-FRB were treated by either DMSO control or 20 nM Rapamycin. The cells were imaged live by confocal microscopy.

For live cell imaging of GFP-EB1, spinning disk confocal microscopy was employed. Stable RPE1 cell lines expressing GFP-EB1 and mCherry-INCENP were imaged live every 1s. Single images were taken each time. Images were then analyzed using the methods that have been previously developed to track EB1 comets (Houghtaling et al., 2009).

2.5 Immunoblots

Cells were incubated in 10 μM nocodazole (Sigma) containing medium for 16 hours before harvest. Cells were then lysed and subjected to SDS-PAGE followed by immunoblotting. Primary antibodies used in immunoblotting are: anti-INCENP (AbCam), anti-cyclin B (BD Biosciences), anti-PP2A (Santa Cruz). IRDye 800 goat anti-rabbit or anti-mouse IgG (Li-Cor) was used according to manufacturer's instructions. Blots were detected and quantified using the Odyssey Infrared Imaging System (Li-Cor).

2.6 Immuno-fluorescence Microscopy

Coverslips were first fixed in 4% formaldehyde in PBS buffer at room temperature for 10 min and then incubated in methanol at -20 °C for 10 min. Subsequently, coverslips were washed with PBS and 0.5% Triton X in PBS (PBS-tx). Washed coverslips were blocked in 5% BSA in PBS-tx for 30 min. Primary antibodies were incubated in 2% BSA in PBS-tx and are from the following sources: anti-Plk1 (Santa Cruz); Rabbit polyclonal anti-PRC1; Aurora B antibody (anti-AIM-1, Signal Transduction Labs); anti-MKLP1 (Santa Cruz); FITC conjugated anti-tubulin DM1-a (Sigma). DNA was stained with DAPI (Invitrogen). Secondary antibodies used are Dylight-conjugated donkey anti-rabbit and anti-mouse antibodies

(Jackson Immunological Laboratories). For RhoA visualization, cells were fixed with 10% Trichloroacetic acid (Sigma) on ice for 10 min and stained with anti-RhoA (Santa Cruz). Images were acquired as Z-stacks with 0.15 μm spacing using a 100x, 1.35 NA objective on a DeltaVision Image Restoration Microscope (Applied Precision Instruments, Issaquah, WA and Olympus, Melville, NY), and processed by iterative constrained deconvolution (SoftWoRx, Applied Precision Instruments). Maximal intensity projections of the entire Z-stack are shown. Linescans for immuno-fluorescence images were generated using ImageJ software. A line with 3.7 μm width was drawn by connecting the two spindle poles and an averaged plot profile was generated.

CHAPTER 3: Examining the dynamics of Aurora kinase-dependent phosphorylation during cell division

3.1 Background information

Dynamic microtubule-based structures are required for the stable propagation of genomes through cell division (Walczak et al., 2008). It is generally agreed that these structures self-organize, a process by which complex architectures arise from the multiplicity of interactions involving key proteins that follow simple rules and respond to positional cues (Nédélec et al., 2003). These cues, which must vary on the relevant length-scale, can be mechanical (e.g. forces that unbind a protein from a microtubule or stall a motor protein) or chemical (e.g. a post-translational modification that can activate an enzyme). At least two different chemical cues that form spatial gradients within single dividing cells have been described. First, a gradient of GTP-bound Ran can be observed before anaphase and contributes to metaphase spindle assembly (Bastiaens et al., 2006; Kalab and Heald, 2008). Second, a gradient of phosphorylated substrates of the chromosomal passenger complex (CPC, comprised of Aurora B kinase, INCENP, Survivin and Borealin) can be observed between segregating chromosomes during anaphase (Fuller et

al., 2008; Ruchaud et al., 2007). In contrast to the Ran gradient, the CPC-substrate phosphorylation gradient remains poorly characterized and its contributions to cell division remain untested.

The CPC is a widely conserved regulator of several processes required for mitosis, including bipolar spindle assembly, chromosome-microtubule attachment and spindle midzone formation (Ruchaud et al., 2007). To carry out these different functions, CPC's localization changes through mitosis, with the protein complex binding along chromosomes when cells enter mitosis, concentrating at the inner centromeres prior to anaphase and relocating to the spindle midzone upon anaphase onset (Carmena and Earnshaw, 2003). A spatial gradient of CPC-substrate phosphorylation at anaphase was observed using FRET-based sensors and antibody-based analyses (Fuller et al., 2008). As the peak of the substrate phosphorylation gradient coincides with CPC localization during anaphase, it is tempting to speculate that kinase localization determines the shape of the gradient. Consistent with this hypothesis, disruption of the spindle midzone using microtubule poisons or knockdown of MKLP2 (a kinesin required for proper CPC localization) prevents the proper establishment of the spatial phosphorylation gradient (Fuller et al., 2008).

However, since these perturbations can interfere with other signaling pathways, such as Polo-like kinase (Plk) signaling (Barr et al., 2004), a proper test of the role of CPC localization in determining the shape of this spatial phosphorylation gradient is lacking.

The possibility that CPC-dependent spatial gradients are present prior to anaphase has been raised by two different observations. First, phosphorylation levels of CPC-substrates at centromeres/kinetochores have been shown to depend on their distance from the inner centromere, where the CPC is concentrated (Lampson and Cheeseman, 2011). Second, it has been shown that chromosomes can enrich and activate the CPC (Kelly et al., 2007), and therefore, there is likely to be higher probability of substrate phosphorylation near chromosomes, than at cell edges that can be several microns away. However, a spatial CPC-substrate phosphorylation gradient has not been observed before anaphase.

As Aurora B kinase localization is dynamic and there is extensive cellular reorganization during cell division, observing gradients of Aurora substrate phosphorylation is likely to require live reporters. The FRET-based sensors previously used to analyze the gradient during anaphase in live cells did not reveal spatial phosphorylation gradients

at earlier stages of cell division (Fuller et al., 2008). This could be in large part due to the fact that these sensors were targeted to chromosomes and, therefore, phosphorylation dynamics could only be analyzed at cellular sites where chromosomes were present (Figure 3.1)(Fuller et al., 2008). Moreover, FRET-sensors freely diffusing in the cytoplasm did not reveal spatial patterns of substrate phosphorylation, most likely due to the degradation of the gradient by diffusion of the sensors (Fuller et al., 2008). Therefore, a sensor that has restricted diffusion and allows continuous measurements of phosphorylation levels across the dividing cell is needed. In this chapter, I describe the development of a microtubule-targeted FRET sensor that allows for characterization of the temporal dynamics of the spatial phosphorylation gradient for Aurora substrates throughout cell division.

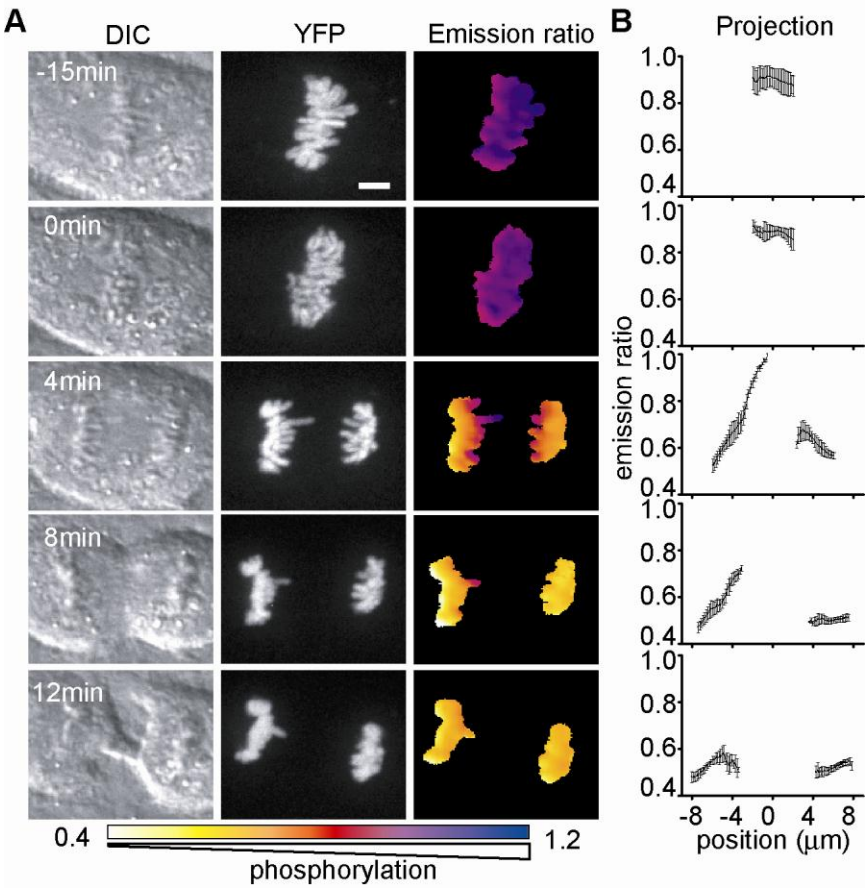

Figure 3.1

The chromatin-targeted FRET sensor for Aurora kinase activity does not readily allow for spatially continuous measurements of substrate phosphorylation during anaphase. (A) A cell expressing chromatin-targeted FRET sensor is imaged through anaphase. DIC, YFP and color-coded emission ratio images are shown. (B) Corresponding linescan projections of emission ratios along the spindle elongation axis are shown. Timestamps are relative to anaphase onset. Error bars, SD. Scale bar, 5µm.

3.2 Development of a microtubule-targeted sensor that reports on Aurora substrate phosphorylation

I developed a microtubule-targeted FRET-sensor by fusing the MAP4 microtubule-binding domain (amino acids 590-964) to the N-terminus of the Aurora cytosolic sensor (Figure 3.2A). Using an hTERT-RPE1 cell line that stably expresses the microtubule-targeted sensor, I verified that the sensor localizes to microtubules (Figure 3.2B), and its expression altered neither the mitotic index nor the error rate of chromosome segregation (Figure 3.2C).

I found that phosphorylation of the microtubule-targeted sensor, measured by calculating CFP:YFP emission ratio, mainly depends on Aurora B kinase activity. Live cell imaging revealed that in mitosis, when Aurora B is activated, the sensor showed a high CFP:YFP emission ratio (0.59 ± 0.05, n = 42 cells), corresponding to a highly phosphorylated state. In interphase, when Aurora B levels are low, the sensor showed a low CFP:YFP emission ratio (0.92 ± 0.05, n = 42 cells), corresponding to a dephosphorylated state (Figure 3.3A,B). Mutation of the phospho-acceptor threonine in the substrate to alanine (Thr to Ala control) or Aurora B knockdown by RNAi led to a low emission ratio in both mitotic and interphase cells (Figure 3.3A,B). From these results, I conclude that the

phosphorylation of the microtubule-targeted sensor by Aurora B kinase could be examined by measuring the CFP:YFP emission ratio of the sensor.

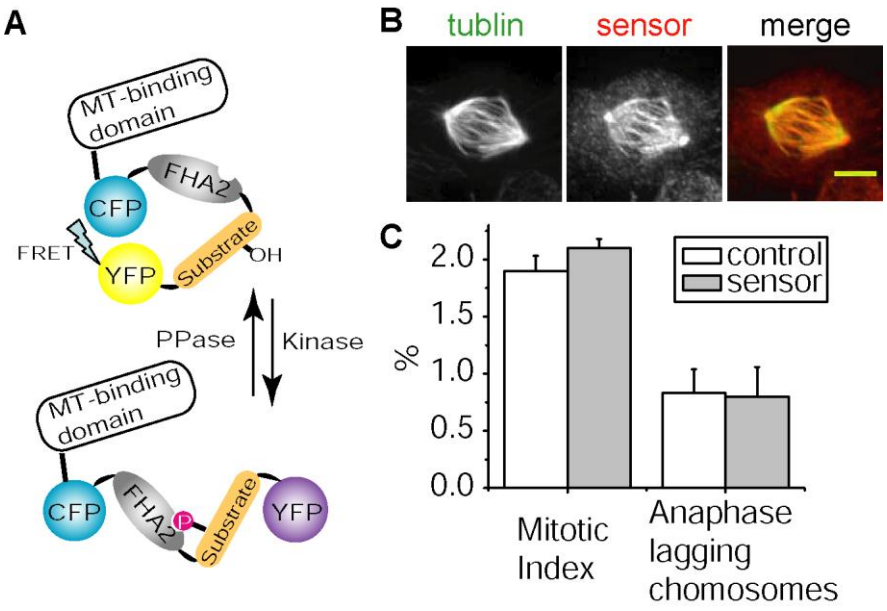

Figure 3.2

Development of a microtubule-targeted FRET sensor.

(A) Schematic shows the design of the microtubule-targeted FRET-sensor of Aurora B activity. The microtubule-binding domain is from MAP4. (B) The microtubule-targeted FRET sensor localizes to microtubule bundles in mitosis. An hTERT-RPE1 cell expressing the sensor was fixed and processed for immuno-fluorescence (tubulin:green and sensor:red). Scale bar, 5μm. (C) Analysis of mitotic index and errors in chromosome segregation during anaphase for cells stably expressing the microtubule-targeted FRET sensor. Comparison between hTERT-RPE1 cells (control) and hTERT-RPE1 cells expressing the microtubule-targeted AurB sensor are shown (N= 4500 cells for mitotic index of each cell line; N > 2000 anaphase cells for lagging chromosome rate of each cell line; three independent experiments).

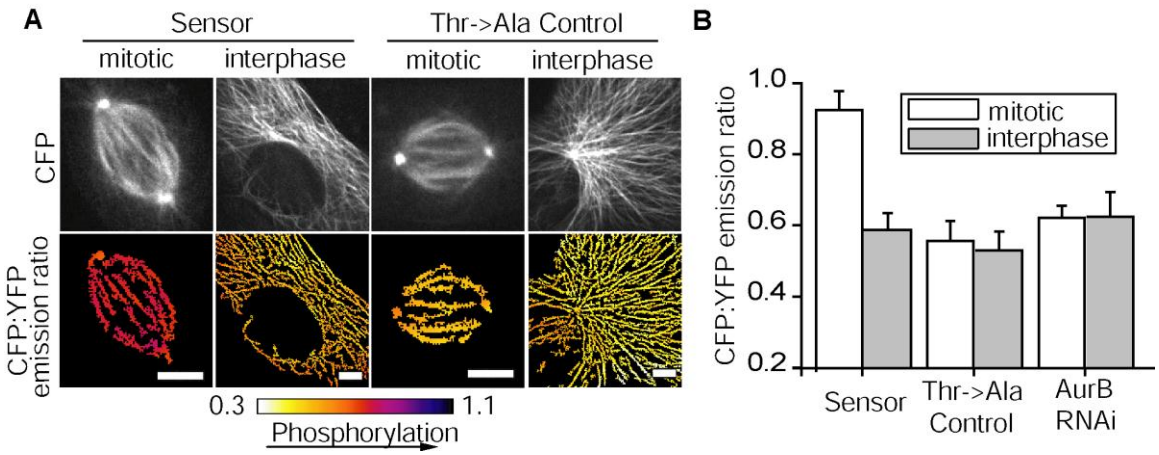

Figure 3.3

Microtubule-associated phosphorylation in mitosis depends on Aurora B. (A) The FRET sensor shows phosphorylation associated with microtubules in mitosis. hTERT-RPE1 cells expressing the FRET sensor, or a mutated sensor (Thr to Ala) as a control, were imaged live. Upper panels, unprocessed CFP images; lower panels, color-coded images of the CFP:YFP emission ratio. Note that higher emission ratio (more yellow/white) indicates high phosphorylation. Scale bars, 5µm. (B) Microtubule-associated phosphorylation in mitosis depends on Aurora B. Analysis of CFP:YFP emission ratios in mitosis and interphase for sensor (N=42 cells), mutated sensor (N=35 cells), and for sensor after knockdown of Aurora B by RNAi (N=23 cells). Imaging of Aurora B depletion in single cells was conducted by fixation, processing for immuno-fluorescence, and relocation using coverslips with grids.

3.3 Temporal and spatial phosphorylation dynamics of microtubule-targeted Aurora sensor during mitosis

I first examined the temporal dynamics of Aurora substrate phosphorylation during mitosis. Time-lapse imaging of the sensor revealed that before nuclear envelope breakdown (NEB) the average CFP:YFP ratio was low (0.62 ± 0.04, n > 10 cells; Figure 3.4A), similar to that during interphase, when the CPC is down-regulated (Honda et al., 2003), and to that observed for the phosphorylation-site mutated sensor (Thr to Ala; Figure 3.3A,B). Together, these data suggest that this ratio likely corresponds to an unphosphorylated state of the sensor. As mitosis progressed, the average CFP:YFP ratio increased and then remained largely constant (CFP:YFP ratio 0.96 ± 0.06, n > 10 cells; Figure 3.4B) until anaphase onset. At anaphase, the average CFP:YFP ratios indicated that the sensor dephosphorylated slowly, with levels reducing ~20% towards the end of cleavage-furrow ingression (Figure 3.4B).

I then examined the spatial dynamics of Aurora substrate phosphorylation throughout cell division. Interestingly, the microtubule-targeted FRET sensor revealed a spatial gradient at the very early stages of mitosis. Just after NEB, CFP:YFP emission ratios were highest at the center of the emerging bipolar spindle and

reduced at astral microtubules that extended from spindle poles to the cell cortex (Figure 3.4C-G, slope 0.02 ± 0.01 μm^{-1}, n = 4 cells). After ~9 minutes the spatial gradient could not be detected (Figure 3.4C, lower panels). As this transient gradient had not been previously captured using chromosome-targeted sensors, I examined the response of the sensor after Aurora B RNAi knockdown or chemical inhibitor treatment. I found that, similar to the chromosome-targeted sensor, the majority of the microtubule-targeted sensor's response depended on the Aurora B kinase at prometaphase, as it did at metaphase and anaphase (Figure 3.4H-M) (Tseng et al., 2010). While it is unlikely that the sensor can discriminate between closely related kinases (e.g. Aurora A and Aurora B), this response likely reflects functional differences between these kinases. Additional studies using antibodies to native phosphorylated substrates will be needed to analyze this further.

Figure 3.4

A microtubule-targeted FRET-sensor reveals a gradient for Aurora substrate phosphorylation at early cell division. (A) The CFP:YFP emission ratio averaged for RPE1 cells expressing the microtubule-targeted sensor (n > 10), as they entered mitosis. Time zero represents nuclear envelope breakdown (NEB). Error bars, SEM. (B) The same analysis was carried out for cells undergoing anaphase (n > 10). Time zero represents anaphase onset. (C) A cell expressing the FRET-sensor was imaged through prophase-prometaphase. DIC, YFP (at two different contrast settings), and color-coded emission ratio images are shown. Time zero represents NEB. (D) Averaged linescan projections along the spindle axis for the corresponding color-coded emission ratio images in (C). Error bars, SD. (E) Color-coded image of emission ratio from 4 min timepoint in (C), adjusted for a smaller range of emission ratios. (F-G) A prometaphase cell was imaged live. DIC, YFP at two different intensity scales, emission ratio images are shown (F). Corresponding averaged linescan projection is shown (G). Error bars, SD. (H-I) A cell expressing the microtubule-targeted sensor lacking the phospho-acceptor threonine (mutated to alanine) was imaged through prophase-prometaphase. DIC, YFP and emission ratio images are shown (H). Corresponding linescan projections are shown (I). (J-K) A prometaphase cell expressing the microtubule-targeted sensor treated with Hesperadin (100nM). DIC, YFP and emission ratio images are shown (J). Corresponding linescan projections are shown (K). (L-M) A prometaphase cell in which Aurora B is depleted by RNAi. DIC, YFP and color-coded images of the CFP:YFP emission ratio are shown (L). Corresponding linescan projections are shown (M). Error bars, SD. Scale bar, 5μm.

Figure 3.4

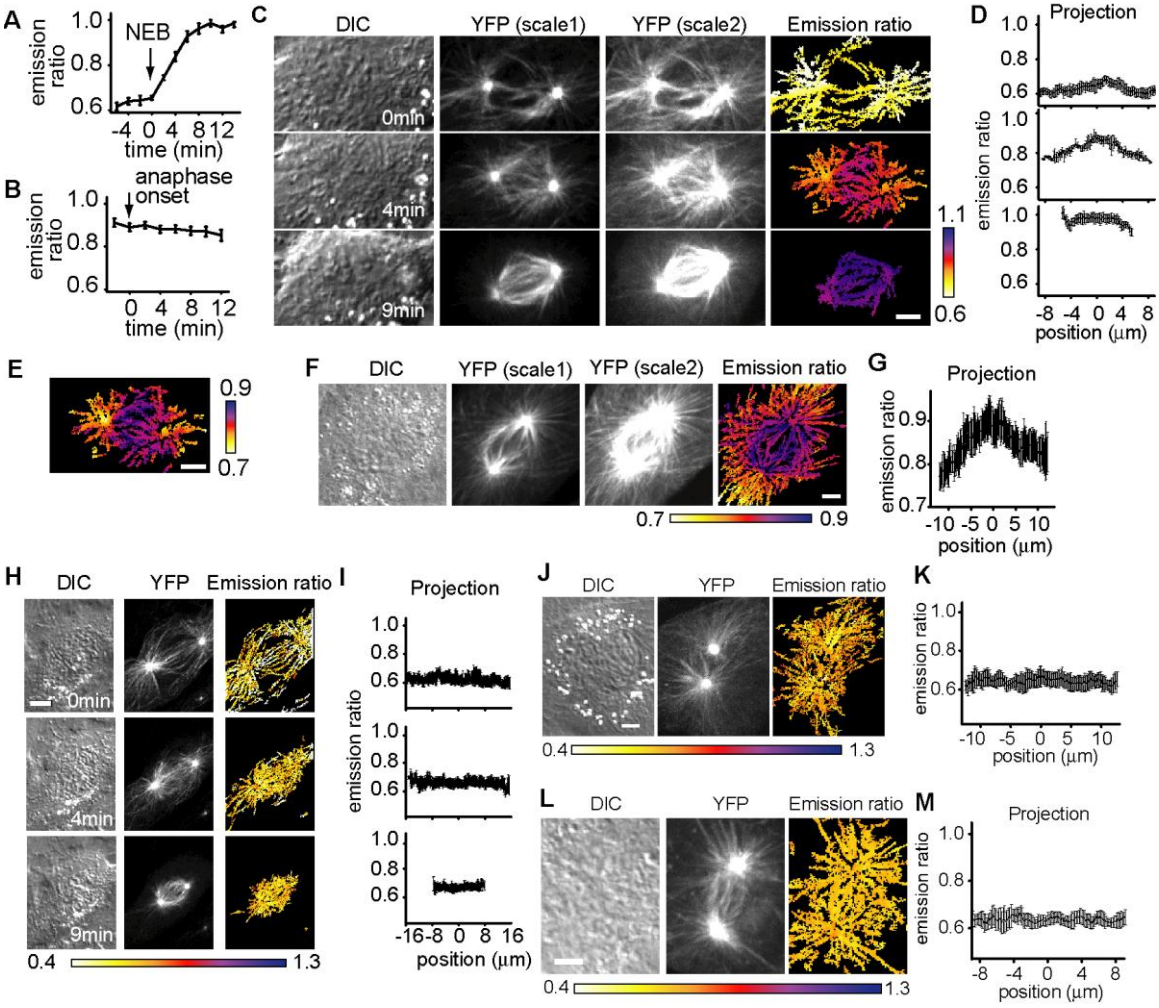
A
emission ratio
1.0
0.8
0.6
NEB
-4 0 4 8 12
time (min)
B
emission ratio
anaphase onset
0 4 8 12
time (min)
C
DIC
YFP (scale1)
YFP (scale2)
Emission ratio
0min
4min
9min
1.1
0.6
D
Projection
emission ratio
-8 -4 0 4 8
position (μm)
E
0.9
0.7
F
DIC
YFP (scale1)
YFP (scale2)
Emission ratio
0.7
0.9
G
Projection
emission ratio
-10 -5 0 5 10
position (μm)
H
DIC
YFP
Emission ratio
0min
4min
9min
0.4
1.3
I
Projection
emission ratio
-16 -8 0 8 16
position (μm)
J
DIC
YFP
Emission ratio
0.4
1.3
K
emission ratio
-10 -5 0 5 10
position (μm)
L
DIC
YFP
Emission ratio
0.4
1.3
M
Projection
emission ratio
-8 -4 0 4 8
position (μm)

To examine if the CPC-substrate phosphorylation gradient could not be detected at metaphase due to the increasing levels of substrate phosphorylation (such that the 'valleys' on either side of the peak are 'filled'), I used the Aurora kinase inhibitor ZM447439 to partially suppress overall phosphorylation. As essentially complete inhibition of substrate phosphorylation is achieved at ~2 μM ZM447439 (Ditchfield et al., 2003), I used 0.3 μM inhibitor for partial inhibition. Under these conditions, the average CFP:YFP ratio is 0.83 ± 0.04 (n=47 cells), indicating that the substrate phosphorylation is partially suppressed and is comparable to that in anaphase cells. A spatial pattern similar to that observed at prometaphase, such that CFP:YFP emission ratios peak between the two spindle poles (the slope was comparable to that in prometaphase cells), was detected in a subset of cells at metaphase (10 out of 47 cells, Figure 3.5A,B). In several other cells, an asymmetric pattern could be detected, with maximal phosphorylation positioned away from the center of the spindle (11 out of 47 cells; Figure 3.5C-F). The reason for this asymmetry could be due to the presence of single or only a few chromosome(s), where the source of the gradient is positioned, at one spindle pole. These chromosomes are likely to be common when the CPC is inhibited (Ruchaud et

al., 2007), and are difficult to detect by DIC imaging in rounded-up metaphase cells. This is also likely to be the reason that a robust gradient cannot be detected in approximately half of the metaphase cells imaged at the presence of low doses of the inhibitor. Together, these data are consistent with the hypothesis that increased levels of substrate phosphorylation at metaphase can mask CPC-dependent spatial patterning of phosphorylation. At this stage, I cannot exclude the possibility that these observations reflect limitations of this sensor-based analysis. As there are no available phospho-specific antibodies against endogenous CPC substrates that distribute uniformly across the spindle, additional tests remain difficult.

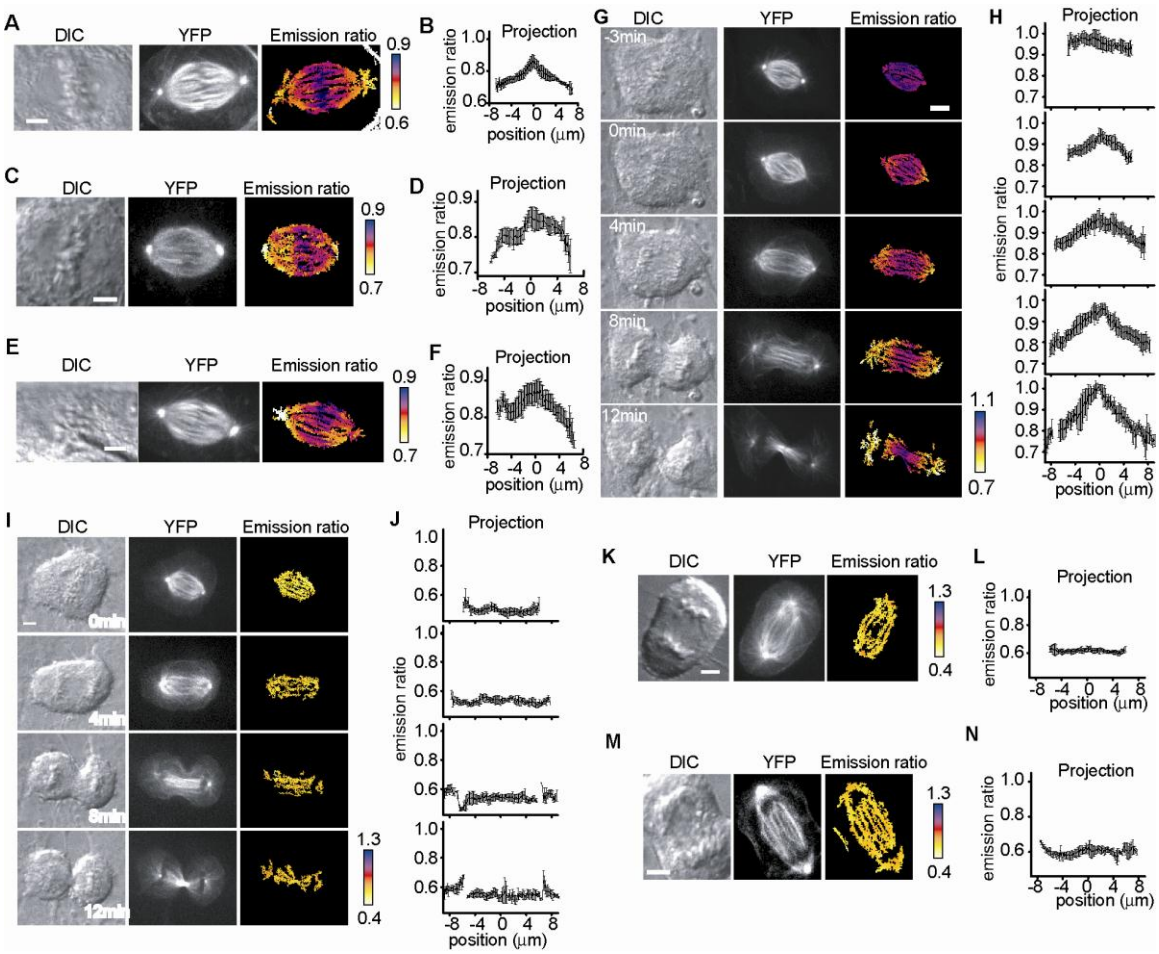

Figure 3.5

DIC, YFP and color-coded emission ratio images, along with corresponding averaged linescan projections along the spindle axis, are shown for cells expressing the microtubule-targeted FRET-sensor. Three metaphase cells treated with 0.3 μM ZM447439 (A-F), a cell at anaphase (G,H), an anaphase cell expressing the microtubule-targeted sensor lacking the phospho-acceptor threonine (mutated to alanine, I,J), an anaphase cell treated with Aurora kinase inhibitor Hesperadin (100nM, K,L), and an anaphase cell in which Aurora B is depleted by RNAi (M,N). Error bars, SD. Scale bar, 5μm.

I next examined the spatial organization of CPC-substrate phosphorylation during anaphase. Similar to what is revealed by chromatin-targeted sensors, the highest levels of phosphorylation coincided with the spindle midzone and phosphorylation levels were reduced near each spindle pole (Figure 3.5G,H). This anaphase gradient also depends on CPC activity, as using the phosphorylation-mutant sensor or inhibition of CPC activity by either chemical inhibitor or Aurora B RNAi abolished the gradient pattern formation (Figure 3.5I-N). In addition, the microtubule-targeted sensor revealed that the gradient emerged when chromosome segregation began. The slope of the gradient, as measured from its peak at the center of the spindle midzone towards a spindle pole, increased over time (from 0.02±0.01 μm^{-1} before the appearance of the cleavage furrow; 0.04±0.02 μm^{-1} after cleavage furrow ingression starts (n = 16 cells); Figure 3.5H). Importantly, the site of maximum phosphorylation remained unchanged throughout anaphase (Figure 3.5H). Interestingly, the appearance of the anaphase gradient also coincided with decreasing phosphorylation after anaphase onset, consistent with the observation that decreased substrate phosphorylation at metaphase reveals CPC-dependent spatial patterning.

3.4 The shape of the Aurora-substrate phosphorylation gradient can be perturbed without altering the overall substrate phosphorylation level

To analyze factors that contribute to the shape of the CPC-substrate phosphorylation gradient, I focused on the analysis of cells undergoing anaphase. In principle, the gradient's shape is controlled by the intracellular localization of the kinase or the phosphatase, which serve as the phosphorylation 'source' and 'sink', respectively. The phosphatase(s) contributing to this phosphorylation gradient are not known. Therefore, I focused on altering the spatial distribution of CPC activity without inhibiting the kinase directly. The relocation of the CPC from centromeres to the spindle midzone depends on the dephosphorylation of INCENP at threonine-59 (Thr-59) (Hümmer and Mayer, 2009). Mutation of Thr-59 to glutamate (Glu) only affects CPC localization after anaphase onset, without disrupting its metaphase functions (Hümmer and Mayer, 2009). Therefore, I knocked down endogenous INCENP using RNAi and added back an mCherry-INCENP T59E mutant (hereafter, referred to as T59E-addback cells) or an mCherry-INCENP wild-type construct (hereafter, WT-addback cells) as a control (Figure 3.6A,B). As anticipated, in T59E-addback cells, the CPC properly concentrated at

centromeres before anaphase (Figure 3.6C), but remained enriched at chromosomal sites during anaphase and could not be detected at the spindle midzone (Figure 3.6C).

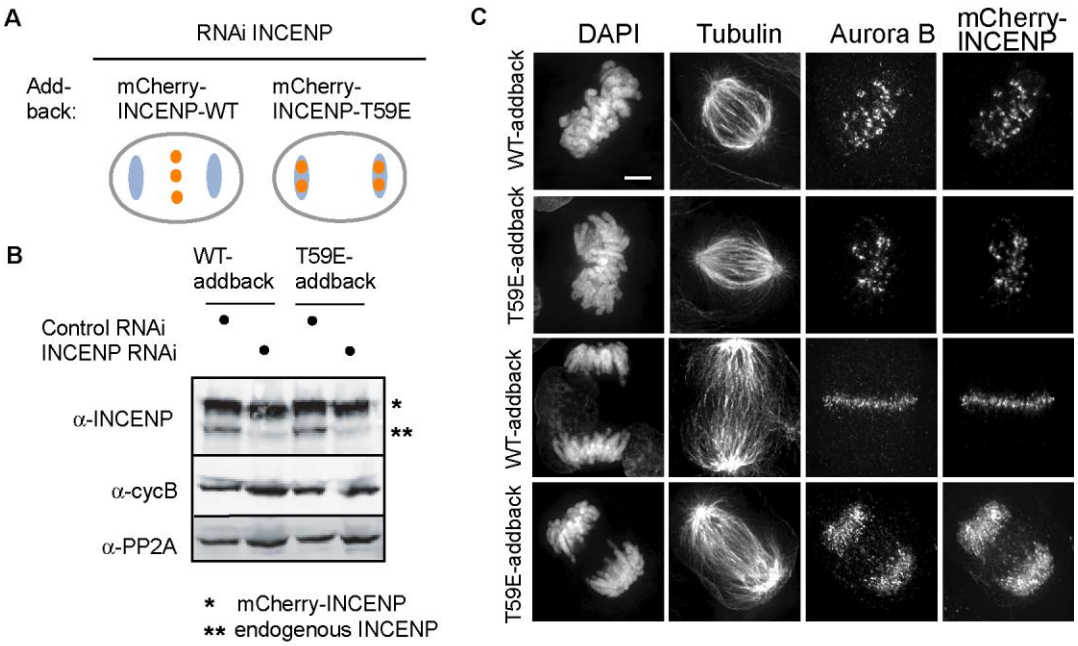

Figure 3.6

Examining CPC localization in cells after INCENP knockdown and add-back of the WT or T59E mutant of INCENP. (A) A schematic of CPC (orange dot) mislocalization on chromosomes (blue) during anaphase. (B) A representative western blot showing knockdown of endogenous INCENP and expression of mCherry-INCENP constructs. Cyclin B (cycB) and PP2A are loading controls. (C) WT- and T59E-INCENP-addback cells were fixed and stained to label chromosomes (DAPI), tubulin, Aurora B and mCherry-INCENP. Pre-anaphase (upper two panels) and anaphase (lower two panels) cells are shown here. Scale bar, 5 μm.

I next examined CPC-substrate phosphorylation in cells where the CPC was mislocalized. While the microtubule-targeted sensor revealed a persistent gradient in WT-addback cells (Figure 3.7A), no robust spatial pattern of CPC-substrate phosphorylation was apparent in T59E-addback cells throughout anaphase (Figure 3.7B). Importantly, the averaged CFP:YFP ratio was similar across microtubules in T59E- and WT-addback cells (Figure 3.7C). In contrast, when an Aurora kinase inhibitor was added to cells entering anaphase, the sensor revealed a ~7-fold lower average phosphorylation during cleavage furrow ingression (t=6 min onward) (Figure 3.7D). Together, these data indicate that in T59E-addback cells the shape of the CPC-substrate phosphorylation gradient was altered without significant changes in overall phosphorylation levels. Therefore, our data suggest that the shape of the substrate phosphorylation gradient is coupled to kinase localization.

Figure 3.7

The microtubule-targeted FRET-sensor reveals that while improper CPC localization disrupts the formation of the spatial phosphorylation gradient, average substrate phosphorylation remains unchanged. (A-B) A WT-(A) or T59E-(B) INCENP-addback cell expressing the microtubule-targeted FRET-sensor was imaged through anaphase. DIC, YFP, color-coded emission ratio images are shown, timestamps are relative to anaphase onset. (C) Overlaid averaged linescan projections along the spindle axis for WT- and T59E-INCENP-addback cells in (A,B). Error bars, SD. (D) Cells expressing microtubule-targeted sensor that are either WT-(n > 10) or T59E-INCENP-addback (n > 20), or treated with Aurora kinase inhibitor ZM447439 (10 μM, added at anaphase onset, n = 3), were imaged live through anaphase. The CFP:YFP emission ratio at each time point was averaged and normalized (setting the interphase ratio to 0, and the metaphase ratio to 100). Note that decreased emission ratio indicates dephosphorylation. Error bars, SEM. Scale bars, 5 μm.

Figure 3.7

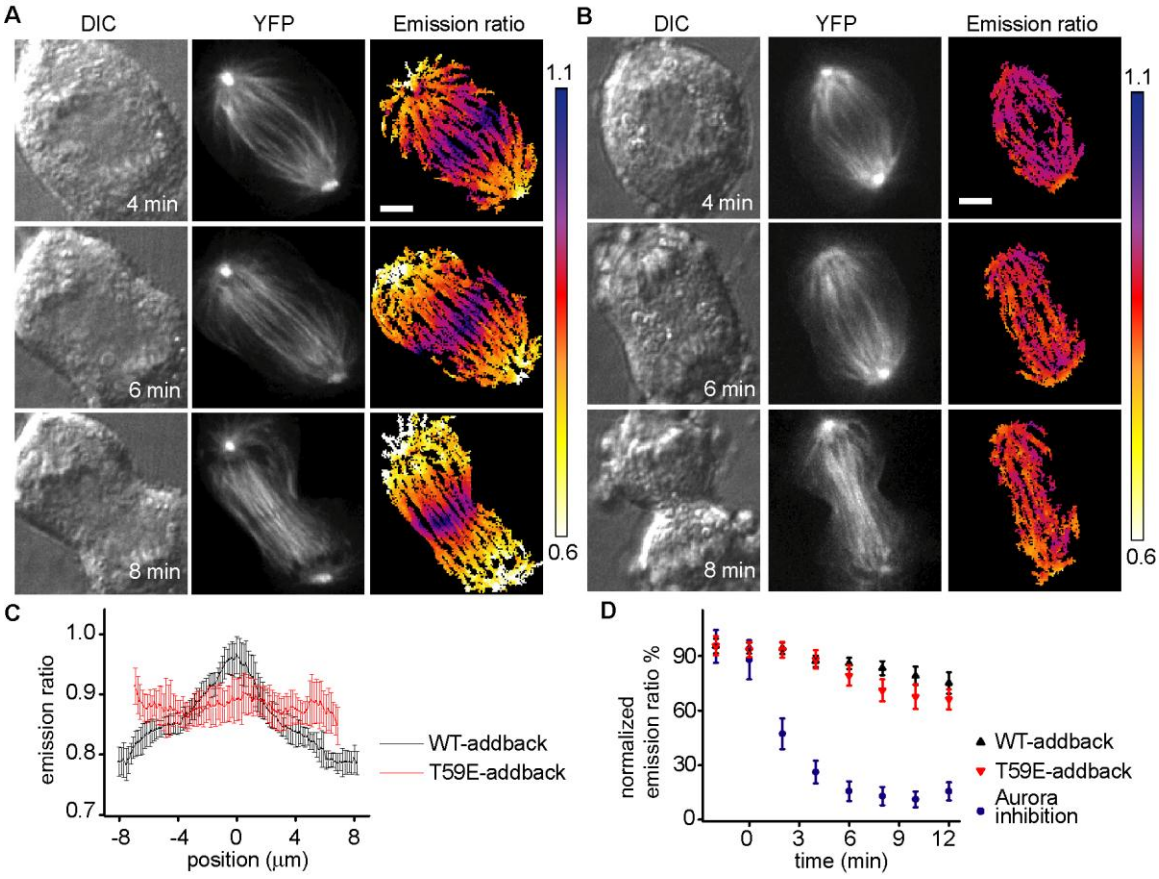
A
DIC
YFP
Emission ratio
4 min
6 min
8 min
1.1
0.6
B
DIC
YFP
Emission ratio
4 min
6 min
8 min
1.1
0.6
C
emission ratio
1.0
0.9
0.8
0.7
-8
-4
0
4
8
position (μm)
WT-addback
T59E-addback
D
normalized emission ratio %
90
60
30
0
0
3
6
9
12
time (min)
WT-addback
T59E-addback
Aurora inhibition

I next asked whether kinase localization at the spindle midzone is sufficient for establishing a substrate phosphorylation gradient. Like Aurora B kinase, Plk1 also localizes to the spindle midzone at anaphase (Figure 3.8A)(Barr et al., 2004). I generated similarly designed microtubule-targeted Plk sensors, with three different unrelated substrate sequences: Myt1, BRCA2, and c-jun ((Fuller et al., 2008; Macurek et al., 2008), M. Lampson unpublished data). These microtubule-targeted Plk sensors did not reveal spatial phosphorylation patterns, while Plk-dependent phosphorylation could be observed (Figure 3.8B-E). These data suggest that kinase localization alone is not likely to be sufficient to generate micron-scale gradients of substrate phosphorylation. At this stage, it is difficult to rule out the possibility that the lack of Plk-dependent spatial gradient is a limitation of the sensors we have used, and further experiments using phospho-specific antibodies against endogenous microtubule-bound Plk1 substrates are needed.

Figure 3.8

Analysis of a microtubule-targeted FRET-sensor for Polo-like kinase activity. (A) Immunofluorescence images of Aurora B or Plk1 (red), tubulin (green) and DNA (blue). (B) Cells expressing the Plk FRET-sensor imaged live. DIC, YFP and CFP:YFP emission ratio images are shown. (C) Analysis of CFP:YFP emission ratios in mitosis and interphase for the Plk sensor (n = 30 cells), and for the sensor in mitosis after Plk inhibition by BI2536 (100 nM; n = 27 cells) or Aurora inhibition by ZM447439 (2 μM; n = 30 cells). (D) Analysis of the Plk sensor in mitotic cells treated with BI2536 (100 nM). Average CFP:YFP emission ratios are plotted against time (n = 10). (E-F) Microtubule-targeted Plk sensor is imaged through anaphase. DIC, YFP and emission ratio images are shown (E). Corresponding linescan projections are shown (F). Timestamps are relative to anaphase onset. (G-H) Images of cells expressing a microtubule-targeted Plk sensor with the phospho-acceptor threonine mutated to alanine. DIC, YFP and emission ratio images are shown (G). Corresponding linescan projections are shown (H). Error bars, SD. Scale bars, 5 μm.

Figure 3.8

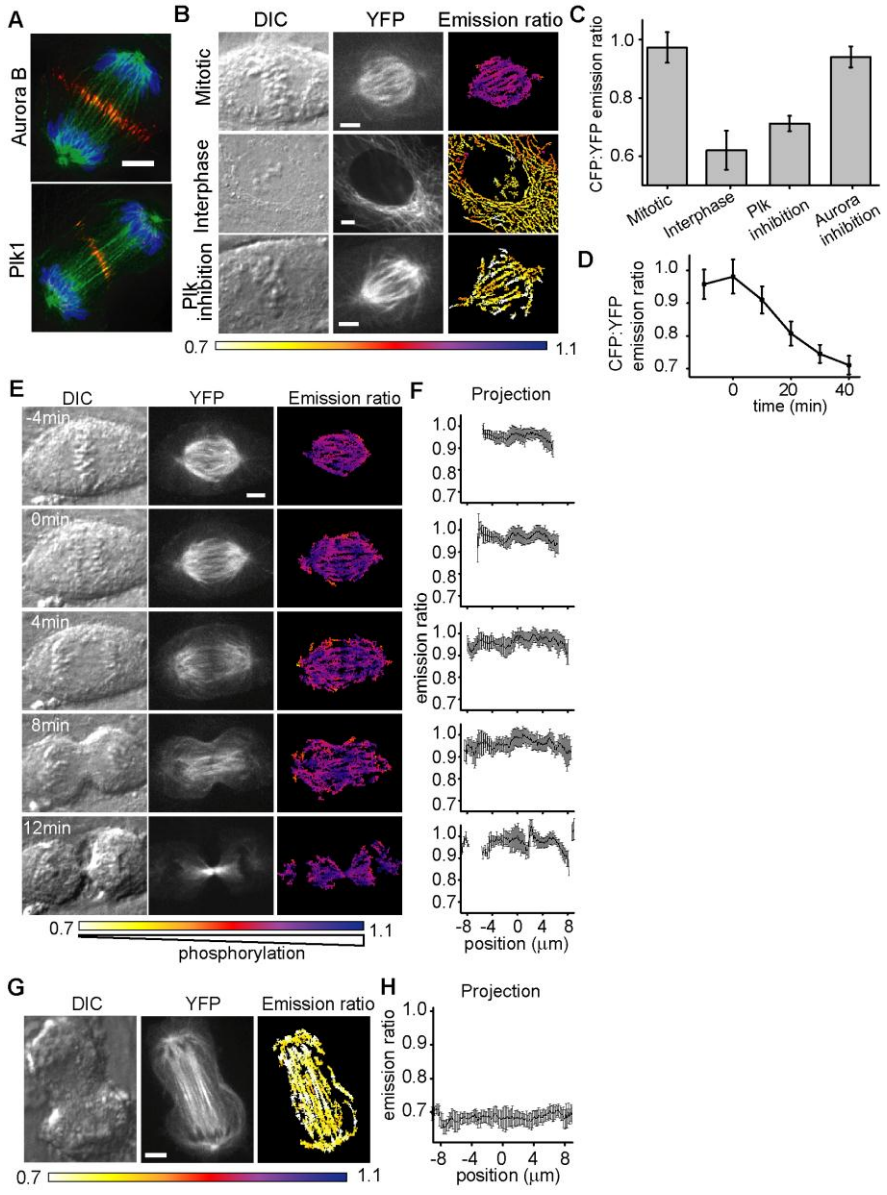
A
Aurora B
Plk1
B
DIC
YFP
Emission ratio
Mitotic
Interphase
Plk inhibition
0.7
1.1
C
CFP:YFP emission ratio
1.0
0.8
0.6
Mitotic
Interphase
Plk inhibition
Aurora inhibition
D
CFP:YFP emission ratio
1.0
0.9
0.8
0.7
0
20
40
time (min)
E
DIC
YFP
Emission ratio
-4min
0min
4min
8min
12min
0.7
1.1
phosphorylation
F
Projection
emission ratio
1.0
0.9
0.8
0.7
-8 -4 0 4 8
position (μm)
G
DIC
YFP
Emission ratio
0.7
1.1
H
Projection
emission ratio
1.0
0.9
0.8
0.7
-8 -4 0 4 8
position (μm)

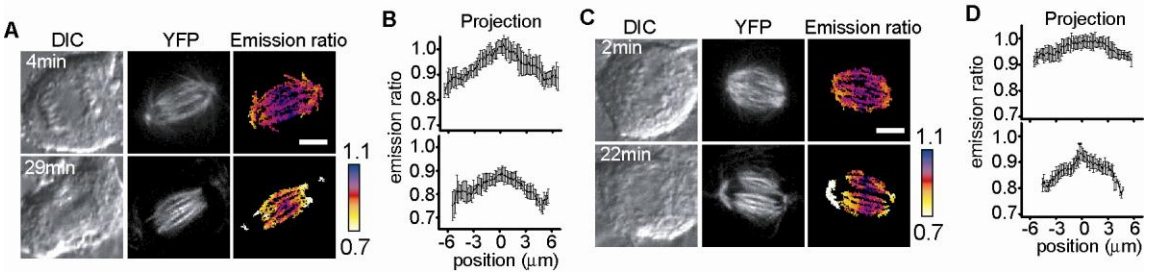

Figure 3.9

The formation of the Aurora-substrate phosphorylation gradient does not depend on cleavage furrow ingression. Cells expressing the microtubule-targeted sensor were treated with either 2 μM latrunculin B (A,B) or 250 nM BI2536 (C,D). DIC, YFP and color-coded emission ratio images, along with corresponding averaged linescan projections along the spindle axis are shown. Time zero represents anaphase onset. Error bars, SD. Scale bars, 5 μm.

To analyze if cleavage furrow ingression also contributes to the shape of the CPC-substrate phosphorylation gradient, I blocked cleavage furrow ingression by either disrupting actin filament formation (using 2 μM latrunculin B (Foe and von Dassow, 2008)), or inhibiting Plk1 activity with a chemical inhibitor (BI2536 at 250 nM (Petronczki et al., 2007)). Under either condition, the microtubule-targeted FRET sensor revealed that the shape of the CPC-substrate phosphorylation gradient emerged and persisted for >20 min (Figure 3.9), which was sufficient time for chromosome decondensation and cleavage furrow ingression in unperturbed cells. These data

show that the CPC-substrate phosphorylation gradient formation at anaphase does not depend on cortical contraction or Plk1 signaling.

3.5 Altering the shape of the Aurora-substrate phosphorylation gradient leads to defects in cytokinesis

To understand the significance of spatially organized CPC signaling, I examined consequences of perturbing the shape of the gradient. As Aurora kinase has numerous roles during anaphase, it is possible that Aurora localization at the midzone and the Aurora-substrate phosphorylation gradient may contribute to multiple processes such as spindle midzone formation (Hauf et al., 2003; Speliotes et al., 2000), compaction of anaphase chromosomes (Mora-Bermudez et al., 2007; Neurohr et al., 2011) or the NoCut pathway (Norden et al., 2006; Steigemann et al., 2009). I focused on spindle midzone formation and compared spindle midzone organization in T59E- vs. WT-addback cells using three different read-outs:

First, I examined the overall density and morphology of the midzone microtubules (Figure 3.10A,C, tubulin panels). In contrast to cells in which the CPC was depleted or inhibited, which had dramatically altered anaphase spindle morphologies (Hauf et al., 2003; Speliotes et al., 2000),

T59E-addback cells had spindle midzone microtubules that appeared similar to those of WT-addback cells.

Second, I analyzed the localization of the CPC substrate MKLP1, a motor protein that binds the RhoA GTPase-activating protein CYK-4 to form the centralspindlin complex(Mishima et al., 2002). As expected, I found that MKLP1 was highly concentrated at the spindle midzone during anaphase in WT-addback cells (Figure 3.10A, WT-addback cells). In contrast, in T59E-addback cells the level of MKLP1 at the spindle midzone was significantly reduced (3-fold reduction indicated by linescans, Figure 3.10A,B, T59E-addback cells).

Third, I examined the extent of antiparallel microtubule overlap using PRC1, a non-motor microtubule-associated protein that marks this cytoskeletal feature (Subramanian et al., 2010). In WT-addback cells, PRC1 localized to the spindle midzone (Figure 3.10C, WT-addback cells). In contrast, in T59E-addback cells, PRC1 still associated with microtubules, but its localization extended over a wider region (2-fold greater distance as indicated by linescans, Figure 3.10C-E, T59E-addback cells). Together, these data show that the proper CPC localization and the spatial organization of its substrate phosphorylation are needed for spindle midzone assembly.

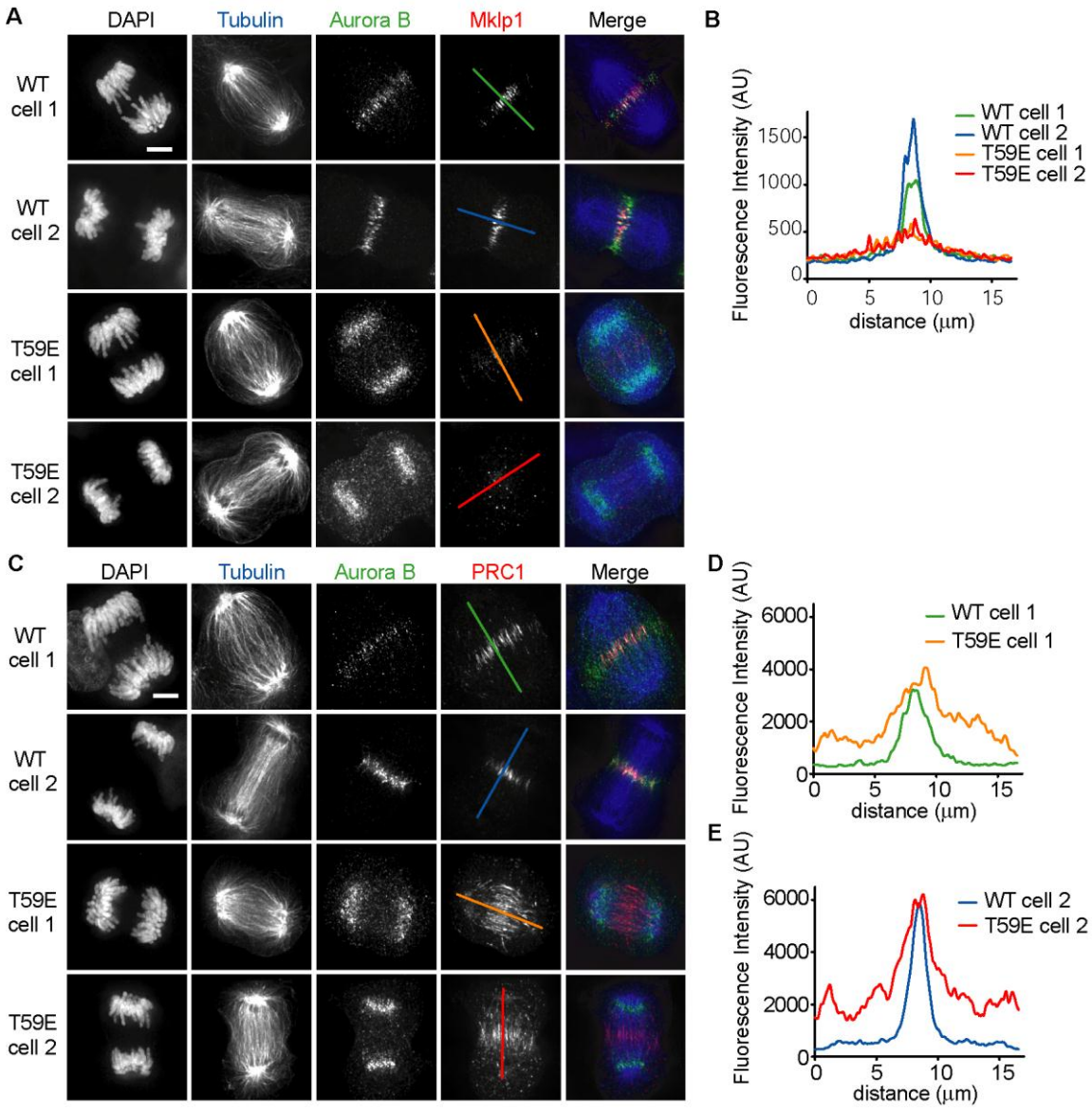

Figure 3.10

Spatially organized CPC activity is needed for proper spindle midzone organization. WT- and T59E-INCENP-addback cells fixed and stained to label chromosomes (DAPI), tubulin (blue), Aurora B (green) and MKLP1 (red, A) or PRC1 (red, C). (B, D-E) Overlaid intensity linescans were generated using lines indicated in the images in (A and C). Scale bars, 5 μm.

I next examined if there are functional consequences of the spindle midzone disruption that I observed in cells lacking spatially organized Aurora signaling. Consistent with redundant signals from the spindle midzone and astral microtubules regulating cleavage furrow formation (Eggert et al., 2006), live cell imaging of the T59E-addback cells revealed no overt defects in either positioning or ingression of the cleavage furrow (Figure 3.11). Therefore, I needed to separate spindle midzone and astral microtubule signaling. To this end, I used a drug-synchronized monopolar cytokinesis assay (Hu et al., 2008). In this assay, astral microtubule distribution is initially symmetric, followed by formation of a monopolar midzone at one end of the cell, where a cleavage furrow ingresses (Figure 3.12A). In T59E-addback cells, Aurora kinase remained at chromosomal sites during anaphase (Figure 3.12B) and an Aurora-substrate phosphorylation gradient could not be detected (Figure 3.12C,D), while overall substrate phosphorylation levels were maintained (Figure 3.12D). Furthermore, consistent with the experiments analyzing bipolar cytokinesis, a properly organized midzone was not observed, and MKLP1 failed to localize to the microtubules (Figure 3.12E). Moreover, the GTPase RhoA (a key regulator of contractile activity needed for cleavage furrow

ingression (Eggert et al., 2006)), which localized at the site of cleavage in WT-addback cells undergoing monopolar cytokinesis (Figure 3.12F, upper panels, (Hu et al., 2008)), remained symmetrically distributed at the cell cortex in >90% of the T59E-addback cells (n>50 cells; Figure 3.12G,H). Importantly, cleavage furrow ingression was also inhibited in these cells (Figure 3.12H). These data suggest that an organized spindle midzone is needed for proper RhoA localization and cleavage furrow formation in monopolar cytokinesis.

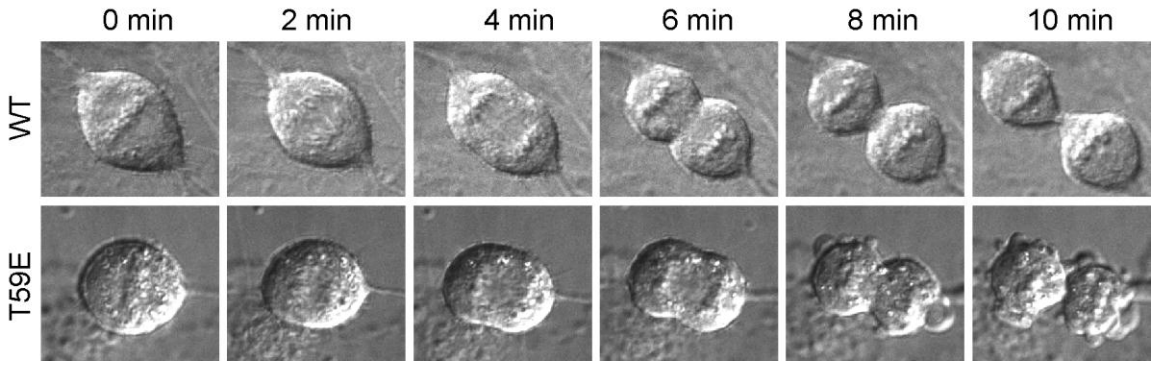

Figure 3.11

Cleavage furrow ingression in WT and T59E-addback cells imaged through anaphase. DIC images are shown. Scale bar, 5 μm.

Figure 3.12

Spatially organized Aurora activity is needed for spindle midzone formation, clustering RhoA and cleavage during monopolar cytokinesis. (A) A schematic showing bipolar and monopolar cells undergoing mitotic exit. Chromosomes, blue; microtubules, green; RhoA, red; CPC, orange dot. (B) WT- and T59E-INCENP-addback cells undergoing monopolar cytokinesis were fixed and stained for chromosomes (DAPI, blue), tubulin (green), Aurora B (red) and mCherry-INCENP. Scale bar, 5 μm. (C-D) WT- and T59E-INCENP-addback cells expressing the microtubule-targeted sensor were induced to undergo monopolar cytokinesis. DIC, mCherry-INCENP, YFP and emission ratio images are shown (C). Scale bar, 5 μm. Overlaid linescan projections along the monopolar cell's long axis (D). Error bars, SD. (E-H) WT- and T59E-INCENP-addback cells undergoing monopolar cytokinesis fixed and analyzed as indicated. (E) Chromosomes (DAPI), tubulin (green), Aurora B (blue) and MKLP1 (red) are shown. Scale bar, 5 μm. (F-G) Chromosomes (DAPI, blue), tubulin (green) and RhoA (red) are shown (F,H). Percent cells ($n \geq 600$) with polarized RhoA localization versus time after mitotic exit is triggered (G). Error bars, SEM. Scale bar, 5 μm in (F) and 10 μm in (H).

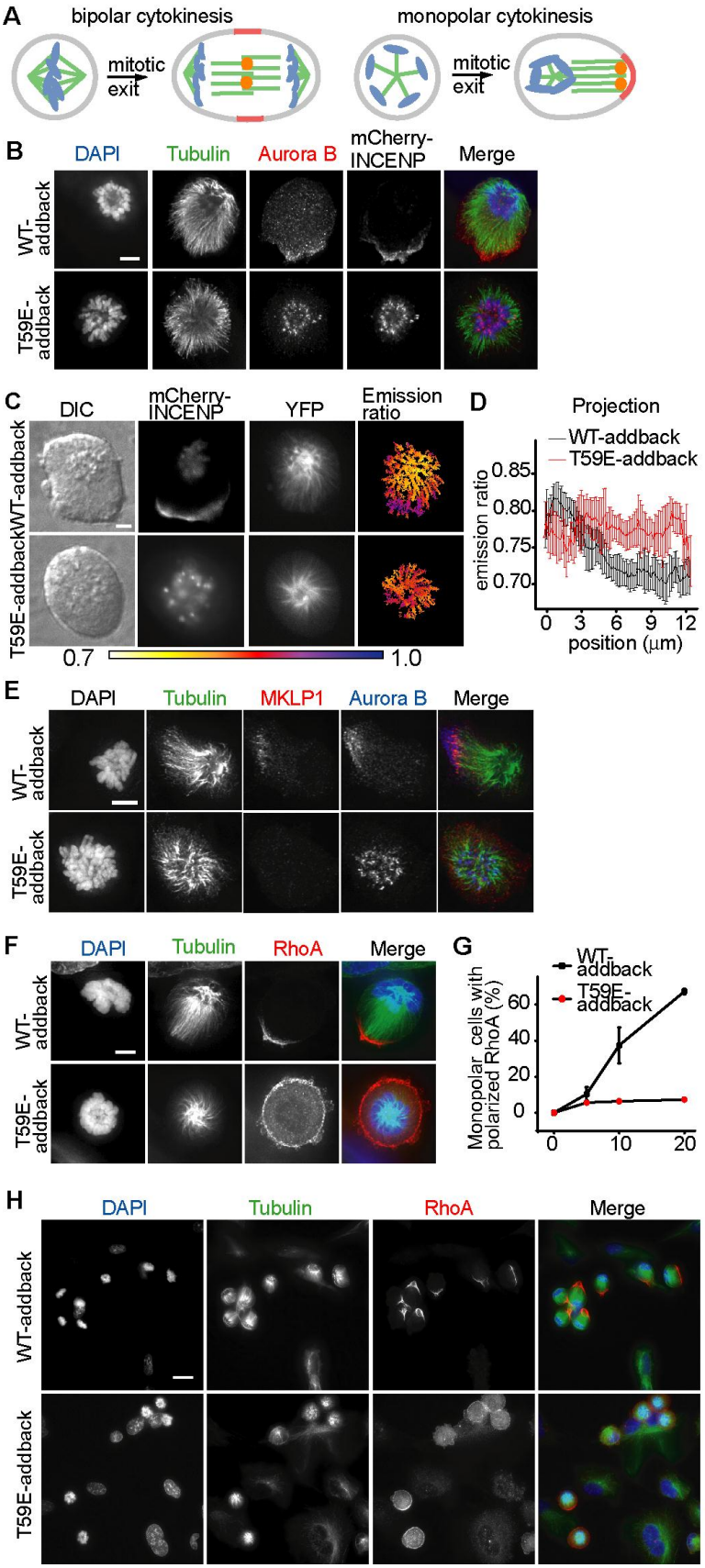
A
bipolar cytokinesis
mitotic exit
monopolar cytokinesis
mitotic exit
B
DAPI
Tubulin
Aurora B
mCherry-INCENP
Merge
WT-addback
T59E-addback
C
DIC
mCherry-INCENP
YFP
Emission ratio
WT-addback
T59E-addback
0.7
1.0
D
Projection
WT-addback
T59E-addback
emission ratio
0.85
0.80
0.75
0.70
0
3
6
9
12
position (μm)
E
DAPI
Tubulin
MKLP1
Aurora B
Merge
WT-addback
T59E-addback
F
DAPI
Tubulin
RhoA
Merge
WT-addback
T59E-addback
G
WT-addback
T59E-addback
Monopolar cells with polarized RhoA (%)
60
40
20
0
0
10
20
H
DAPI
Tubulin
RhoA
Merge
WT-addback
T59E-addback

I next analyzed if the cortical recruitment of RhoA also depended on a properly organized spindle midzone during bipolar cytokinesis. As cleavage furrow ingression was not blocked in T59E-addback cells, it was unlikely that RhoA failed to target. However, it was possible that the dynamics of RhoA recruitment could be sensitive to the loss of the Aurora-substrate phosphorylation gradient. Quantitative analysis of the cortical signals for fluorophore-tagged human RhoA in live cells is limited by high cytosolic background (Roberts et al., 2008). Therefore, I used GFP-tagged anillin, which is a scaffold protein linking RhoA to actomyosin at the cortex (Piekny and Glotzer, 2008), as an alternative reporter for cleavage furrow assembly. As expected, GFP-anillin distributed symmetrically in metaphase cells and, within a few minutes after anaphase, concentrated to the site of cell cleavage (Figure 3.13A, upper panels). In contrast, GFP-anillin accumulated at the cortex in T59E-addback cells, but its levels were reduced (Figure 3.13A, lower panels) and the recruitment kinetics were slower (~1.7-fold, n>10 cells, Figure 3.13B). These data suggest that proper midzone organization is needed for the efficient assembly of the cleavage furrow in bipolar cytokinesis.

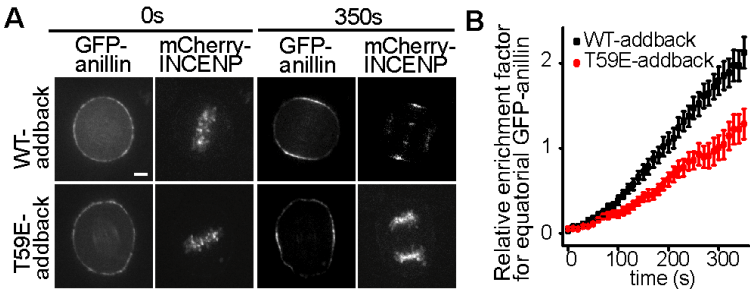

Figure 3.13

Spatially organized CPC activity is needed for efficient anillin recruitment to the equatorial cortex during bipolar cytokinesis. GFP-anillin and mCherry-INCENP images at anaphase onset (0 s) and 350 s post-anaphase onset are shown (A). Relative enrichment of GFP-anillin at the equatorial cortex versus time for WT- (n = 15) and T59E- (n = 12) addback cells (B). Error bars, SEM. Scale bar, 5 μm.

3.6 Other attempts to disrupt the gradient and examine its function

3.6.1 Other attempts to disrupt the gradient

In addition to experiments based on INCENP RNAi with T59E-mutant addback, I tried three different approaches to alter the shape of the gradient. These approaches were not successful for various reasons.

First, I transiently expressed a chimeric construct of Aurora B-mCherry-H2B into HeLa cells to mislocalize Aurora B to the chromosomes. In these cells, I observed chromosome segregation defects (Figure 3.14), the severity of these defects correlate with mCherry fluorescence signal. This suggests that Aurora B-mCherry-H2B is likely perturbing mitosis prior to anaphase onset. Consistent with this, I co-expressed the chromosome-targeted CPC sensor with Aurora B-mCherry-H2B. Live cell imaging of the sensor showed that the CFP:YFP emission ratio measured in these cells is higher than in normal cells, both during metaphase and anaphase (~20% higher at metaphase). This suggests that CPC substrates are hyper-phosphorylated upon Aurora B-mCherry-H2B expression. Although this perturbation altered the shape of the gradient (Figure 3.14B), it also likely affects processes prior to anaphase, as a result of CPC substrate hyper-phosphorylation. Therefore, any anaphase

defect could be due to errors at metaphase and this approach is not suitable to examine the phenotype associated with gradient perturbation.

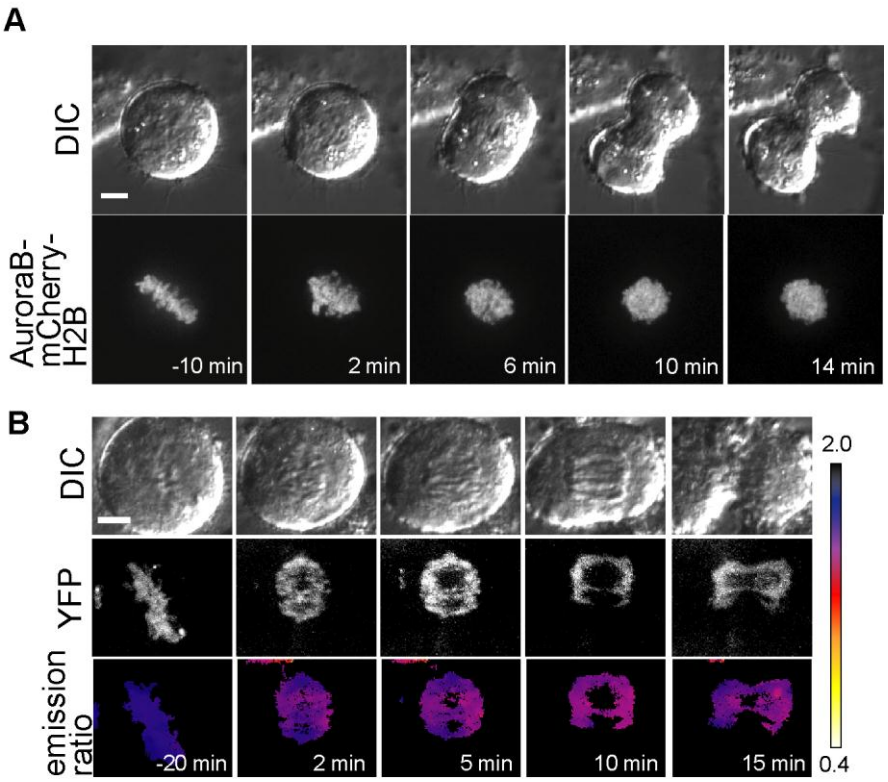

Figure 3.14 Expression of Aurora B-mCherry-H2B in HeLa cells perturbs the anaphase gradient and chromosome segregation, but also leads to sensor hyper-phosphorylation prior to anaphase. (A) A HeLa cell expressing Aurora B-mCherry-H2B was imaged through anaphase. (B) A HeLa cell co-expressing Aurora B-mCherry-H2B and the chromosome-targeted FRET sensor for CPC was imaged through anaphase. Time zero is anaphase onset. Scale bars, 5 μm.

Second, I used a small molecule Rapamycin-mediated FKBP-FRB dimerization system, aiming to trigger

mislocalization of Aurora B after anaphase onset. FKBP and FRB are well-folded domains that can form heterodimers upon addition of Rapamycin. To optimize this system towards fast kinetics to match the timescale of anaphase (~8 min), I used a non-chromosome binding protein ppp2R5B as a model protein. I found that co-expression of H2B-mCherry-FRB and FKBP-GFP-ppp2R5B with addition of 20 nM Rapamycin has the fastest kinetics of recruiting target proteins to chromosomes (Figure 3.15A, B). I applied this configuration to my system and co-expressed H2B-mCherry-FRB and FKBP-GFP-Aurora B in HeLa cells. I first added Rapamycin to cells before anaphase onset and found that GFP fluorescence signal gets recruited to the chromosomes within minutes (Figure 3.15D). This relocalization depends on Rapamycin, as DMSO addition does not change GFP localization (Figure 3.15C). In these Aurora B mistargeted cells, I observed phenotypes of chromosome mis-segregation with occasional cleavage furrow misplacement (Figure 3.15C,D), similar to the phenotype of the Aurora B-mCherry-H2B transient expression. The shape of the gradient is perturbed in these cells as well (Figure 3.15E,F).

Figure 3.15

Rapamycin-induced dimerization system to mis-target CPC. (A) A cell expressing FKBP-GFP-ppp2R5B and H2B-mCherry-FRB with Rapamycin addition. (B) Time course for relocalization kinetics for cells with Rapamycin addition (time zero represents drug addition). (C,D) Time course for HeLa cells co-expressing FKBP-GFP-Aurora B and H2B-mCherry-FRB after addition of DMSO (C) or Rapamycin (D) (time zero). The cleavage furrow, marked by a pair of red arrows, does not ingress in the middle of separating chromosomes, accompanied by chromosome mis-segregation. (E,F) Cells expressing chromosome-targeted FRET sensor, FKBP-mCherry-Aurora B and H2B-FRB were treated with DMSO (E) or Rapamycin (F).

Figure 3.15

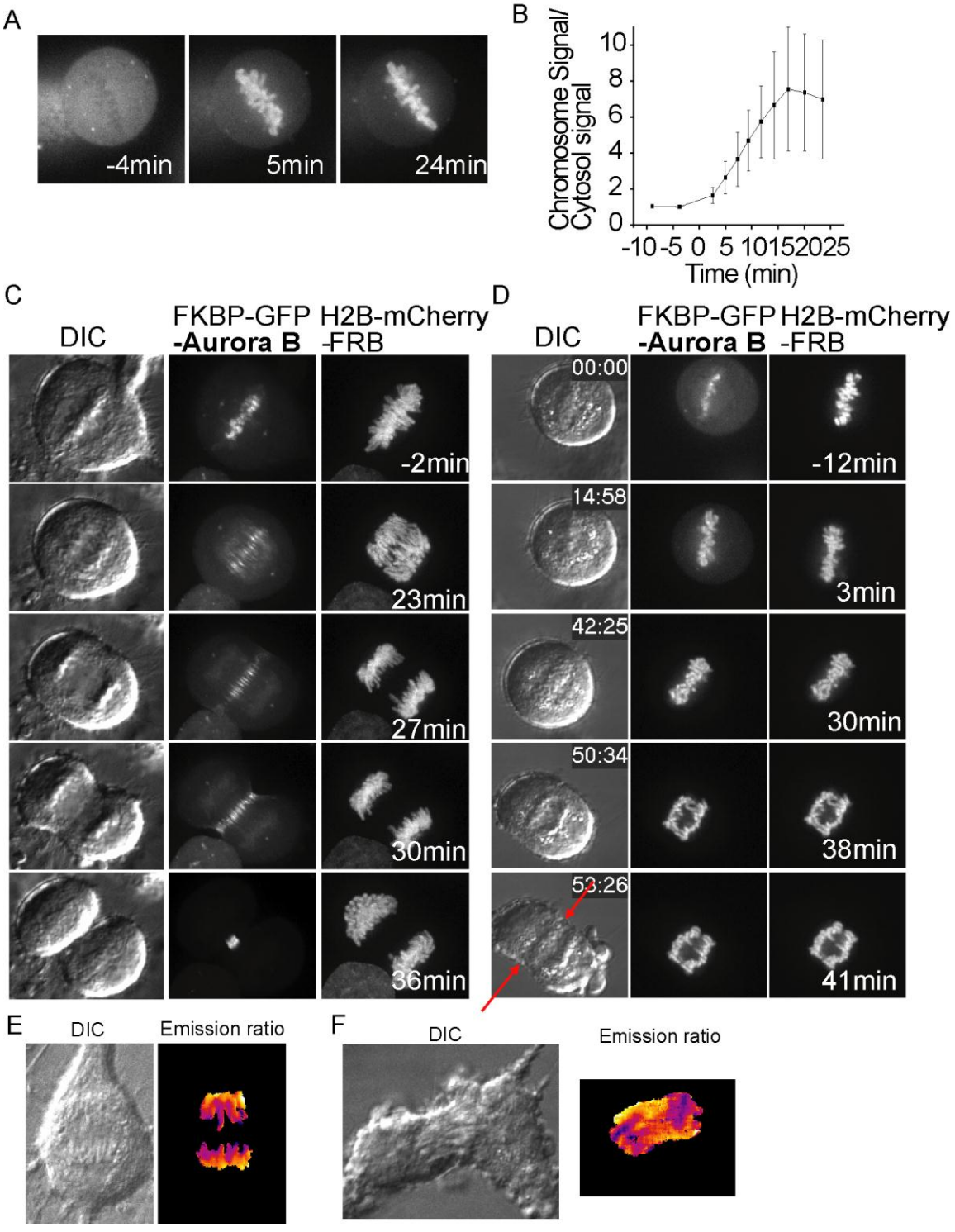
A
-4min
5min
24min
B
Chromosome Signal/
Cytosol signal
10
8
6
4
2
0
-10 -5 0 5 10 15 20 25
Time (min)
C
DIC
FKBP-GFP
-Aurora B
H2B-mCherry
-FRB
-2min
23min
27min
30min
36min
D
DIC
FKBP-GFP
-Aurora B
H2B-mCherry
-FRB
00:00
-12min
14:58
3min
42:25
30min
50:34
38min
53:26
41min
E
DIC
Emission ratio
F
DIC
Emission ratio

To induce mislocalization only at anaphase, I added Rapamycin post anaphase onset. Surprisingly, the efficiency of Aurora B mislocalization to chromosomes dropped dramatically (Figure 3.16). A significant amount of FKBP-GFP-Aurora B still localizes to the spindle midzone (Figure 2.16A). It is likely that the endogenous pathway that recruits Aurora B to the spindle midzone at anaphase is so efficient that the Rapamycin-induced dimerization could not compete with it. I tried to improve the mis-localization efficiency by raising the concentration of Rapamycin from 20 nM to 2 μM, but I found that a significant amount of FKBP-GFP-Aurora B still localizes to the spindle midzone. Due to this limited mislocalization efficiency post anaphase onset, I did not further pursue this approach. I have, however, shown that for multiple proteins dimerization-induced mislocalization works well during metaphase. As many protein localizations are key to their function in mitosis, this dimerization system will potentially be useful for other studies.

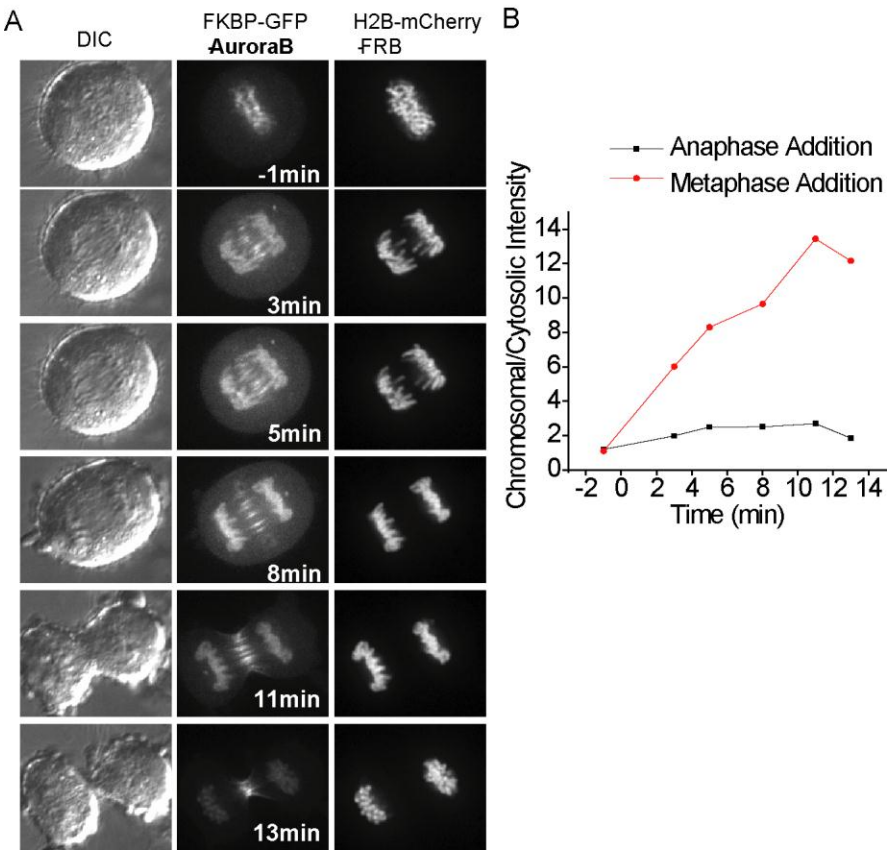

Figure 3.16 Rapamycin addition after anaphase onset fails to efficiently recruit Aurora B to the chromosomes. (A) Cells expressing FKBP-GFP-Aurora B and H2B-mCherry-FRB with Rapamycin added after anaphase onset. (B) Quantification of the amount of Aurora B mis-targeted to chromosomes for both metaphase and anaphase Rapamycin addition.

Third, I attempted to disrupt the shape of the CPC-substrate phosphorylation gradient with knockdown of PRC1 levels through RNAi. PRC1 is a microtubule crosslinking protein required for spindle midzone assembly (Mollinari et al., 2002). Imaging of the microtubule-targeted FRET sensor showed that, in most cells, the phosphorylation gradient

becomes shallower upon PRC1 RNAi, but the basic shape is retained (Figure 3.17). Especially at telophase, the gradient shape became very evident (Figure 3.17). Therefore, PRC1 RNAi is not an ideal approach to study perturbation of the gradient, as it could not completely alter its shape.

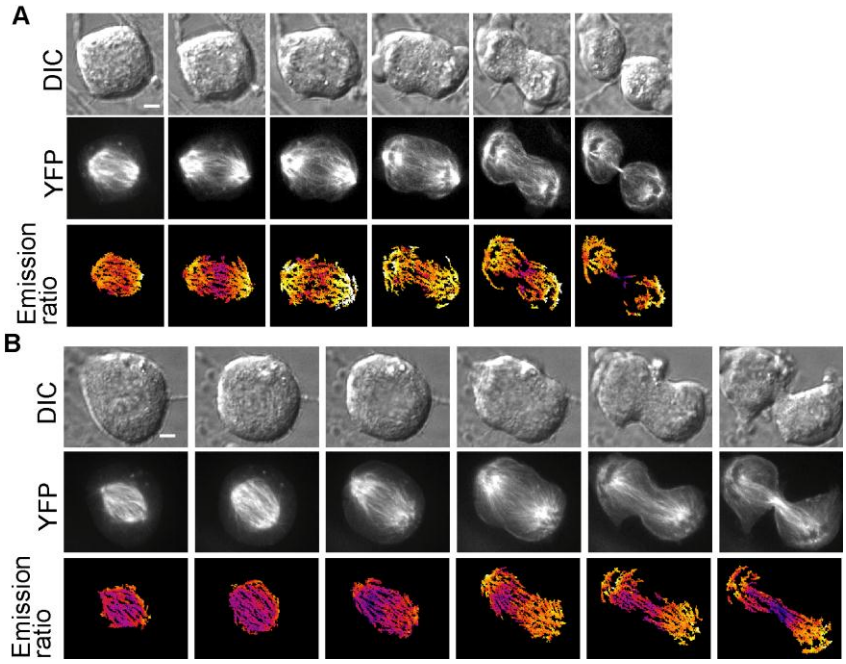

Figure 3.17 PRC1 RNAi does not completely abolish the CPC-substrate phosphorylation gradient. Two cells expressing the microtubule-targeted FRET sensor were treated with PRC1 RNAi and imaged live. Images were taken every 2 min. Scale bars, 5 μm.

In conclusion, these perturbations turned out to be not as ideal as the INCENP RNAi-addback for studying perturbation of the CPC-substrate phosphorylation gradient. Therefore I didn't pursue these approaches further.

3.6.2 Other attempts to examine the role of the gradient

To test whether the CPC phosphorylation gradient contributes to transmitting cleavage signals from the spindle midzone to the cell cortex, which occurs over micron distances, I developed a cell-pushing assay. In sea urchin eggs, a displacement of the spindle midzone from the cleavage furrow triggers the cleavage furrow to re-position itself to where the spindle midzone is (Bement et al., 2005). If the CPC-substrate phosphorylation gradient is crucial for signal transmission from the spindle midzone to the cell cortex, I hypothesized that perturbation of the gradient might inhibit repositioning after physical spindle displacement. With the help of Dr. Yuta Shimamoto in the Kapoor lab, I set up a micromanipulation device, with a glass needle controlled by a piezo actuator (Figure 3.18A). To clearly measure the physical displacement of the spindle midzone compared with the cleavage furrow, I co-expressed GFP-PRC1, to label the midzone, and GFP-Anillin, to label the cleavage furrow (Figure 3.18B). Similar to previous findings in sea urchin eggs, in human cells the cleavage furrow position couples with the spindle midzone position after the spindle midzone is physically displaced (Figure 3.18B,C). To test the gradients role in this process, I

depleted endogenous INCENP and added back T59E mutant to disrupt the gradient. Preliminary analyses suggest the coupling between the spindle midzone and the cleavage furrow is intact in T59E-INCENP-addback cells (Figure 3.18D).

This negative result could be explained in multiple ways. My finding could simply mean the CPC-substrate gradient is not required for dynamic coupling between the spindle midzone and the cleavage furrow in human cells. Alternatively, there might be technical issues in this assay that limit the interpretation of the results. For example, as the spindle size is large relative to cell size in human somatic cells compared with sea urchin egg cells, it is very difficult to physically displace the midzone relative to the furrow without moving the cell body as a whole or dislodging the entire cell. To partially circumvent this issue, I coated the coverslip with collagen to increase attachments between the cell and the glass surface. Furthermore, during the pushing experiment, I specifically chose cells that were very well spread out, which usually indicates a strong attachment to the coverslip. However, the coupling phenomenon that I observed could still be due to cell movement in response to spindle displacement, instead of signaling from the midzone to the

cleavage furrow. To test this hypothesis, future experiments with actin cytoskeleton inhibition together with spindle displacement are needed.

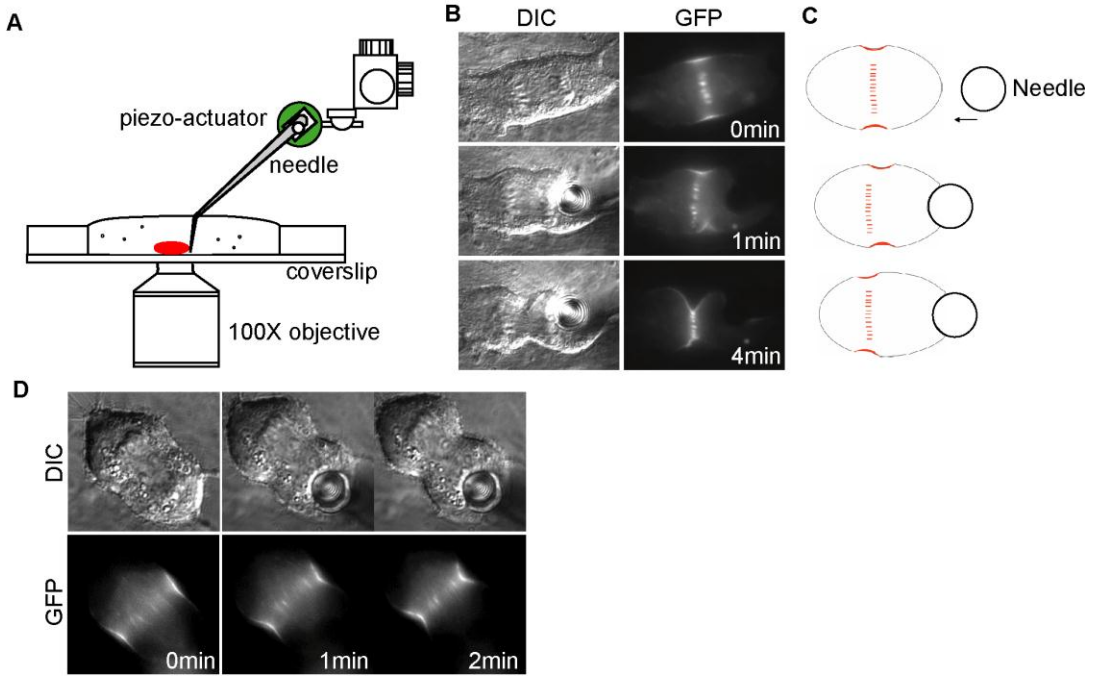

Figure 3.18 A cell pushing assay to examine the dynamic coupling between the spindle midzone and the cleavage furrow. (A) A schematic for the experimental set-up. (B,C) An RPE1 cell co-expressing GFP-PRC1 and GFP-Anillin was imaged live and pushed by a glass needle at anaphase. DIC and GFP images are shown (B). A schematic is shown (C). (D) An RPE1 cell co-expressing GFP-PRC1, GFP-Anillin and mCherry-INCENP T59E mutant was treated with INCENP RNAi, imaged live and pushed by a glass needle.

3.6 Discussion

My findings reveal a CPC substrate phosphorylation gradient early in mitosis with maximal phosphorylation centered between the two spindle poles. This gradient cannot be detected using FRET-based sensors during metaphase, but appears again upon anaphase onset and persists through cell cleavage. These data suggest that the gradient is detected at stages of cell division when the overall CPC-substrate phosphorylation levels are lower than at metaphase, when substrate phosphorylation is highest, most likely due to suppression of overall phosphatase activity (Mochida and Hunt, 2007) and robust CPC activation by chromosomes (Kelly et al., 2007). As partial suppression of substrate phosphorylation at metaphase can reveal a spatial gradient, I propose that increased levels of substrate phosphorylation can mask spatial gradients, while the CPC retains its capacity to generate such gradients.

It has been suggested that formation of intracellular signaling gradients involve the following three components. First, an effector molecule that exists in two states, S and S* (e.g., a motor protein in non-phosphorylated and phosphorylated forms). Second, an enzyme ('source', e.g. kinase) that converts S to S* and binds to a cellular structure (e.g. spindle midzone). Third, another enzyme

('sink', e.g. phosphatase) that converts S* back to S and is localized in the cytoplasm or is bound to another cellular structure. Proximal to where the 'source' is located, S is converted to S*. Diffusion moves S* away, allowing it to interact with the 'sink', which in turn regenerates S. The shape of the S* concentration gradient depends on the kinetics of interconversion between S and S* and on the diffusion coefficient of S*. This framework has been used to explain the Ran gradient (Bastiaens et al., 2006) and can be used to describe my observations relating to the CPC-substrate phosphorylation gradient. I find that the proper localization of the CPC, which is the 'source', is important for establishing the spatial gradient at anaphase. At the spindle midzone, the CPC phosphorylates substrates (generating S*). These substrates diffuse away and are then acted upon by phosphatases. PP1γ, a phosphatase that gets recruited to chromosomes by Repo-Man during anaphase, has been shown to oppose CPC activity during metaphase (Liu et al., 2010) and could be the relevant 'sink' for phosphorylated CPC substrates at anaphase. When the CPC is mislocalized to chromosomes during anaphase, it could be insufficiently separated from the phosphatase and thus no spatial gradient is observed. Further, consistent with the model, which indicates that rates of

interconversion between S and S* are important for establishing a gradient, my findings suggest that the mechanism of kinase activation and recruitment to substrates are critical. Polo-like kinase has similar localization to CPC at anaphase, but no spatial phosphorylation pattern is revealed using FRET-sensors. An explanation for these differences could be that non-linear increases in substrate phosphorylation at sites proximal to the kinase can be established by CPC, whose activation depends on clustering and auto-phosphorylation (Kelly et al., 2007), and not by Polo-like kinase, which is targeted to its substrates via recognition of phospho-peptide docking sites (Barr et al., 2004). Finally, the diffusion of S*, a key parameter for establishing a gradient, needs to be limited through anchoring substrates to intracellular sites, as the gradient is not observed when FRET-sensors diffuse freely in the cytoplasm. Proper tests of the contributions of these different factors will probably require in vitro reconstitution of the phosphorylation gradient with purified components.

Although CPC activity is known to be needed for spindle midzone formation, my results show that defects in spindle midzone and cleavage furrow assembly can be observed when total CPC-substrate phosphorylation levels are unchanged,

but the spatial distribution of these post-translational modifications are altered. While different models can account for this, I favor the model in which the proper localization of CPC at the spindle midzone sets up a gradient that allows threshold levels of phosphorylation to be achieved at specific intracellular sites. At anaphase onset, an initial 'shallow' gradient becomes apparent, which may lead to the highest levels of phosphorylated CPC-substrates, such as MKLP1, at the center of the cell. It has been proposed that CPC-phosphorylation relieves 14-3-3-mediated inhibition of MKLP1 and allows the motor to cluster into multi-protein assemblies that can make sufficiently long-lived associations with microtubules (Douglas et al., 2010; Hutterer et al., 2009). Therefore, local MKLP1 phosphorylation and clustering-dependent persistent filament binding and motility, could lead to a rapid non-linear increase in the levels of active MKLP1 at the center of a dividing cell (Figure 3.19, right panels). In contrast, uniform phosphorylation across the spindle microtubules could result in a distribution of phosphorylated MKLP1 such that the probability of interaction with another phosphorylated MKLP1 would be too low for clustering. As a result, MKLP1 would fail to slide microtubules to properly organize the spindle midzone

(Figure 3.19, left panels). In normal cells, as the spindle midzone gets more focused, possibly by MKLP1-dependent reductions in antiparallel filament overlap (Nislow et al., 1992), the CPC becomes more concentrated at a narrower region, which further sharpens the phosphorylation gradient, as we have observed.

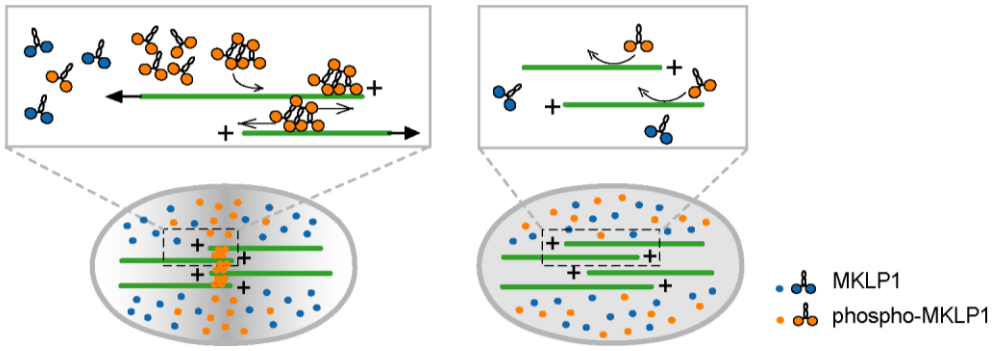

Figure 3.19
A schematic for how the CPC may coordinate spindle midzone organization. Gray shading represents phosphorylation.

It is likely that the contribution of the spatially organized CPC-dependent signaling to the regulation of different cell division processes, such as chromosome condensation, spindle assembly, or the NoCut pathway could vary and depend on the substrates' distinct phosphorylation kinetics, localization, and diffusion. For example, Op18, a cytosolic substrate for CPC (Kelly et al., 2007), and a microtubule destabilizer, is likely to function properly during anaphase without a CPC-dependent phosphorylation gradient (i.e. phosphorylation alone may be sufficient for

its proper function and spatially organized post-translational modifications may not be needed). This could potentially explain my observation that the microtubule density is not dramatically altered in the anaphase spindle upon CPC mislocalization, while the midzone microtubule organization is affected. Interestingly, previous studies have suggested that a gradient of inactivated Op18 around mitotic chromosomes contributes to metaphase spindle assembly (Niethammer et al., 2004). It will be important to examine whether Op18 phosphorylation, which modulates its binding to tubulin, is also spatially organized during anaphase and if this organization is sensitive to CPC localization.

My results suggest how a kinase may establish an intracellular spatial gradient of post-translational marks to control cytoskeleton self-organization during the final stages of cell division. Although I believe that the shape of the gradient is needed for proper microtubule organization at the spindle midzone, my experiments do not distinguish the function of the shape of the gradient from that of the CPC localization itself, and from protein concentration. Future studies on phenotypes associated with altering the shape of the gradient with high level of substrate phosphorylation all across the cell would help

address the problem. Further in vitro reconstitution experiments discussed in Chapter 5 would also shed new light on separating functional contributions from system components.

CHAPTER 4: Efforts towards examining PRC1's role in cytokinesis

4.1 Background information

Proper microtubule organization is required for error-free cell division. During anaphase when chromosomes are separated to the two cell ends, the mitotic spindle reorganizes to prepare for cytokinesis. There are two major changes to the mitotic spindle during anaphase. First, the two spindle poles move further away from each other and the spindle elongates. This anaphase spindle elongation has been shown to contribute to correcting merotelic attachment (Courtheoux et al., 2009) and positioning the cleavage furrow (Dechant and Glotzer, 2003). Second, an antiparallel microtubule array that are bundled at their overlapping plus ends, forms between the segregated chromosomes. This microtubule array is termed the spindle midzone. Previous studies have shown that the spindle midzone is needed for successful cytokinesis (Eggert et al., 2006).

The formation of the spindle midzone depends on a widely conserved microtubule cross-linking protein, PRC1 (protein required for cytokinesis 1) (Jiang et al., 1998). Without PRC1, the spindle midzone, an antiparallel microtubule array in the mid-cell at anaphase, could not

form properly (Mollinari et al., 2002). In these cells, multinucleation is observed, likely due to failed cytokinesis. In other organisms, PRC1 homologs are also involved in processes that depend on microtubule organization, such as cell shape determination in fission yeast, and directional cellular growth in plants (Hamada, 2007; Loïodice et al., 2005).

Previously it has been shown that PRC1 organizes the spindle midzone by crosslinking antiparallel microtubules (Bieling et al., 2010; Subramanian et al., 2010). Besides PRC1's mechanical role, it has also been found to interact with other proteins such as kinesin motor KIF4A, which controls overlap size by overlap length-dependent microtubule growth inhibition (Bieling et al., 2010; Hu et al., 2011). However, currently the PRC1-depletion phenotype has not yet been carefully examined using live cell imaging.

In this chapter, I describe three parts of work examining PRC1's role by live cell imaging: 1) Detailed characterization of spindle and cell morphology of PRC1-depletion phenotype. 2) Analysis of microtubule dynamics by quantitative tracking of GFP-EB1 in PRC1-depleted cells. 3) Analysis of a chimeric PRC1 mutant that still binds microtubules but could not organize microtubules. Unfortunately I find that microtubule dynamics measured by

tracking EB1-GFP do not change significantly upon PRC1 depletion, and the chimeric PRC1 mutant does not seem to bundle microtubules in cells. Therefore most of this chapter is descriptive and there is not a single clear conclusion that could be drawn based on this body of work to shed new light on mechanism of PRC1 function. But I hope these data would generate some hypotheses to motivate interesting future experiments discussed in Chapter 5 Future directions.

4.2 Cell and Spindle morphology in PRC1-depleted cells

4.2.1 PRC1 depletion by RNAi

I depleted PRC1 by RNAi in hTERT-RPE1 cells (Jiang et al., 1998) (Figure 4.1A). Consistent with previous findings (Zhu et al., 2006), immunofluorescence against tubulin shows that organized microtubule bundles cannot form at the spindle midzone upon PRC1 RNAi (Figure 4.1B). I also observed that multinucleated cell index increases from less than 1% to over 30% (Figure 4.1C), indicating failure in cytokinesis. These data confirms that PRC1 knockdown efficiently disrupt the spindle midzone.

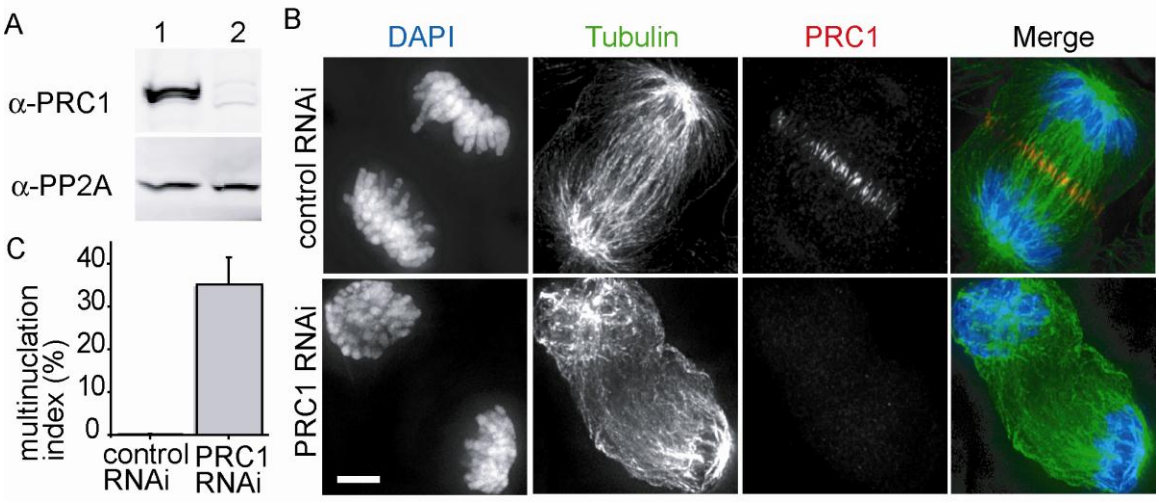

Figure 4.1

PRC1 depletion in RPE1 cells disrupts microtubule bundle formation at the spindle midzone. (A) A representative western blot is shown for control (Lane 1) and PRC1 RNAi (Lane 2) cell lysates. (B) Control and PRC1 RNAi cells were fixed and stained for DNA, tubulin and PRC1. Scale bar, 5μm. (C) Control and PRC1 RNAi cells were fixed and stained for DNA and tubulin. Multinucleated and single nucleated cells were counted to determine the multinucleation index in three independent experiments (N > 500 cells in each experiment).

4.2.2 PRC1 depletion leads to abnormal anaphase cell and spindle elongation

To examine the phenotype associated with PRC1 depletion, I imaged live cells expressing GFP-tubulin upon control or PRC1 RNAi(Figure 4.2). GFP-tubulin images confirmed that the spindle midzone is disrupted in PRC1-depleted cells (Figure 4.2). Furthermore, I also observed

that cells depleted of PRC1 tended to elongate to a greater extent at anaphase (Figure 4.2).

Next I quantified the anaphase cell length over time for both control and PRC1 RNAi cells, and found that PRC1 depleted cells elongate at similar rates as the control cells (Figure 4.3A,B). However, while control cells elongated more slowly 10 minutes post anaphase onset, PRC1 depleted cells tended to continue elongating at a similar rate beyond the 10 minute timepoint (Figure 4.3A,B). These data suggest that unlike fission yeast, spindle midzone in human cells is not essential for anaphase spindle elongation. Instead, the spindle midzone seems to prevent the anaphase spindle from abnormal elongation.

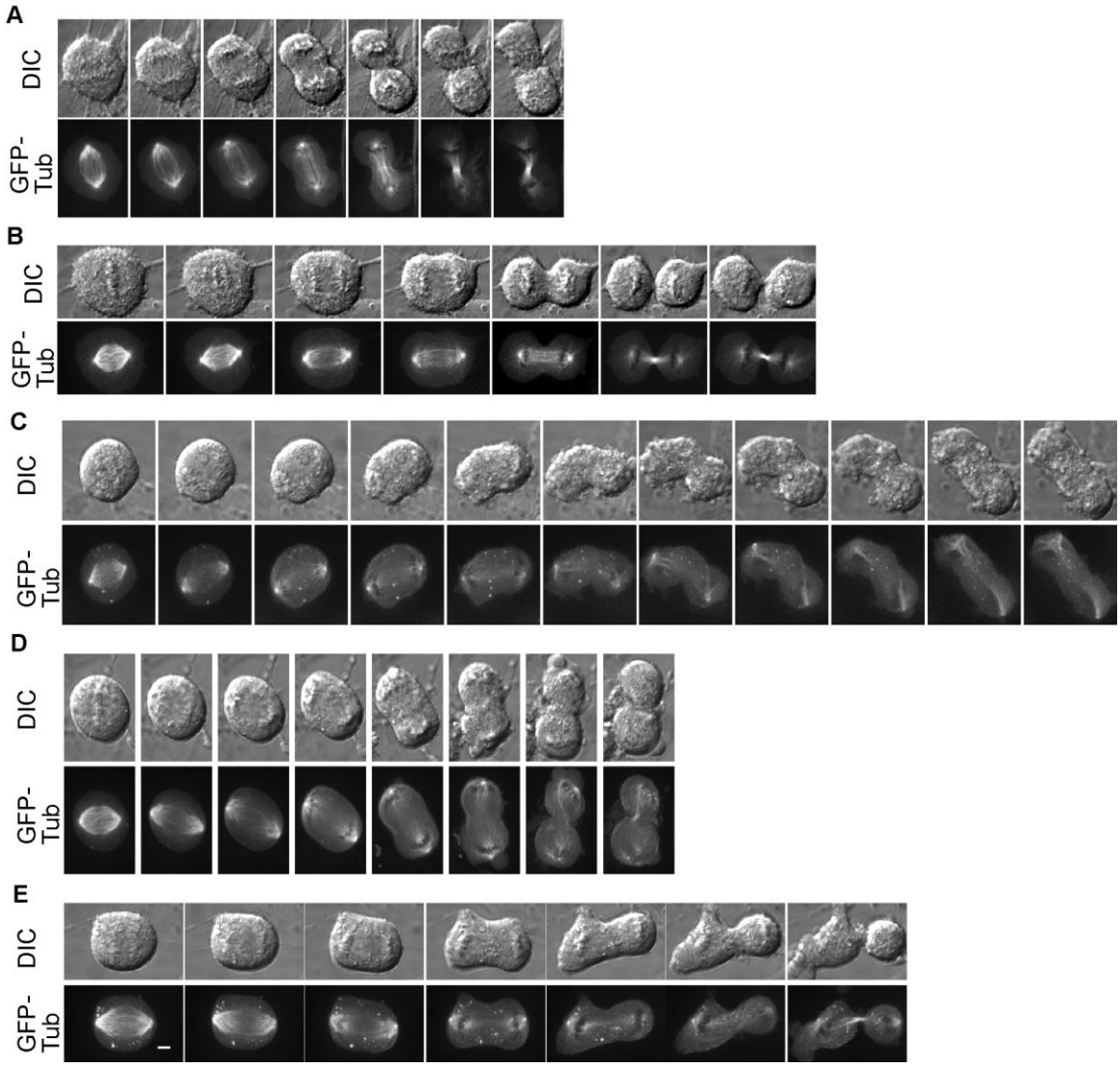

Figure 4.2

PRC1 depletion disrupts microtubule bundle formation at the spindle midzone. Control (A,B) and PRC1 RNAi (C-E) cells expressing GFP-tubulin were imaged live. DIC and GFP-tubulin images were acquired every 2 min. Scale bars, 5μm.

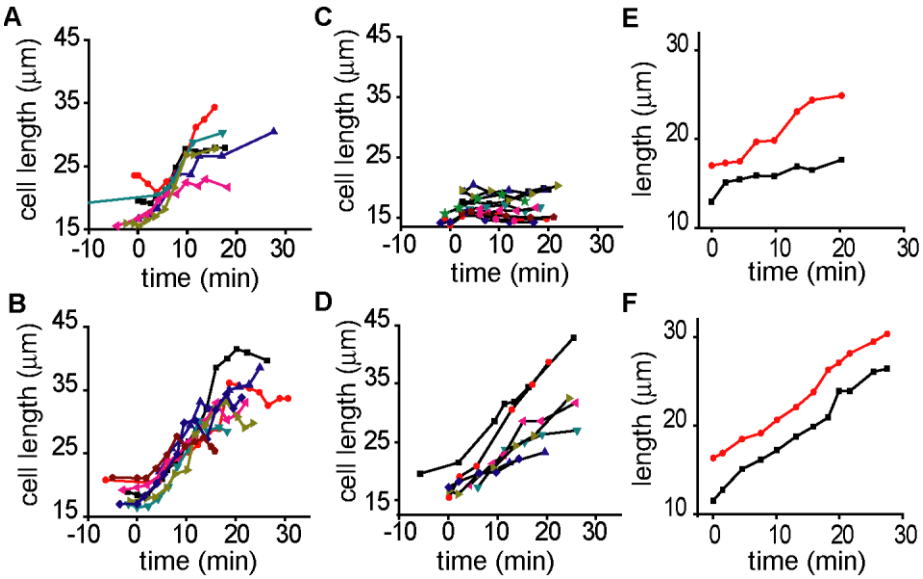

Figure 4.3

PRC1 depletion leads to anaphase cell abnormal elongation. (A,B) RPE1 cells treated with control (A) or PRC1 (B) RNAi were imaged live. Cell lengths were measured in DIC images over time. (C,D) RPE1 cells treated with control (C) or PRC1 (D) RNAi were imaged live, in the presence of Latrunculin B (20 μm). Cell lengths were measured in DIC images over time. (E,F) RPE1 cells expressing GFP-tubulin were treated with control (E) or PRC1 (F) RNAi and imaged live. Cell lengths (red) and spindle lengths (black) were measured in DIC and GFP-tubulin images over time. Time zero corresponds to anaphase onset.

4.2.3 The abnormal cell and spindle elongation in PRC1 depleted cells depend on microtubules

The abnormal elongation in PRC1 depleted cells is possibly due to unbalanced force within the spindle. As the actin cytoskeleton and microtubule networks are known

force-generating components, I tested their role in the observed abnormal elongation in PRC1-depleted cells. As expected, inhibition of actin filament formation by Latrunculin B (20 μM) blocks the cleavage furrow ingression in both control and PRC1 depleted cells (Figure 4.4A,B). It also completely suppressed cell elongation in control cells (Figure 4.3A,C). However, Latrunculin B addition did not suppress cell elongation in PRC1 depleted cells (Figure 4.3D, 4.4B), indicating that the actin cytoskeleton does not provide the forces required for this process. In contrast, inhibition of microtubule formation by Nocodazole (10 μM) blocks cell elongation and cleavage furrow ingression in both control and PRC1 depleted cells (Figure 4.4C,D). This indicates that abnormal elongation in PRC1 depleted cells depends on microtubule-based processes, but not on the actin cytoskeleton. To further test the idea that microtubules are driving the abnormal elongation, I examined the correlation between spindle length (pole-to-pole distance) and cell length over time for a single cell. In control cells, spindle elongation is nearly complete within the first 5 min post anaphase onset (Figure 4.2A, B, 4.3E). This is followed by significant cell elongation, which starts 5 min post anaphase onset (Figure 4.2A, B, 4.3E). However, in PRC1 depleted cells, the cell length

abnormal elongation correlates with the spindle abnormal elongation (Figure 4.2 C,D, 4.3F). These data suggest that in PRC1-depleted cells, the abnormal elongation depends on microtubule-based processes, likely antiparallel microtubule sliding by microtubule motors.

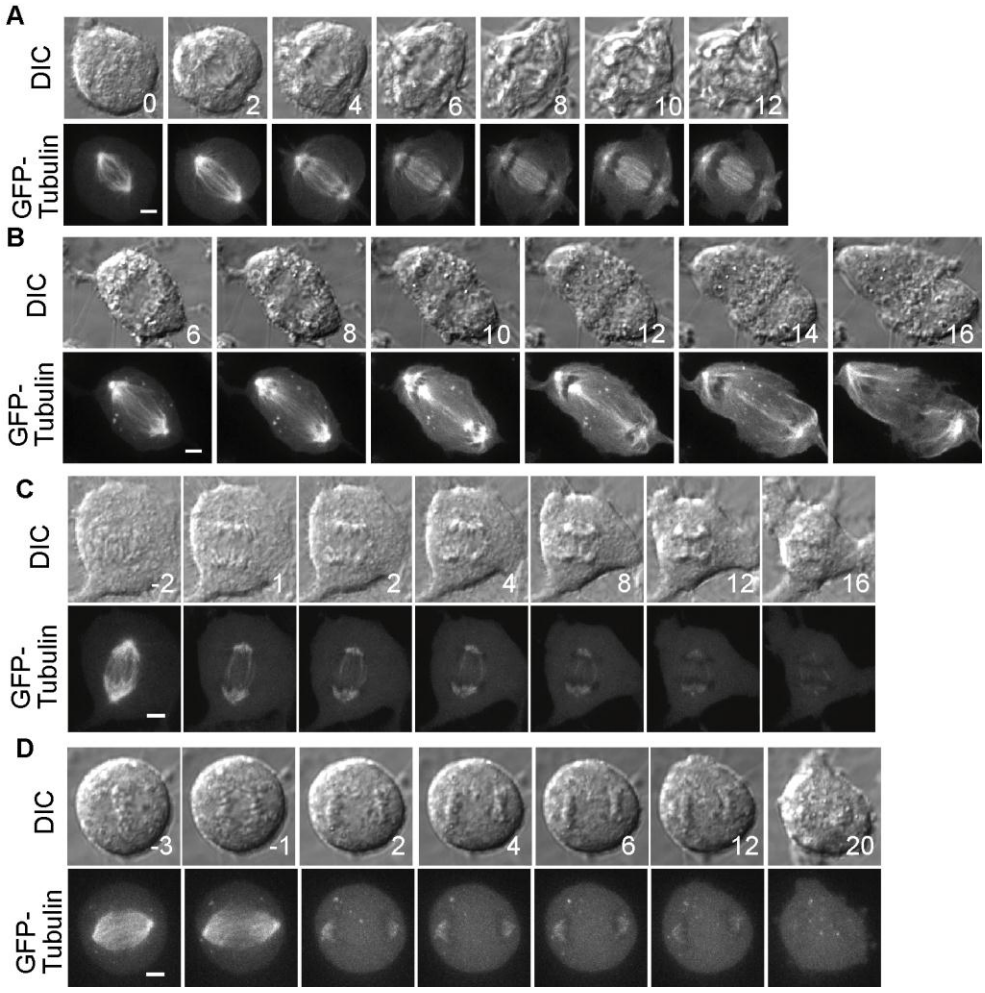

Figure 4.4

Abnormal elongation in PRC1 depleted cells depends on microtubules, but not actin. RPE1 cells expressing GFP-tubulin were treated with control (A,C) or PRC1 (B,D) RNAi. Latrunculin B (20 μM, A, B) or Nocodazole (10 μM, C, D) were

added at anaphase. Time zero corresponds to the time of adding the drugs. Time mark is in minute. Scale bars, 5μm.

4.3 Examining microtubule dynamics in PRC1-depleted cells

In this second part, I examined microtubule dynamics by quantitative imaging of GFP-tagged EB1, a reporter that binds to the plus ends of growing microtubules (Tirnauer et al., 2002). As cleavage furrow ingression dynamics are different between control and PRC1 cells (Figure 4.2), I blocked cleavage furrow formation by Latrunculin B (20 μM) during these experiments, to minimize influence from furrow ingression. In control cells, a dense distribution of EB1 tracks outlined the shape of the anaphase spindle and astral microtubules (Figure 4.5A). Upon PRC1 depletion, EB1 tracks appeared to be more randomly distributed in the cell (Figure 4.5A), consistent with the previous observation that microtubules are not properly organized in PRC1 knockdown cells. According to a current model which suggests that microtubule plus-end polymerization is inhibited by PRC1 binding partner KIF4A at the spindle midzone (Bieling et al., 2010; Hu et al., 2011), EB1 tracks should appear to be diminished at the spindle equator. Surprisingly, I did not observe the expected EB1 comet pattern in control cells (Figure 4.5A). Furthermore, though both immunofluorescence and live cell imaging show a region of microtubules at the middle of PRC1-depleted cells, the density of EB1 tracks at the spindle equator in PRC1

knockdown cells is not different from that at other parts of the spindle (Figure 4.5A). Quantification of control and PRC1 knockdown cells revealed similar numbers of tracks detected in unit time (two-tailed T-test, p=0.77), with an average number of 19 tracks/s (N=3 cells, S.D. = 3 tracks/s), and 17 tracks/s in control cells (N=3 cells, S.D. = 3 tracks/s) (Figure 4.6A). The rates of the growing EB1 tracks in PRC1 RNAi cells are slightly higher than those in control cells (13.5 ± 0.6 μm/min in PRC1-depleted cells vs. 11.6 ± 1.1 μm/min in control cells, two-tailed T-test, p=0.13) and the lifetime of the tracks in PRC1 RNAi cells is slightly lower than control (7.2 ± 0.8s in PRC1-depleted cells vs. 8.6 ± 0.6s in control cells), but the differences are not significant (Figure 4.6B, C, two-tailed T-test, p=0.33). Furthermore, there is no discernible difference in EB1 comet run-length between control and PRC1 RNAi cells (1.43 ± 0.05 μm vs. 1.4 ± 0.1 μm, two-tailed T-test, p=0.09, Figure 4.6D). These data show that PRC1 depletion disrupts microtubule bundle formation at the spindle midzone, without significantly altering the dynamics of EB1-bound microtubule plus-ends. These data also suggest that there are microtubules at the mid-cell for motor proteins to slide apart to drive spindle elongation.

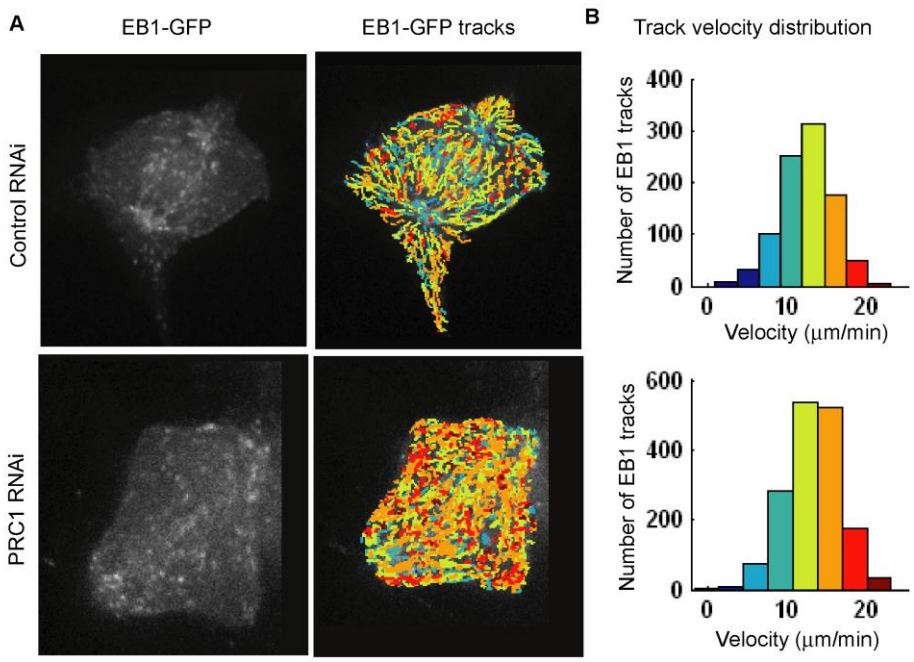

Figure 4.5

The spatial distribution of microtubule polymerization rates is not dramatically altered upon PRC1 depletion. (A) Control and PRC1 RNAi cells expressing GFP-EB1 were imaged live (left panels). EB1 comets from time-lapse sequence were detected and tracked using automated software (Houghtaling et al., 2009). Tracks were colored to reflect velocity, with blue colors being slower than red colors. Colored EB1 tracks were overlaid onto a single frame from the time-lapse (right panels). (B) Histogram of EB1 track velocities detected in control and PRC1 RNAi cells.

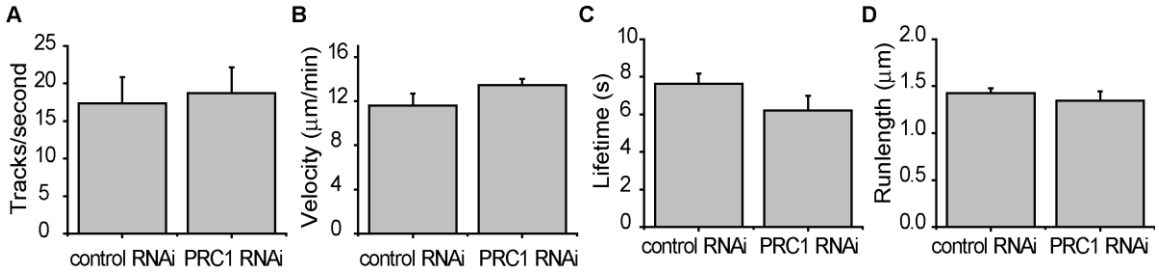

Figure 4.6

The plus-end microtubule tip dynamics are not dramatically altered upon PRC1 depletion. (A) The number of EB1 tracks per second detected in control and PRC1 RNAi cells (N>3 cells). (B) The average velocity of EB1 tracks in control and PRC1 RNAi cells (N>3 cells). (C) The average lifetime of EB1 tracks in control and PRC1 RNAi cells (N>3 cells). (D) The average run-length of EB1 tracks in control and PRC1 RNAi cells (N>3 cells). Error bars, SD.

I then analyzed whether PRC1 knockdown disrupts the distribution of EB1-bound microtubule plus-ends. As no obvious patterns are detected for all of the EB1 tracks in control cells (Figure 4.5), I segmented EB1 tracks based on their growth direction and assigned the same color to tracks moving towards the same spindle pole (Figure 4.7A). This analysis revealed an interesting pattern in control cells: Most of the EB1 tracks growing towards one pole are present at the opposite half of the spindle, from which the microtubules emanate; very few EB1 tracks cross over to the other half of the spindle (Figure 4.7A). The PRC1 RNAi cells have a similar pattern in this analysis. I then

quantified the pattern by comparing the ratio of the number of tracks present at the populated half vs. the unpopulated half of the spindle (Figure 4.7B). The ratio is not significantly different between control and PRC1 RNAi cells (Figure 4.7C), which suggests that PRC1 depletion does not dramatically alter the distribution of EB1-bound microtubule plus-ends.

I next analyzed the microtubule plus-end dynamics at the mid-spindle. EB1 tracks present in a 3 μm area at the midpoint of the two spindle poles are grouped together (Figure 4.8A). Similar to the whole cell analysis, no discernible difference was found for the detected EB1 track number in unit time and the runlength of the tracks (1.9 ± 0.4 tracks/s in control cells vs. 2.1 ± 0.4 tracks/s in PRC1-depleted cells, two-tailed T-test, p=0.63, and 1.5 ± 0.1 μm in control cells vs. 1.4 ± 0.1 μm in PRC1-depleted cells, two-tailed T-test, p=0.12). EB1 tracks in PRC1 RNAi cells have slightly higher growth velocity but shorter lifetime than those in control cells (Figure 4.8, 11.6 ± 0.7 μm/min in control cells vs. 14.1 ± 0.7 μm/min in PRC1-depleted cells, two-tailed T-test, p=0.0003, and 9.1 ± 0.8 s in control cells vs. 7.3 ± 1.0 s in PRC1-depleted cells, two-tailed T-test, p=0.01). These data suggest that PRC1

depletion does not significantly alter dynamics of EB1-bound microtubule plus-ends at the middle of the anaphase spindle.

My results show that PRC1 depletion does not significantly affect the dynamics and distribution of the EB1-bound microtubule plus-ends, though PRC1 is critical for microtubule bundle formation at the spindle midzone. These data also suggest that there are dynamic microtubules at the mid-cell when PRC1 is depleted.

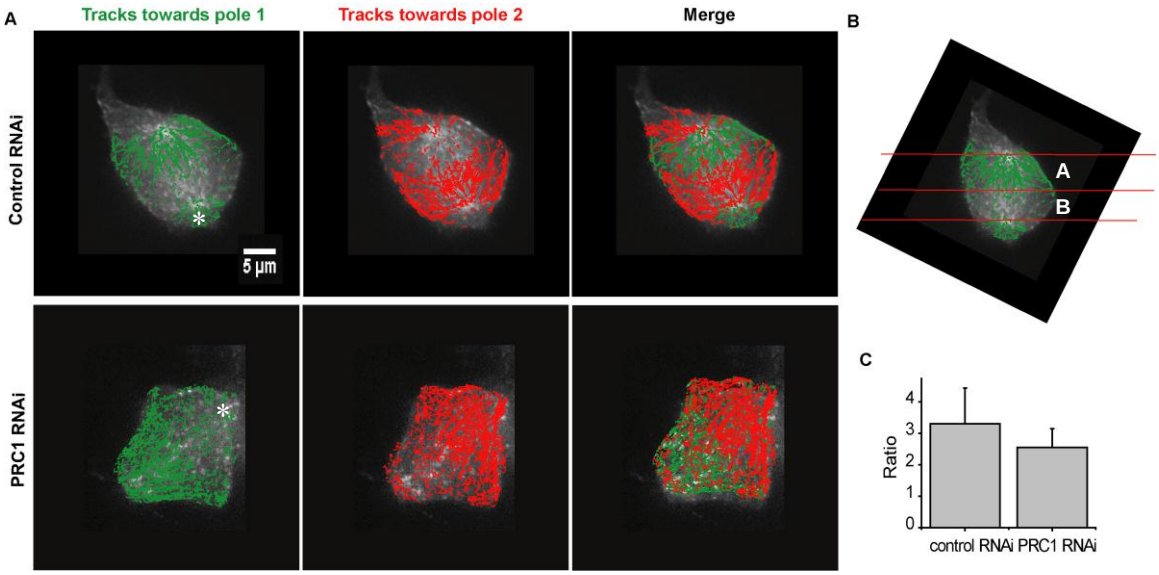

Figure 4.7

The distribution of polymerizing microtubule plus-ends running towards one pole is not significantly altered upon PRC1 depletion. (A) EB1 tracks that are running towards one pole are colored green or red. Colored EB1 tracks were overlaid onto a single frame from the EB1 time-lapse movie. (B) A sample image with EB1 tracks running towards one pole overlaid onto a single frame (pole 1 is labeled with *). Two spindle pole positions were manually identified and a Matlab program was used to generate three red lines perpendicular to the spindle axis. Two red lines crosses spindle poles and the other line lies in the middle of the two poles. Two areas, A and B, are defined as the space between the two adjacent red lines. The area with more EB1 tracks is assigned as A. (C) Average ratio for number of EB1 tracks found in Area A vs. Area B in control and PRC1 RNAi cells (N = 3 cells).

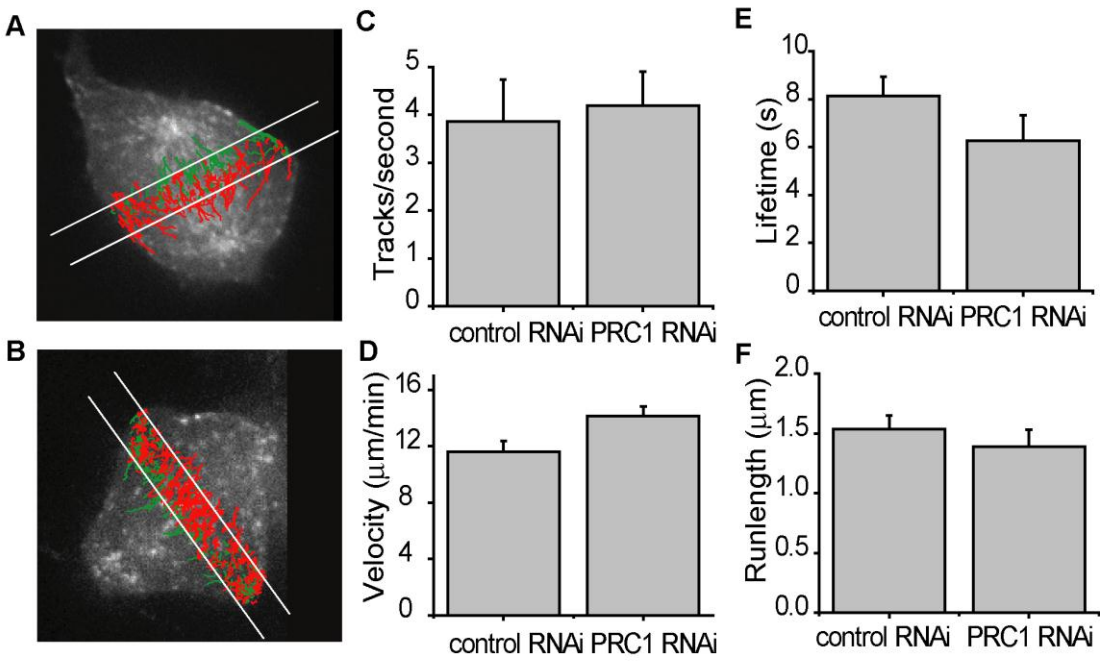

Figure 4.8

The dynamics of polymerizing microtubule plus-ends at the spindle midzone is not significantly altered upon PRC1 depletion. (A,B) The EB1 tracks located within a 3 μm area in the middle of the control (A) or PRC1 RNAi (B) spindle were colored green or red based on their direction and overlaid onto a single frame from the EB1 time-lapse movie. (C) The number of EB1 tracks per second detected in control and PRC1 RNAi spindle midzone (N>3 cells). (D) The average velocity of EB1 tracks in control and PRC1 RNAi spindle midzone (N>3 cells). (E) The average lifetime of EB1 tracks in control and PRC1 RNAi spindle midzone (N>3 cells). (F) The average runlength of EB1 tracks in control and PRC1 RNAi spindle midzone (N>3 cells). Error bars, SD.

4.4 Analysis of a chimeric PRC1 that binds microtubules but does not organize microtubules properly

In this section, I describe experiments analyzing a chimeric PRC1 that binds microtubules but does not organize microtubules properly. I focused on examining the spindle midzone formation and protein recruitment to the mid-cell during anaphase.

I first confirmed that PRC1 depletion by RNAi disrupts spindle midzone formation and localization of three key cytokinesis proteins, Aurora B, MKLP1 and Plk1 (Figure 4.9, 4.10, 4.11) (Kurasawa et al., 2004). In certain telophase cells with PRC1 knockdown, Plk1 localizes at the middle of the cell, but its localization is less pronounced when compared with control cells (Figure 4.11). These data show that PRC1 is required for recruiting these key regulators to the mid-cell.

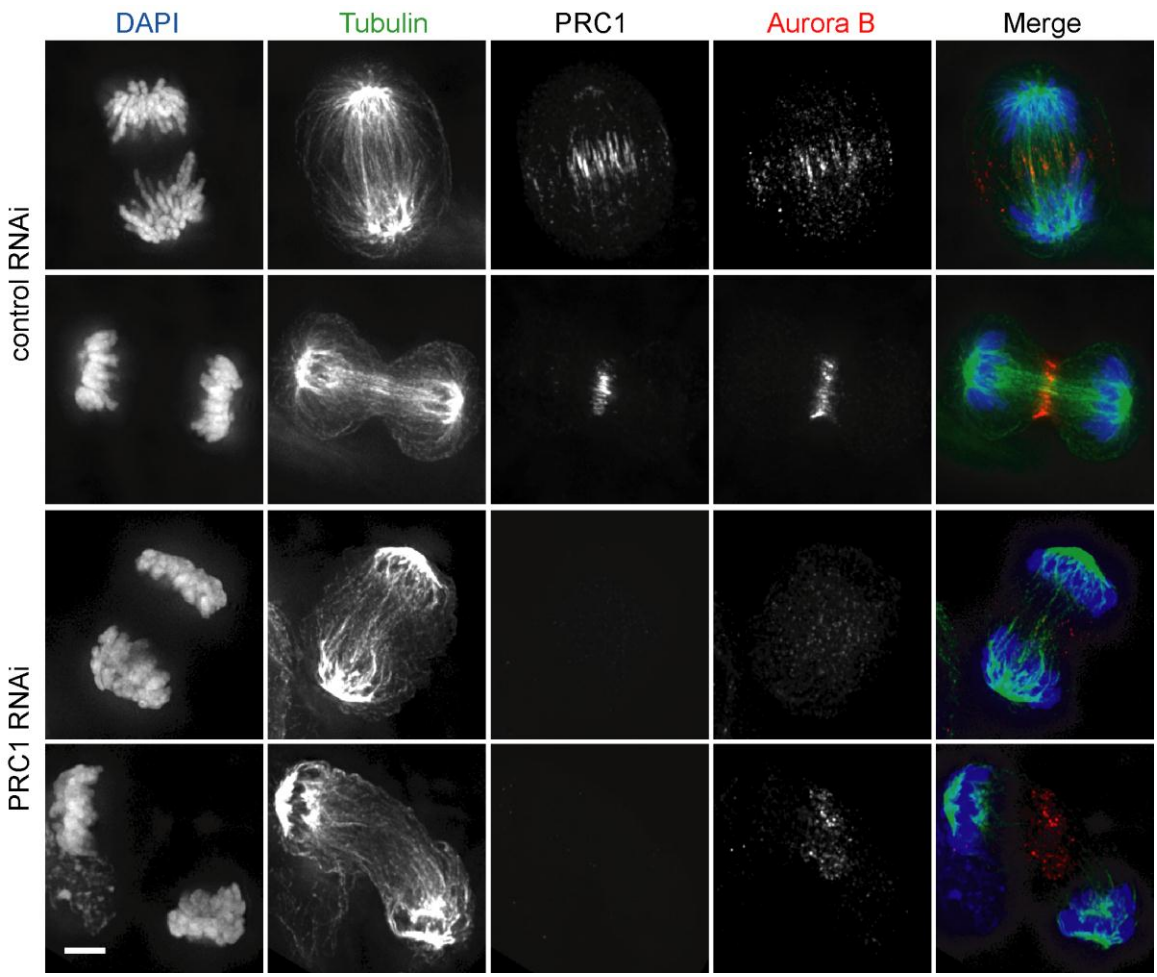

Figure 4.9

PRC1 depletion in RPE1 cells leads to defects in Aurora B kinase localization. Control and PRC1 RNAi cells were fixed and stained for DNA, tubulin, PRC1 and Aurora B. Scale bar, 5μm.

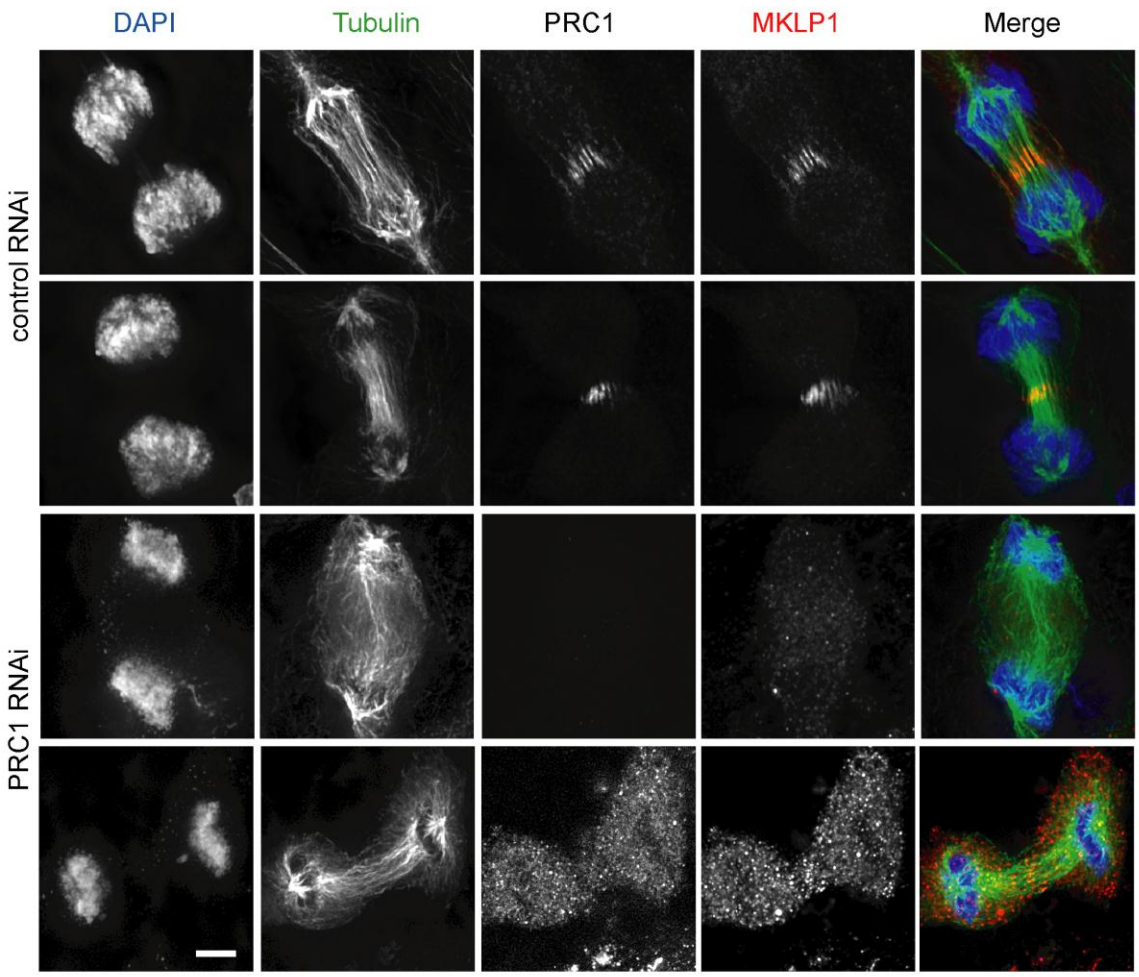

Figure 4.10

PRC1 depletion in RPE1 cells leads to defects in MKLP1 localization. Control and PRC1 RNAi cells were fixed and stained for DNA, tubulin, PRC1 and MKLP1. Scale bar, 5μm.

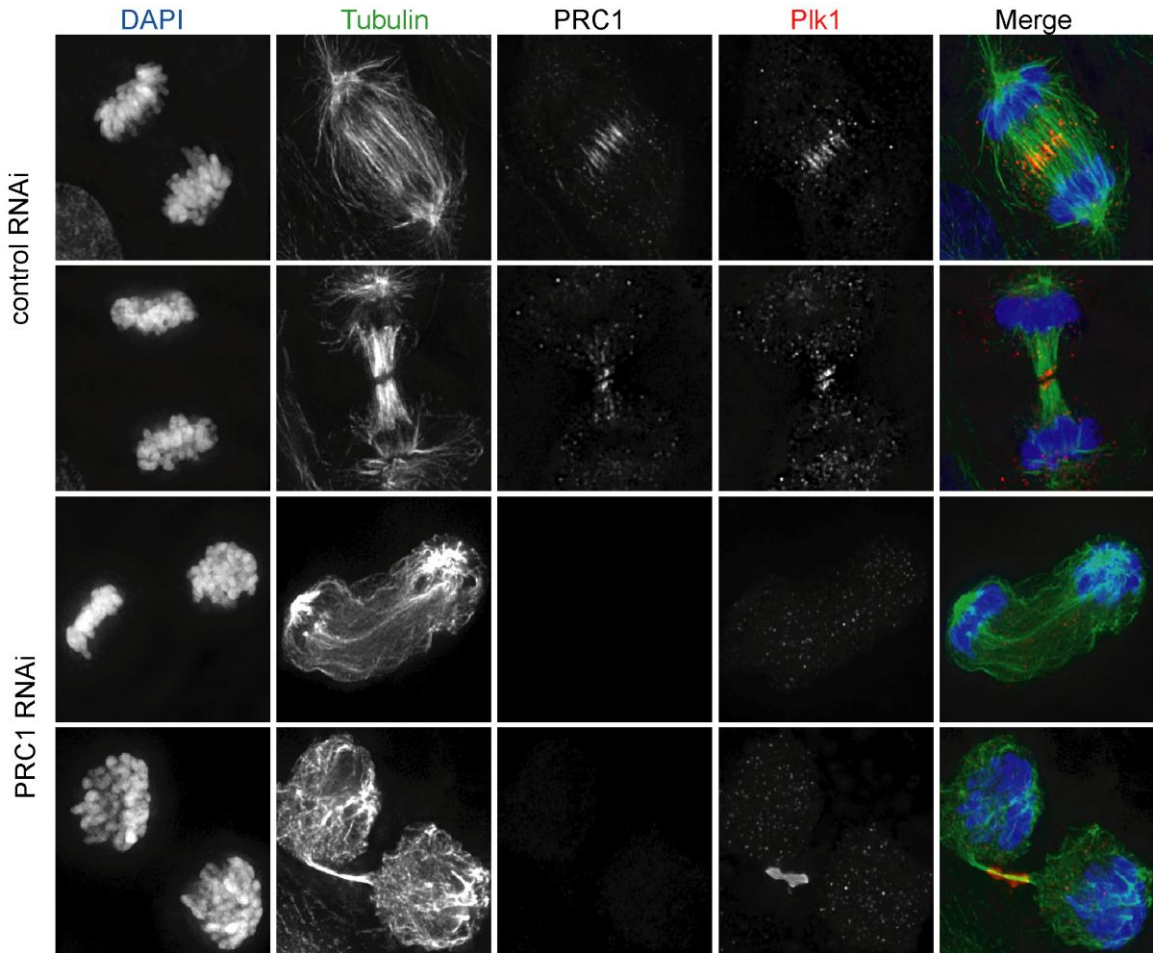

Figure 4.11

PRC1 depletion in RPE1 cells leads to defects in Plk1 localization. Control and PRC1 RNAi cells were fixed and stained for DNA, tubulin, PRC1 and Plk1. Scale bar, 5μm.

I then collaborated with Dr. Radhika Subramanian in the Kapoor lab and Dr. Elizabeth M.Wilson-Kubalek (Milligan Lab, The Scripps Institute) to design a PRC1 mutant that could still bind microtubules and interact with other proteins, but could not properly organize microtubules. Based on the published electron microscopy (EM) analysis, the dimerization domain in PRC1 is tilted 20 degrees relative to the microtubule spectrin domain only when PRC1 is crosslinking two microtubules (Subramanian et al., 2010), which suggests that the junction between the spectrin domain and the dimerization domains is likely to be important for crosslinking specificity. Therefore, we introduced floppy linkers consisting of 9 or 19 Gly-Ser repeats (hereafter L9 and L19 mutant) at the junction (Figure 4.12A) in order to increase flexibility and likely affect PRC1's ability to organize microtubules.

To biochemically characterize the mutant, linkers were introduced in PRC1-NSdeltaC (aa. 1-486) instead of the full length protein, as this construct recapitulates all the key features of PRC1 activity but is easier and faster to purify (Subramanian et al., 2010)(Fig. 4.12B). The insertion of these floppy linkers does not affect solubility, oligomeric state or microtubule binding activity of these mutant proteins (Figure 4.12C, D).

Interestingly, while the wild type protein results in well-organized lateral microtubule arrays, bundling by mutants results in disorganized arrays (Figure 4.12E), which suggests promiscuous crosslinking by these proteins, likely resulting from a loss in crosslinking specificity. EM analysis of the mutants also revealed crosslinking difference from the wildtype PRC1. While the wildtype PRC1 shows regular striations between microtubules with a precise inter-filament spacing, the mutants show no regular striations and don't maintain the precise filament spacing (Figure 4.12F). We observe that the inter-microtubule distances are frequently shorter than those seen in wild type protein. These observations show that the PRC1 linker mutant retains ability to bind and bundle microtubules, but loses its ability to form organized microtubule bundles in vitro.

Figure 4.12

Insertion of a flexible linker into PRC1 disrupts its ability to facilitate the formation of organized anti-parallel microtubule bundles in vitro. (A) Schematic shows the strategy for designing a mutant PRC1, which has a floppy linker between PRC1's dimerization domain (purple line) and its microtubule-binding spectrin domain (green triangle). (B) Schematic of the constructs used for this analysis. (C) Coomasie-stained SDS-PAGE. (D) Gel filtration chromatography suggests that the oligomerization state of the mutants is similar to the wild-type protein. (E) Microtubule bundling by PRC1 wild-type and mutant proteins. 1 μM protein was added to a coverslip decorated with microtubules polymerized with X-Rhodamine tubulin and imaged by TIRF microscopy. (F) Negative stain EM images of microtubules decorated by wild-type and mutant PRC1. Striations of PRC1 are indicated by arrow heads in wild-type panel.

Note: Data from this figure are from experiments done by Dr. Radhika Subramanian, Dr. Elizabeth M.Wilson-Kubalek (Milligan Lab, The Scripps Institute) and David Snead.

Figure 4.12

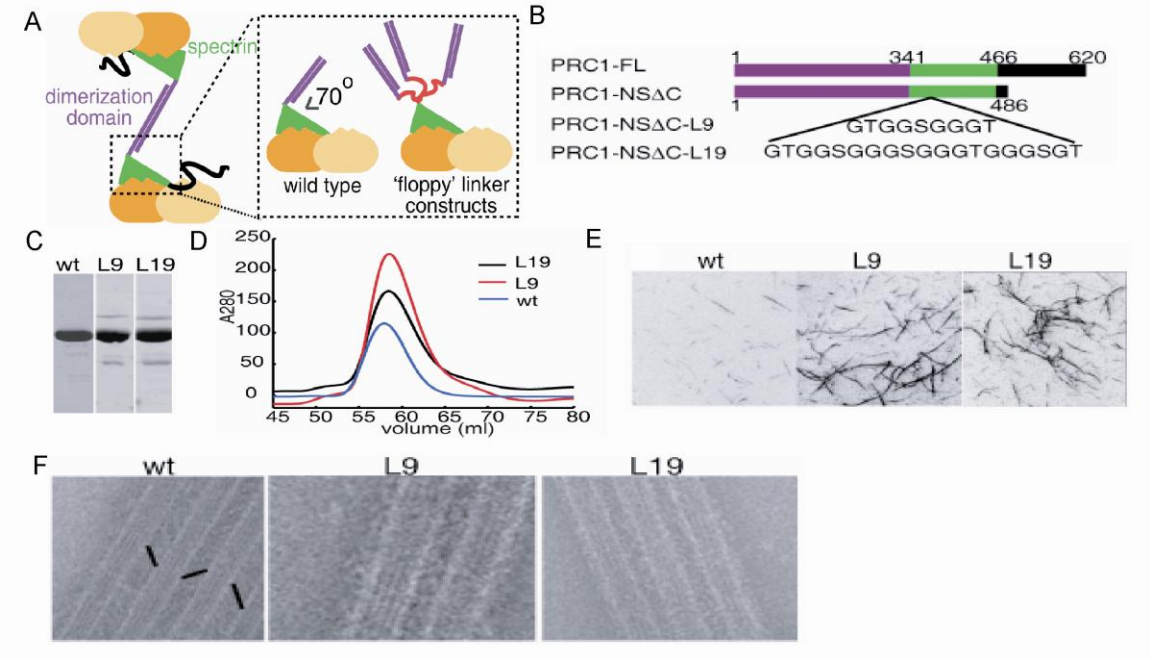
A
spectrin
dimerization domain
70°
wild type
'floppy' linker constructs
B
PRC1-FL
PRC1-NSΔC
PRC1-NSΔC-L9
PRC1-NSΔC-L19
1
341
466
620
1
486
GTGGSGGGT
GTGGSGGGSGGGTGGGSGT
C
wt L9 L19
D
A280
250
200
150
100
50
0
45 50 55 60 65 70 75 80
volume (ml)
L19
L9
wt
E
wt
L9
L19
F
wt
L9
L19

To examine the L19 mutant behavior in vivo, I depleted endogenous PRC1 by RNAi and expressed RNAi-resistant GFP-fused wild type (WT-addback) or L19 mutant (L19-addback) PRC1 in RPE1 cells (Figure 4.13). First I examined L19 mutant localization in cells, by both immunofluorescence and live cell imaging, to confirm that it could bind microtubules in vivo. Immunofluorescence reveals that wild type PRC1 localizes to the mid-spindle in early anaphase and is tightly focused at spindle midzone at late anaphase (Figure 4.14A). However, the L19 mutant localization during early anaphase is widely dispersed over the spindle microtubules (Figure 4.14B, upper panel). In about half of the late anaphase cells, the L19 mutant accumulates at the tips of the microtubules in the middle of the cell (Figure 4.14B, lower panel). These immunofluorescence data demonstrate that the L19 mutant can bind microtubules, consistent with biochemical characterization. In live cell imaging, both wild type and L19 mutant PRC1 localize over the metaphase spindle, before anaphase onset (Figure 4.14C,D,E). During early anaphase, wild type quickly gets recruited to the spindle midzone and gets more concentrated at late anaphase (Figure 4.14C). However, the L19 mutant still localizes to the entire early anaphase spindle and at late anaphase gets accumulated at the tips of microtubules

in the middle of the cell (Figure 4.14D,E). The tip localization of L19 mutant during late anaphase is likely due to interaction with its binding partners. This is consistent with the previous report that PRC1 accumulates at the plus-ends of microtubules during monopolar cytokinesis (Hu et al., 2008). These data indicate that the PRC1 L19 mutant is still able to bind microtubules and could localize to the microtubule tips at the anaphase spindle.

Although L19 mutant could bind microtubules in cells, immunofluorescence experiments show that microtubule bundles at the spindle midzone could not form robustly in L19-addback cells, compared to WT-addback cells (Figure 4.14A, B).

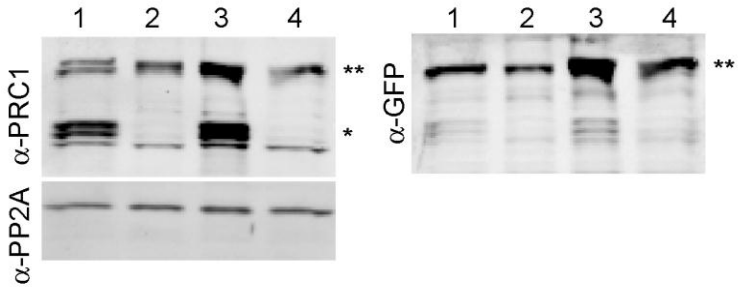

Figure 4.13

Depletion of PRC1 by RNAi and addback of GFP-PRC1 wildtype, or the linker mutant. A representative western blot with cells expressing GFP-PRC1 wild-type (Lane 1,2) or L19 mutant (Lane 3,4) treated with control RNAi (Lane 1,3) or PRC1 RNAi (Lane 2,4). * marks PRC1 and ** marks GFP-PRC1.

Figure 4.14

PRC1 with a flexible linker accumulates at microtubule ends and it does not rescue microtubule bundle formation at the spindle midzone. (A,B) PRC1 RNAi with WT-addback (A) or L19-addback (B) cells were fixed and stained for DNA, tubulin and GFP-PRC1. (C-E) PRC1 RNAi with WT-addback (C) or L19-addback (D,E) cells were imaged live. DIC and projection of GFP-PRC1 are shown. Time unit is minute and time zero is anaphase onset. Scale bars, 5 μm.

Figure 4.14

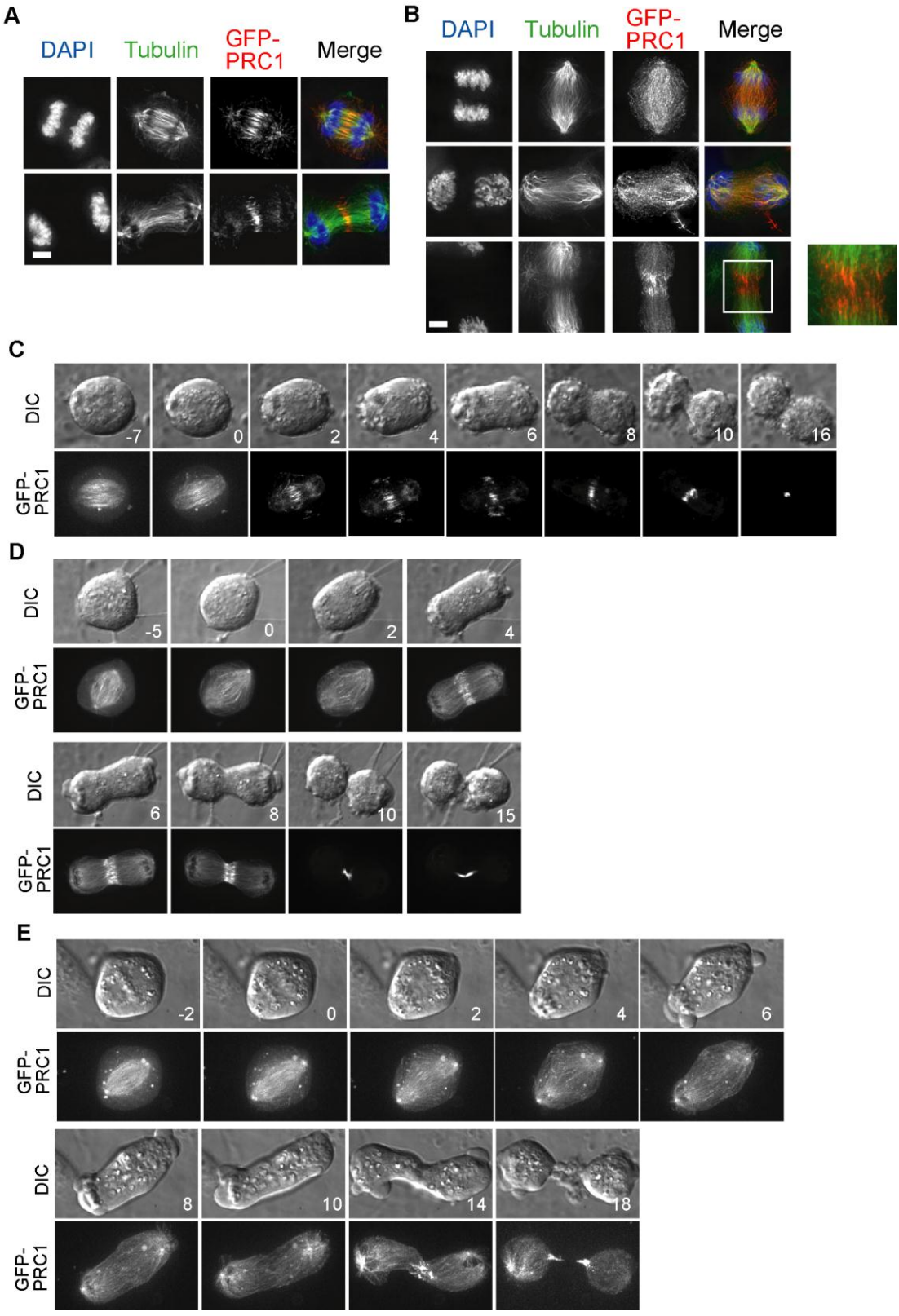
A
DAPI
Tubulin
GFP-PRC1
Merge
B
DAPI
Tubulin
GFP-PRC1
Merge
C
DIC
GFP-PRC1
-7
0
2
4
6
8
10
16
D
DIC
GFP-PRC1
-5
0
2
4
6
8
10
15
E
DIC
GFP-PRC1
-2
0
2
4
6
8
10
14
18

I next examined whether key cytokinesis regulators Aurora B, MKLP1 and Plk1 could be recruited to the mid-cell, without the PRC1-crosslinked microtubule array at the spindle midzone. Immunofluorescence shows that these proteins properly localize to the spindle midzone in WT-addback cells (Figure 4.15). In L19-addback cells where the L19 mutant is spread out over a broader region of the spindle microtubules, these proteins do not have any focused localization (Figure 4.15). Interestingly, in L19-addback cells where L19 mutant localizes to microtubule tips, these protein co-localize with L19 at the mid-cell (Figure 4.15). These data suggest that microtubule bundles at the spindle midzone are dispensable for concentrating key cytokinesis regulators such as Aurora B, MKLP1 and Plk1 at the mid-cell.

I then examined whether cytokinesis could succeed given that the key cytokinesis regulators are recruited to the mid-cell. Immunofluorescence experiments reveal that L19-addback cells have a similar multinucleation index as PRC1 RNAi cells (Figure 4.16, 4.1C), indicating that the L19 mutant cannot rescue cytokinesis failure. These data suggest that the recruitment of Aurora B, MKLP1 and Plk1 to the mid-cell is not likely to be sufficient for successful cytokinesis.

Figure 4.15

PRC1 with a flexible linker could accumulate MKLP1, Plk1 and Aurora B to microtubule ends. PRC1 RNAi with WT- or L19-addback cells were fixed and stained for DNA, tubulin, GFP-PRC1 and MKLP1 (A), Plk1 (B) or Aurora B kinase (C). Scale bar, 5 μm.

Figure 4.15

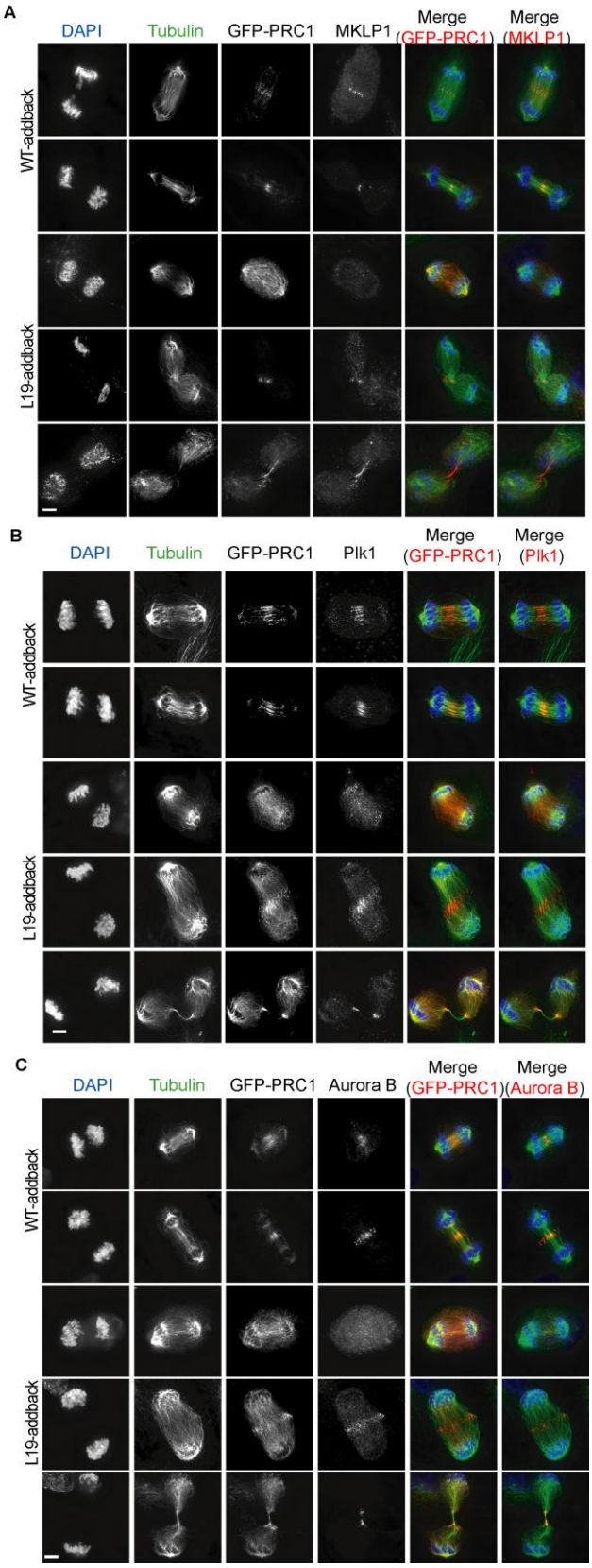
A
DAPI
Tubulin
GFP-PRC1
MKLP1
Merge (GFP-PRC1)
Merge (MKLP1)
WT-addback
L19-addback
B
DAPI
Tubulin
GFP-PRC1
Plk1
Merge (GFP-PRC1)
Merge (Plk1)
WT-addback
L19-addback
C
DAPI
Tubulin
GFP-PRC1
Aurora B
Merge (GFP-PRC1)
Merge (Aurora B)
WT-addback
L19-addback

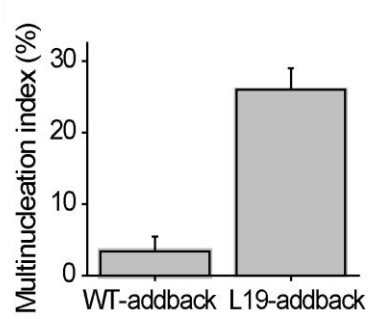

Figure 4.16

The PRC1 linker mutant could not rescue cytokinesis. PRC1 RNAi with WT- or L19-addback cells were fixed and stained for DNA and tubulin. Multinucleate and single nucleated cells were counted to calculate multinucleation index in three independent experiments (N > 500 cells in each experiment).

4.5 Discussion

As my results show that PRC1 depletion disrupts the spindle midzone structure, without disrupting the EB1-marked microtubules, I propose that there are two subsets of microtubules during anaphase: the first subset is the PRC1-crosslinked microtubule array that has reduced dynamics due to KIF4A function. The second subset is a dynamic population of microtubules, revealed by my EB1-GFP imaging. The EB1-bound microtubule subpopulation could probably undergo efficient plus-end polymerization and provide the tracks for motors to slide microtubules apart (Figure 4.17C). Consistent with my model, it has been shown in budding yeast that EB1 provide structural support for the anaphase spindle (Gardner et al., 2008). I propose that in normal anaphase cells, these two subsets of microtubules balance each other to set the length of the anaphase spindle. Once PRC1 is depleted and the crosslinked array cannot form, it is likely that the antiparallel microtubule sliding could not be balanced, resulting in the observed abnormal elongation of the anaphase spindle. Here I propose that this balancing process determines the length of the anaphase spindle and prevents the cell from undergoing abnormal elongation.

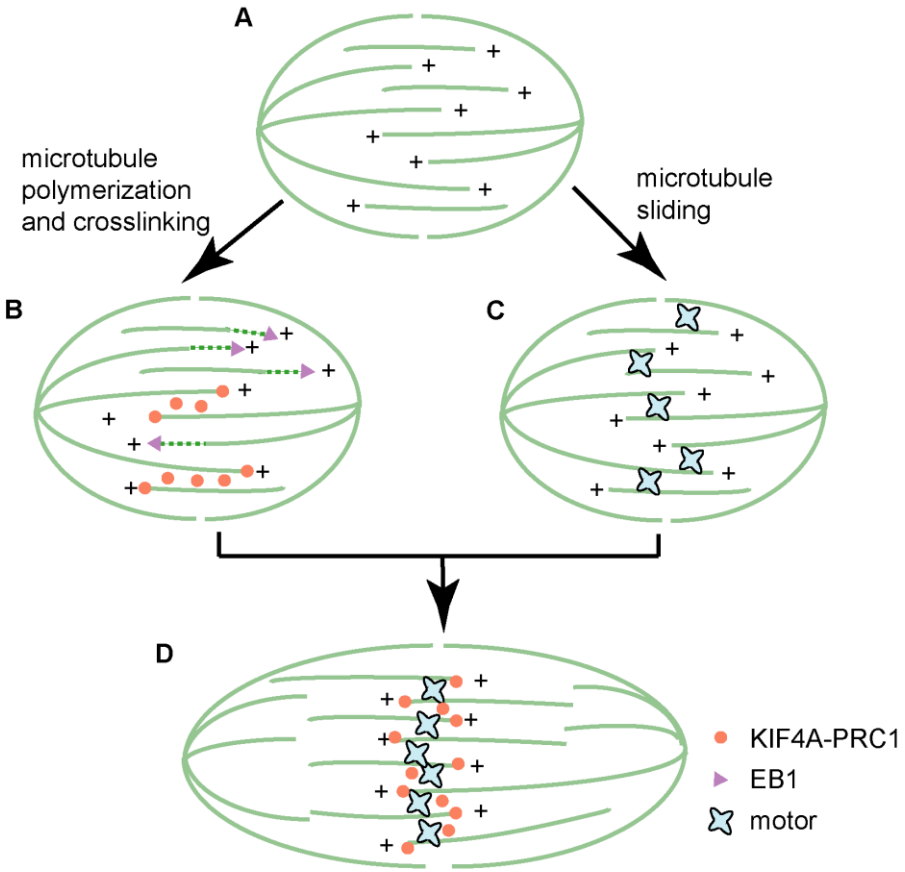

Figure 4.17

A schematic for anaphase spindle elongation. (A) Metaphase spindle. (B) At anaphase, there are two subsets of microtubules: PRC1-KIF4A crosslinked population and EB1-marked dynamic population. (C) Microtubule-based motors slide antiparallel microtubules apart. (D) A balance of microtubule bundling and antiparallel microtubule sliding sets the steady-state length of the anaphase spindle.

Previous studies on KIF4A, a PRC1 interacting partner and processive motor that regulates microtubule plus-end dynamics, have shown that KIF4A depletion leads to longer anti-parallel microtubule overlaps and longer anaphase

spindles (Bieling et al., 2010; Hu et al., 2011; Kurasawa et al., 2004). Based on these findings, it has been hypothesized that KIF4A is controlling the anti-parallel overlap size at the spindle midzone and hence regulating the spindle length. As KIF4A depends on PRC1 for proper localization and function (Kurasawa et al., 2004), my observations could, in theory, be explained by a loss of KIF4A function. I do not favor this model because the PRC1 floppy linker mutant still likely interacts with KIF4A and recruits it to microtubules; however, it fails to rescue both the midzone bundle formation and the abnormal elongation in PRC1 depleted cells. Therefore it is unlikely that the cell abnormal elongation phenotype in PRC1 depleted cells could be simply explained by loss of KIF4A function. To further test this, a KIF4A-PRC1 linker mutant interaction needs to be examined, and KIF4A localization needs more detailed study.

My results have also suggested that without the PRC1-crosslinked microtubule array at the spindle midzone, recruitment of cytokinesis regulators (i.e. Aurora B kinase, Plk1 and MKLP1) to the mid-cell is not sufficient for successful cytokinesis. It is possible that the PRC1-crosslinked microtubule array could be essential to fully activate the cytokinesis regulators (Fuller et al., 2008),

and by concentrating the regulators at the mid-cell alone does not allow these proteins to reach the threshold activity level needed for proper function. Other technical reasons might explain this result as well. For example, there might be essential cytokinesis proteins that could not be recruited by the PRC1 linker mutant. Further cell biological and biochemical experiments are needed to test these hypotheses.

My results suggest a mechanism how PRC1 participate in setting up the length for the anaphase spindle. The molecular mechanism for how PRC1 function in this process is not clear yet. Further experiments testing carefully-designed separation of function mutants for PRC1 are needed to address this further.

CHAPTER 5: FUTURE DIRECTIONS

5.1 Examining CPC-substrate phosphorylation gradient

My results on the CPC-substrate phosphorylation gradient have shown that the gradient emerges in mitosis at both early prometaphase and anaphase. Although we know that the anaphase gradient is involved in organizing the spindle midzone, we do not yet know what the minimal set of components to generate the CPC-substrate phosphorylation gradient is. Furthermore, we do not know if the CPC-substrate phosphorylation gradient alone is sufficient to organize microtubules either. Here I propose several experiments that might further our understanding along these directions.

5.1.1 CPC-substrate phosphorylation gradient for different substrates

The CPC has multiple substrates localized at different subcellular locations (Table 1). It would be interesting to examine the contribution of substrate sequence, localization and diffusion constants to the spatio-temporal dynamics of substrate phosphorylation.

Because the kinetic parameters of a substrate with its kinase(s) or phosphatase(s) can differ for different

sequences, the spatio-temporal patterning of substrate phosphorylation may also be substrate-specific. To address this, one could construct multiple CPC sensors containing different substrate sequences (Table 1, known CPC substrate phosphorylation sites). As shown in the previous chapters, these sensors could then be expressed in cells and examined by live cell imaging. Sensors should first be validated to ensure that their response is specific to CPC activity and that the response is higher than noise. After validation, FRET imaging could be applied, and the phosphorylation dynamics measured by these sensors could be compared (Appendix, Figure A1). If the measurements were similar, this would suggest that the CPC phosphorylation gradient is consistent across different substrate sequences. If the phosphorylation dynamics measurements were different, this potentially could be a mechanism for CPC to co-ordinate different events. Following the live cell imaging, in vitro studies measuring the phosphorylation and dephosphorylation reaction rates could be performed, as mathematical modeling suggests these reaction rates are important parameters for phosphorylation dynamics and spatial patterning. Then, the phosphorylation and dephosphorylation reaction rates for different sensors could be compared with the live cell imaging results. These experiments might generate some

hypotheses for how enzymes co-ordinate multiple cellular events by having differential reaction dynamics for substrates, so that further functional tests could be done in physiological relevant context.

Aside from sequences, CPC substrates also have diverse localizations (Table I). Previous studies have shown that cleavage furrow components, such as Myosin II regulatory light chain (MRLC) and MRLC kinase, are substrates for CPC (Ruchaud et al., 2007). It has also been found that CPC itself localizes at the equatorial cortex during anaphase (Ruchaud et al., 2007). Given these observations, it would be interesting to examine the substrate phosphorylation dynamics at the cell cortex. Membrane targeting motifs from Lyn kinase, RhoA GTPase, Anillin could be used to target the FRET sensor to the cell cortex. I constructed a membrane-targeted sensor using Lyn kinase membrane targeting motif, but the sensor did not respond to Aurora B inhibitor (Appendix Figure A2). In my experience constructing the chromosome- and microtubule-targeted sensors, it is common that the identity of the targeting domains significantly affect whether the sensor responds to CPC activity or not. This could be the case for membrane-targeted sensor, as there are different membrane micro-domains (e.g. lipid rafts) to which certain proteins prefer

to localize (Lingwood and Simons, 2010). Therefore, it may be fruitful to try other membrane-targeting domains for the CPC FRET sensor. The membrane-targeted sensor would not only allow for analysis of CPC phosphorylation dynamics, but it would also provide a starting point to construct similar sensors for other mitotic kinases such as Plk1.

Mathematical modeling also predicts that substrate diffusion is a key parameter for gradient formation (Brown and Kholodenko, 1999); our system would be useful to test this in a controlled way. For example, one could use Rapamycin-mediated FKBP-FRB dimerization to target the sensor to microtubules. Then either by using FKBP-FRB mutants with different binding affinities or by using mutants of MAP4 microtubule-binding domain with different microtubule binding ability, sensors with a range of diffusion rates on microtubules could be created. FRAP experiments could be used to quantify the turnover rate of these sensors, and the turnover rates could be correlated to the gradient shape measured in ratiometric FRET imaging. Therefore, the relationship between substrate diffusion and gradient formation could be tested.

Table I. CPC substrates and known phosphorylation sites

Protein/Phosphorylation site	Function	Reference
Chromosome/Centromere/ Kinetochore		
INCENP (S598, S599)	CPC regulation	(Bishop and Schumacher, 2002)
Survivin (T117)	CPC regulation	(Wheatley et al., 2004)
Condensin Cnd2 (S52)	Chromosome condensation	(Nakazawa et al., 2011)
Histone H3 (S10)	Chromosome condensation	(Hsu et al., 2000)
CENPA (S7)	Centromere protein	(Zeitlin et al., 2001)
MCAK (T95, S110, S196)	Microtubule motor	(Andrews et al., 2004)
Zwint-1 (S250, T251, S262)	Kinetochore component	(Andrews et al., 2004)
KNL1 (S24, S60)	Kinetochore component	(Welburn et al., 2011)
Ndc80 (S5, S15, T49, S55, S69)	Kinetochore component	(DeLuca et al., 2006)
Dsn1 (S100, S109)	Kinetochore component	(Welburn et al., 2011)
CENPE (T422)	Kinetochore motor	(Kim et al., 2010)
mDia3 (S196, T882)	Kinetochore component	(Cheng et al., 2011)
Ska1 (T157, S185, T205, S242)	Kinetochore component	(Chan et al., 2012)
Ska3 (S87, S110, S159)	Kinetochore component	(Chan et al., 2012)
Plk1 (T182)	Kinetochore kinase	(Carmena et al., 2012)
Spindle midzone		
MgcRac1GAP (S387)	GTPase activating protein (GAP) for RhoA GTPase.	(Minoshima et al., 2003)
ZEN-4/MKLP1 (S680, S708)	Central spindle organization	(Guse et al., 2005)
Vimentin (Ser72)	Intermediate filament protein	(Goto et al., 2003)
Desmin (S11, T16, S59)	Intermediate filament protein	(Kawajiri et al., 2003)

5.1.2 In vitro reconstitution of the CPC-substrate phosphorylation gradient

The mechanism of how the CPC-substrate phosphorylation gradient is generated and how it may facilitate the microtubule organization at the spindle midzone could be further examined by in vitro reconstitution. in which individual components could be tested separately. For instance, although it has been shown that the kinesin MKLP2 is responsible for recruiting CPC to the spindle midzone (Gruneberg et al., 2004), potentially by transporting CPC as a cargo along microtubules, this interaction has not yet been tested in vitro. Therefore, reconstitution of the gradient could be done in two steps. First, we would need to reconstitute of the CPC recruitment to microtubule ends by MKLP2. This step requires purification of recombinant MKLP2 and in vitro assembly of the CPC (Jeyaprakash et al., 2007; Neef et al., 2003). MKLP2-CPC interaction should be examined in vitro, possibly by IP-western technique. Once an interaction is confirmed, we would be able to examine if MKLP2 directly brings CPC to the tips of microtubules in vitro by comparing the imaging of GFP-MKLP2 with microtubules, GFP-CPC with microtubules, and of MKLP2, GFP-CPC with microtubules on glass coverslips,. Second, MKLP2, mCherry-CPC, phosphatase (e.g. PP1γ) and microtubules would

be mixed and added on to a coverslip. Recombinant microtubule-targeted FRET sensor would then be added to the mix to analyze the phosphorylation dynamics. During this reconstitution of the gradient, we could examine different parameters involved in the formation of a gradient. For example, the CPC kinase concentration, the phosphatase concentration, the substrate diffusion rate and the substrate sequence. If the first step (i.e., reconstitution of MKLP2-CPC transport along microtubules) were not successful, reconstitution of the gradient might be achieved in other approaches. Given that INCENP antibody coated beads can locally activate CPC (Kelly et al., 2007), this could potentially substitute MKLP2-dependent CPC clustering and serve as source of phosphorylation for generating the gradient. The reconstitution of the gradient would allow us to experimentally test parameters that are predicted to be important for gradient pattern formation and would provide an experimental basis for mathematical modeling of the CPC-substrate phosphorylation gradient.

Reconstitution could also be used to test our model that the CPC-substrate gradient is organizing the spindle midzone by spatially differentiated regulation of MKLP1, or, more specifically, the MKLP1-MgcRacGAP-centralspindlin complex. To this end, one could add purified

centralspindlin complex (Hutterer et al., 2009) into the reconstituted gradient system on the coverslip. Under such conditions, microtubule organization could be observed to examine if there is a correlation between directed microtubule movements and the shape of the gradient. As post-translational control of protein activity is commonly used during cell division, different site-mutants of the individual components could be tested in this reconstitution. For example, the INCENP TSS mutant could serve as negative control, as it could not activate CPC complex (Honda et al., 2003). Furthermore, there are known Plk1 phosphorylation sites on both INCENP and MKLP2 (Carmena and Earnshaw, 2006; Neef et al., 2003). By using phosphorylation site mutants in the reconstitution, one might uncover crosstalk between Plk1 and CPC in regulating microtubule organization. Therefore, this reconstitution would provide insights into how the CPC-substrate gradient organizes microtubule organization.

5.1.3 Other functions of the CPC-substrate phosphorylation gradient

The CPC has multiple substrates involved in various processes during cell division including chromosome condensation, spindle assembly, kinetochore-microtubule

attachment, spindle checkpoint, spindle midzone assembly and abscission (Ruchaud et al., 2007). Given that my results show that the CPC-substrate gradient emerges both at early prometaphase and at anaphase, the CPC-substrate phosphorylation gradient might function during both stages of cell division.

Several lines of evidence suggest that CPC provides spatial cues for spindle assembly. First, it has been shown in Xenopus egg extracts that the CPC must interact with both chromosomes and microtubules to support spindle assembly (Tseng et al., 2010). Based on this finding, it has been proposed that dual detection of chromosomes and microtubules by the CPC ensures that spindles assemble only around chromosomes (Tseng et al., 2010). Second, it has been found in human cells that CPC substrate MCAK localizes to microtubule plus-ends throughout the spindle and that its accumulation is strongly reduced on microtubule plus-ends near chromatin (Tanenbaum and Medema, 2011). This pattern depends on CPC, suggesting that CPC generates signals emanating from chromosomes to negatively regulate MCAK plus-end binding. It has been proposed that CPC could spatially control the dynamics of non-kinetochore microtubules during spindle assembly. These two pieces of evidence, together with my discovery of the early

prometaphase CPC-substrate phosphorylation gradient, suggest that CPC could facilitate spindle formation around chromosomes by establishing a gradient centered on chromosomes. Although CPC activity is dispensable for spindle assembly in somatic human cells (Ruchaud et al., 2007), it might still contribute to the chromosome-mediated spindle assembly: functions for the CPC and the CPC-dependent gradient could be masked by the redundant pathways that support spindle assembly. Further experiments that suppress the centrosome pathway of spindle assembly could be helpful in examining the contribution of the CPC and the CPC-dependent phosphorylation gradient to spindle assembly in mammalian cells.

Besides spindle assembly, the CPC-substrate phosphorylation gradient could also be involved in abscission step during cytokinesis. It has been shown that, in both yeast and in human cells, the CPC is needed for an abscission checkpoint, which delays the final resolution of two daughters until all chromosomes are pulled out of the cleavage plane (Steigemann et al., 2009). Two of my observations suggest that CPC-substrate phosphorylation gradient might be involved in the abscission checkpoint. First, by imaging the microtubule-targeted sensor, I found that the gradient persists through telophase and that the

slope of the gradient becomes steeper over time. Second, when I induced anaphase lagging chromosomes by nocodazole washout (Cimini et al., 2003), I found that sensor phosphorylation remains to be high on lagging chromosomes (Appendix Figure A3). These results suggest that the CPC gradient is a potential mechanism for to co-ordinating cytokinesis with chromosome segregation. Long-term live-cell imaging of the microtubule-targeted sensor in conditions where the telophase gradient is perturbed is needed to test this hypothesis.

5.2 Examining PRC1's function at cytokinesis

My results on PRC1 show that this protein is required for controlling anaphase spindle length and spindle midzone formation. PRC1 is also needed for key cytokinesis regulators (e.g. Aurora B kinase, Polo-like kinase and MKLP1) to be efficiently and properly recruited to the spindle midzone. There are several interesting aspects in this project that might be worth examining.

5.2.1 The function of PRC1's microtubule tip localization

It has been shown that PRC1 preferably binds to anti-parallel microtubule overlaps and that it crosslinks microtubules to organize the spindle midzone (Subramanian

et al., 2010). However, several lines of evidence show that PRC1 also localizes to the microtubule tips. First, PRC1 has been observed to accumulate on the tips of microtubules when monopolar cells polarize as they are forced to exit mitosis (Hu et al., 2008). T monopolar cells likely do not have anti-parallel microtubule overlaps at the polarized end of the cell(given that the two centrosomes are not separated and localize at the same pole) Second, the PRC1 floppy linker mutant, which does not support spindle midzone formation, localizes to the tips of the microtubules (Figure 4.15). As this floppy linker mutant likely preserves the ability to bind PRC1 interaction partners, this result might also reveal PRC1's tendency to accumulate at the microtubule plus-end tips.

The microtubule tip binding of PRC1 is not well characterized. It would be interesting to do a truncation screening to identify the domain(s) or motif(s) that is essential for PRC1 recruitment to microtubule tips. In the screen, one might be able to get a separation-of-function mutant that still crosslinks anti-parallel microtubules, but does not localize to microtubule tips. Phenotypic analysis of such a separation-of-function mutant would help understand the function of PRC1's microtubule tip accumulation.

5.2.2 Reconstitution of anaphase spindle elongation with PRC1 and microtubule motors

I found that PRC1 is required for controlling the anaphase spindle length. In chapter 4, I proposed a model in which initially dynamic microtubules are stabilized once they are crosslinked by PRC1 and bound to KIF4, counteracting the outward pushing forces generated by microtubules motors. To test this model, one could reconstitute a minimal system in vitro, with PRC1, KIF4, a microtubule motor (e.g. Eg5) and microtubules. TIRF imaging would reveal microtubule dynamics and movement with these microtubule-binding proteins. The reconstitution would help us understand key parameters needed for microtubule organization during anaphase.

An alternative approach to test PRC1 and KIF4A's role in anaphase spindle elongation is to use the isolated diatom spindles. Previously, elegant studies have used this system to show that microtubule growth and antiparallel microtubule sliding are two key elements in anaphase spindle elongation (Masuda and Cande, 1987). As genomes for diatoms are now available (Armbrust et al., 2004) and gene silencing techniques have been developed (De Riso et al., 2009), one could use isolated diatom spindle

system to test the role of PRC1 and KIF4 in a more controlled way than in mammalian cell culture. Biotin-tubulin could be used to track newly incorporated tubulin in the anaphase spindle. Furthermore, free tubulin and ATP concentration could be easily manipulated in this system. Results from the diatom spindle would provide insights into the contribution of PRC1 and KIF4A to specific steps of the anaphase spindle elongation.

5.3 Establishing spatial order from micron scale to sub-micron scale

Anaphase is a highly dynamic process, in which chromosome segregation, spindle elongation and cleavage furrow ingression finish within 10 min. Spatial order is needed at different length scales, from tens of microns to sub-microns. I favor the model that molecular interactions such as PRC1-KIF4-microtubules form basic functional modules within short range of distance (i.e. sub-micron scale) and that these modules are further coordinated by a long range gradient, such as the CPC-substrate phosphorylation gradient that extends over tens of microns.

To test this model, I propose an in vitro reconstitution experiment that would be based on the reconstitution experiments proposed earlier in this chapter.

Once the CPC-substrate phosphorylation gradient were be reconstructed in vitro, PRC1, KIF4A and microtubule motors that could slide antiparallel microtubules apart could be added into the system one-by-one or altogether. This would allow us to test whether long range gradients like the CPC-substrate phosphorylation gradient could coordinate events that are at sub-micron scale to achieve spatial order. Furthermore, information from the reconstitution would lend itself to future mathematical modeling of spatial patterning in anaphase.

APPENDIX: Supplement to Chapter 5 Future Directions

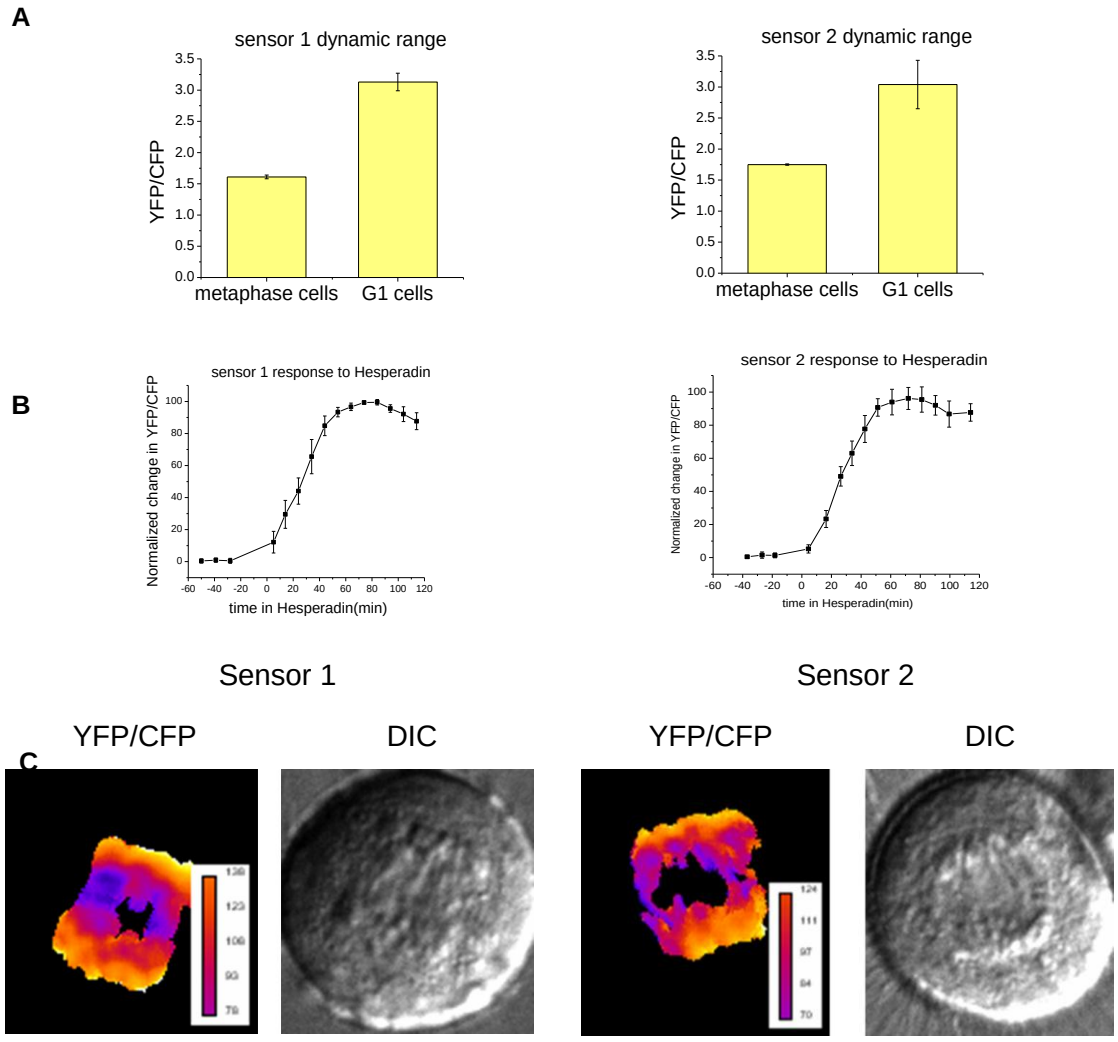

Figure A1 Phosphorylation dynamics of CPC-substrates measured by two FRET sensors with different substrate sequences. Sensor 1 uses Kif2a substrate sequence KVNKIVKNRRTVAI and Sensor 2 uses CENP-A substrate sequence: PRRRTRKIEAPRR. (A) Dynamic range of sensor 1 and sensor 2. (B) Sensor 1 and sensor 2 responds to Aurora kinase inhibitor Hesperadin (100nM). Data averaged and normalized for more than five cells. (C) Ratiometric image and DIC image for sensor 1 and sensor 2.

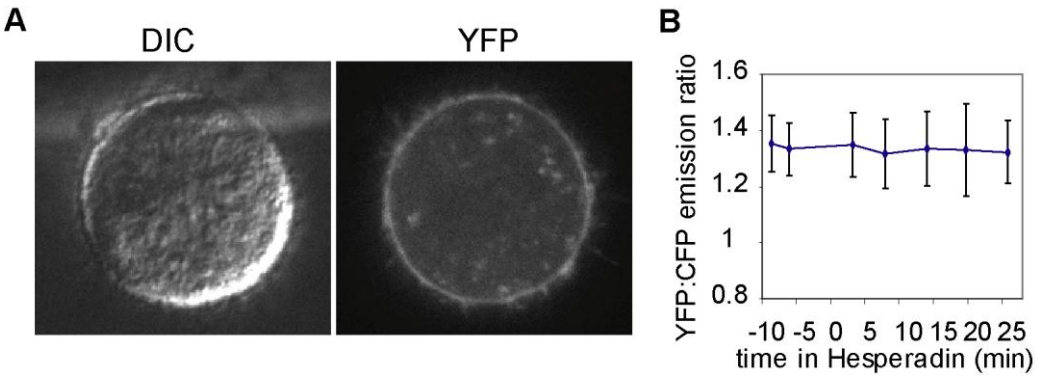

Figure A2 Failed attempt to construct a membrane-targeted FRET sensor. Membrane targeting motif from Lyn is used to target the FRET sensor to the membrane. (A) DIC and YFP image of a cell expressing the membrane-targeted sensor. (B) The membrane-targeted sensor expressing cells were treated with 100 nM Hesperadin. Time zero represents Hesperadin addition. Data was averaged for 5 cells.

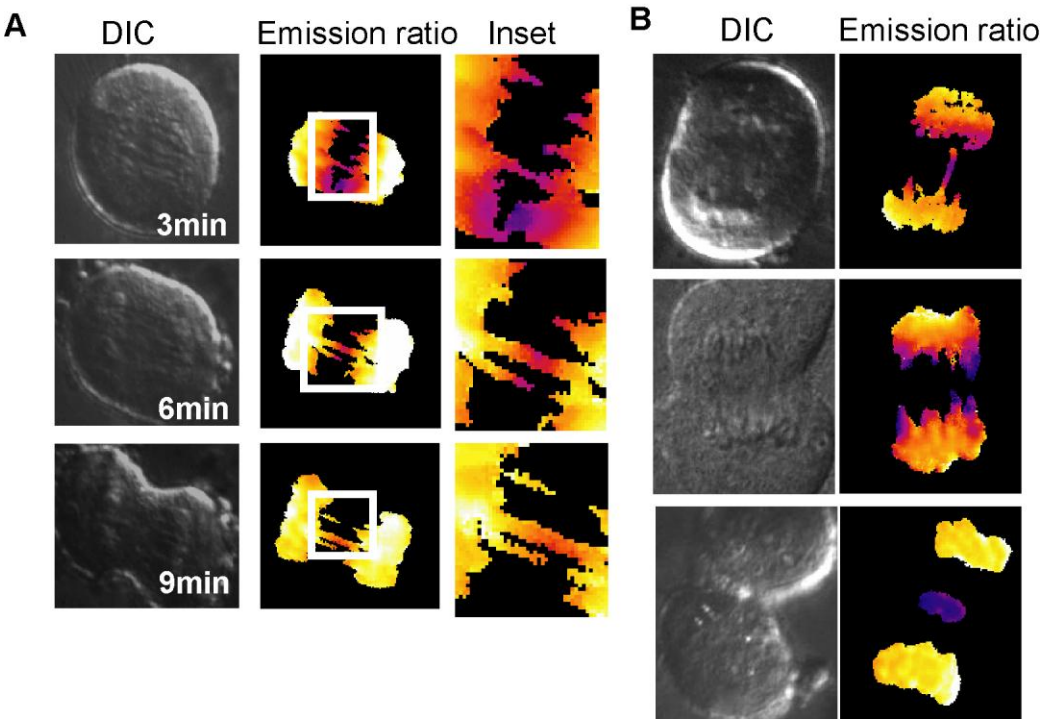

Figure A3 Gradient measurement on lagging chromosomes by nocodazole washout. (A) Time course of a cell expressing chromosome-targeted AurB FRET sensor with lagging chromosomes. Time zero represents anaphase onset. The inset highlights the white box area of the FRET ratio image. For the projection graph: the distance axis on the projection graph was the distance from the pixel to the center of the separating chromosomes, projected along the spindle elongation axis. The FRET ratio was averaged over pixels with the same projected distance. The projection graphs are for the FRET ratio image. (B) Single time-point images of three cells expressing chromosome-targeted FRET sensor.

REFERENCES:

Adams, D.W., and Errington, J. (2009). Bacterial cell division: assembly, maintenance and disassembly of the Z ring. Nat Rev Micro 7, 642-653.

Andrews, P.D., Ovechkina, Y., Morrice, N., Wagenbach, M., Duncan, K., Wordeman, L., and Swedlow, J.R. (2004). Aurora B Regulates MCAK at the Mitotic Centromere. Developmental Cell 6, 253-268.

Armbrust, E.V., Berges, J.A., Bowler, C., Green, B.R., Martinez, D., Putnam, N.H., Zhou, S., Allen, A.E., Apt, K.E., Bechner, M., et al. (2004). The Genome of the Diatom Thalassiosira Pseudonana: Ecology, Evolution, and Metabolism. Science 306, 79-86.

Ashe, H.L., and Briscoe, J. (2006). The interpretation of morphogen gradients. Development *133*, 385-394.

Barr, F.A., Sillje, H.H.W., and Nigg, E.A. (2004). Polo-like kinases and the orchestration of cell division. Nat Rev Mol Cell Biol *5*, 429-441.

Bastiaens, P., Caudron, M., Niethammer, P., and Karsenti, E. (2006). Gradients in the self-organization of the mitotic spindle. Trends Cell Biol *16*, 125-134.

Bement, W.M., Benink, H.l.n.A., and von Dassow, G. (2005). A microtubule-dependent zone of active RhoA during cleavage plane specification. The Journal of Cell Biology *170*, 91-101.

Bi, E., and Lutkenhaus, J. (1991). FtsZ ring structure associated with division in Escherichia coli. Nature *354*, 161-164.

Bieling, P., Telley, I.A., and Surrey, T. (2010). A Minimal Midzone Protein Module Controls Formation and Length of Antiparallel Microtubule Overlaps. Cell *142*, 420-432.

Bishop, J.D., and Schumacher, J.M. (2002). Phosphorylation of the Carboxyl Terminus of Inner Centromere Protein (INCENP) by the Aurora B Kinase Stimulates Aurora B Kinase Activity. Journal of Biological Chemistry 277, 27577-27580.

Brown, G.C., and Kholodenko, B.N. (1999). Spatial gradients of cellular phospho-proteins. FEBS Letters 457, 452-454.

Carmena, M., and Earnshaw, W.C. (2003). The cellular geography of Aurora kinases. Nat Rev Mol Cell Biol *4*, 842-854.

Carmena, M., and Earnshaw, W.C. (2006). INCENP at the kinase crossroads. Nat Cell Biol 8, 110-111.

Carmena, M., Pinson, X., Platani, M., Salloum, Z., Xu, Z., Clark, A., MacIsaac, F., Ogawa, H., Eggert, U., Glover, D.M., *et al.* (2012). The Chromosomal Passenger Complex Activates Polo Kinase at Centromeres. PLoS Biol *10*, e1001250.

Caudron, M.w., Bunt, G., Bastiaens, P., and Karsenti, E. (2005). Spatial Coordination of Spindle Assembly by Chromosome-Mediated Signaling Gradients. Science *309*, 1373-1376.

Chan, Y.W., Jeyaprakash, A.A., Nigg, E.A., and Santamaria, A. (2012). Aurora B controls kinetochore-microtubule attachments by inhibiting Ska complex-KMN network interaction. The Journal of Cell Biology *196*, 563-571.

Cheng, L., Zhang, J., Ahmad, S., Rozier, L., Yu, H., Deng, H., and Mao, Y. (2011). Aurora B Regulates Formin mDia3 in Achieving Metaphase Chromosome Alignment. Developmental Cell *20*, 342-352.

Cimini, D., Moree, B., Canman, J.C., and Salmon, E.D. (2003). Merotelic kinetochore orientation occurs frequently during early mitosis in mammalian tissue cells and error correction is achieved by two different mechanisms. Journal of Cell Science 116, 4213-4225.

Clarke, P.R., and Zhang, C. (2008). Spatial and temporal coordination of mitosis by Ran GTPase. Nat Rev Mol Cell Biol *9*, 464-477.

Courtheoux, T., Gay, G., Gachet, Y., and Tournier, S. (2009). Ase1/Prc1-dependent spindle elongation corrects merotely during anaphase in fission yeast. The Journal of Cell Biology *187*, 399-412.

Dajkovic, A., Lan, G., Sun, S.X., Wirtz, D., and Lutkenhaus, J. (2008). MinC Spatially Controls Bacterial Cytokinesis by Antagonizing the Scaffolding Function of FtsZ. Current Biology *18*, 235-244.

Dechant, R., and Glotzer, M. (2003). Centrosome Separation and Central Spindle Assembly Act in Redundant Pathways that Regulate Microtubule Density and Trigger Cleavage Furrow Formation. Developmental Cell *4*, 333-344.

de Boer, P.A.J., Crossley, R.E., Hand, A.R., and Rothfield, L.I. (1991). The MinD protein is a membrane ATPase required for the correct placement of the Escherichia coli division site. EMBO Journal *10*, 4371-4380.

de Boer, P.A.J., Crossley, R.E., and Rothfield, L.I. (1989). A division inhibitor and a topological specificity factor coded for by the minicell locus determine proper placement of the division septum in E. coli. Cell *56*, 641-649.

De Riso, V., Raniello, R., Maumus, F., Rogato, A., Bowler, C., and Falciatore, A. (2009). Gene silencing in the marine diatom Phaeodactylum tricornutum. Nucleic Acids Research 37, e96.

DeLuca, J.G., Gall, W.E., Ciferri, C., Cimini, D., Musacchio, A., and Salmon, E.D. (2006). Kinetochore Microtubule Dynamics and Attachment Stability Are Regulated by Hec1. Cell 127, 969-982.

Ditchfield, C., Johnson, V.L., Tighe, A., Ellston, R., Haworth, C., Johnson, T., Mortlock, A., Keen, N., and Taylor, S.S. (2003). Aurora B couples chromosome alignment with anaphase by targeting BubR1, Mad2, and Cenp-E to kinetochores. J Cell Biol *161*, 267-280.

Douglas, M.E., Davies, T., Joseph, N., and Mishima, M. (2010). Aurora B and 14-3-3 Coordinately Regulate Clustering of Centralspindlin during Cytokinesis. Curr Biol *20*, 927-933.

Dutta, R., and Robinson, K.R. (2004). Identification and Characterization of Stretch-Activated Ion Channels in Pollen Protoplasts. Plant Physiology *135*, 1398-1406.

Eggert, U.S., Mitchison, T.J., and Field, C.M. (2006). Animal Cytokinesis: From Parts List to Mechanisms. Annual Review of Biochemistry *75*, 543-566.

Foe, V.E., and von Dassow, G. (2008). Stable and dynamic microtubules coordinately shape the myosin activation zone during cytokinetic furrow formation. J Cell Biol *183*, 457-470.

Fu, X., Shih, Y.-L., Zhang, Y., and Rothfield, L.I. (2001). The MinE ring required for proper placement of the division site is a mobile structure that changes its cellular location during the Escherichia coli division cycle. Proceedings of the National Academy of Sciences *98*, 980-985.

Fuller, B.G., Lampson, M.A., Foley, E.A., Rosasco-Nitcher, S., Le, K.V., Tobelmann, P., Brautigan, D.L., Stukenberg, P.T., and Kapoor, T.M. (2008). Midzone activation of aurora B in anaphase produces an intracellular phosphorylation gradient. Nature *453*, 1132-1136.

Gierer, A. (1982). Generation of biological patterns and form: Some physical, mathematical, and logical aspects. Progress in Biophysics and Molecular Biology *37*, 1-47.

Glotzer, M. (2009). The 3Ms of central spindle assembly: microtubules, motors and MAPs. Nat Rev Mol Cell Biol *10*, 9-20.

Goto, H., Yasui, Y., Kawajiri, A., Nigg, E.A., Terada, Y., Tatsuka, M., Nagata, K.-i., and Inagaki, M. (2003). Aurora-B Regulates the Cleavage Furrow-specific Vimentin Phosphorylation in the Cytokinetic Process. Journal of Biological Chemistry 278, 8526-8530.

Gruneberg, U., Neef, R.d., Honda, R., Nigg, E.A., and Barr, F.A. (2004). Relocation of Aurora B from centromeres to the central spindle at the metaphase to anaphase transition requires MKlp2. The Journal of Cell Biology 166, 167-172.

Gruss, O.J., Carazo-Salas, R.E., Schatz, C.A., Guarguaglini, G., Kast, J.r., Wilm, M., Le Bot, N., Vernos, I., Karsenti, E., and Mattaj, I.W. (2001). Ran Induces Spindle Assembly by Reversing the Inhibitory Effect of Importin-b on TPX2 Activity. Cell *104*, 83-93.

Guberman, J.M., Fay, A., Dworkin, J., Wingreen, N.S., and Gitai, Z. (2008). PSICIC: Noise and Asymmetry in Bacterial Division Revealed by Computational Image Analysis at Sub-Pixel Resolution. PLoS Comput Biol *4*, e1000233.

Guse, A., Mishima, M., and Glotzer, M. (2005). Phosphorylation of ZEN-4/MKLP1 by Aurora B Regulates Completion of Cytokinesis. Current Biology 15, 778-786.

Hachet, O., Berthelot-Grosjean, M., Kokkoris, K., Vincenzetti, V., Moosbrugger, J., and Martin, SophieÂ G. (2011). A Phosphorylation Cycle Shapes Gradients of the DYRK Family Kinase Pom1 at the Plasma Membrane. Cell *145*, 1116-1128.

Hale, C.A., Meinhardt, H., and de Boer, P.A.J. (2001). Dynamic localization cycle of the cell division regulator MinE in Escherichia coli. EMBO J *20*, 1563-1572.
Hepler, P.K., Kunkel, J.G., Rounds, C.M., and Winship, L.J. (2012). Calcium entry into pollen tubes. Trends in Plant Science *17*, 32-38.

Hamada, T. (2007). Microtubule-associated proteins in higher plants. Journal of Plant Research *120*, 79-98.

Hauf, S., Cole, R.W., LaTerra, S., Zimmer, C., Schnapp, G., Walter, R., Heckel, A., van Meel, J., Rieder, C.L., and Peters, J.-M. (2003). The small molecule Hesperadin reveals a role for Aurora B in correcting kinetochore-microtubule attachment and in maintaining the spindle assembly checkpoint. J Cell Biol *161*, 281-294.

Holdaway-Clarke, T.L., Feijó, J.A., Hackett, G.R., Kunkel, J.G., and Hepler, P.K. (1997). Pollen Tube Growth and the Intracellular Cytosolic Calcium Gradient Oscillate in Phase while Extracellular Calcium Influx Is Delayed The Plant Cell *9*, 1999-2010.

Holdaway-Clarke, T.L., and Hepler, P.K. (2003). Control of pollen tube growth: role of ion gradients and fluxes. New Phytologist *159*, 539-563.

Honda, R., Korner, R., and Nigg, E.A. (2003). Exploring the Functional Interactions between Aurora B, INCENP, and Survivin in Mitosis. Mol Biol Cell *14*, 3325-3341.

Houghtaling, B.R., Yang, G., Matov, A., Danuser, G., and Kapoor, T.M. (2009). Op18 reveals the contribution of nonkinetochore microtubules to the dynamic organization of the vertebrate meiotic spindle. Proceedings of the National Academy of Sciences *106*, 15338-15343.

Hsu, J.-Y., Sun, Z.-W., Li, X., Reuben, M., Tatchell, K., Bishop, D.K., Grushcow, J.M., Brame, C.J., Caldwell, J.A., Hunt, D.F., et al. (2000). Mitotic Phosphorylation of Histone H3 Is Governed by Ipl1/aurora Kinase and Glc7/PP1 Phosphatase in Budding Yeast and Nematodes. Cell 102, 279-291.

Hu, C.-K., Coughlin, M., Field, C.M., and Mitchison, T.J. (2008). Cell polarization during monopolar cytokinesis. J Cell Biol *181*, 195-202.

Hu, C.-K., Coughlin, M., Field, Christine M., and Mitchison, T.J. (2011). KIF4 Regulates Midzone Length during Cytokinesis. Current Biology *21*, 815-824.

Hu, Z., and Lutkenhaus, J. (1999). Topological regulation of cell division in Escherichia coli involves rapid pole to pole oscillation of the division inhibitor MinC under the control of MinD and MinE. Molecular Microbiology *34*, 82-90.

Hu, Z., Mukherjee, A., Pichoff, S., and Lutkenhaus, J. (1999). The MinC component of the division site selection system in Escherichia coli interacts with FtsZ to prevent polymerization. Proceedings of the National Academy of Sciences *96*, 14819-14824.

Hu, Z., and Lutkenhaus, J. (2000). Analysis of MinC Reveals Two Independent Domains Involved in Interaction with MinD and FtsZ. Journal of Bacteriology *182*, 3965-3971.

Hu, Z., and Lutkenhaus, J. (2003). A conserved sequence at the C-terminus of MinD is required for binding to the membrane and targeting MinC to the septum. Molecular Microbiology *47*, 345-355.

Hümmer, S., and Mayer, T.U. (2009). Cdk1 Negatively Regulates Midzone Localization of the Mitotic Kinesin Mklp2 and the Chromosomal Passenger Complex. Curr Biol *19*, 607-612.

Hutterer, A., Glotzer, M., and Mishima, M. (2009). Clustering of Centralspindlin Is Essential for Its Accumulation to the Central Spindle and the Midbody. Curr Biol *19*, 2043-2049.

Hutterer, A., Glotzer, M., and Mishima, M. (2009). Clustering of Centralspindlin Is Essential for Its Accumulation to the Central Spindle and the Midbody. Current Biology 19, 2043-2049.

Iwano, M., Entani, T., Shiba, H., Kakita, M., Nagai, T., Mizuno, H., Miyawaki, A., Shoji, T., Kubo, K., Isogai, A., *et al.* (2009). Fine-Tuning of the cytoplasmic Ca2+ concentration is essential for pollen tube growth. Plant Physiology *150*, 1322-1334.

Jeyaprakash, A.A., Klein, U.R., Lindner, D., Ebert, J., Nigg, E.A., and Conti, E. (2007). Structure of a Survivin-Borealin-INCENP Core Complex Reveals How Chromosomal Passengers Travel Together. Cell 131, 271-285.

Jiang, W., Jimenez, G., Wells, N.J., Hope, T.J., Wahl, G.M., Hunter, T., and Fukunaga, R. (1998). PRC1: A Human Mitotic Spindle-Associated CDK Substrate Protein Required for Cytokinesis. Molecular cell *2*, 877-885.

Kalab, P., and Heald, R. (2008). The RanGTP gradient: a GPS for the mitotic spindle. Journal of Cell Science *121*, 1577-1586.

Kalab, P., Pralle, A., Isacoff, E.Y., Heald, R., and Weis, K. (2006). Analysis of a RanGTP-regulated gradient in mitotic somatic cells. Nature *440*, 697-701.

Kalab, P., Pu, R.T., and Dasso, M. (1999). The Ran GTPase regulates mitotic spindle assembly. Current Biology *9*, 481-484.

Kalab, P., Weis, K., and Heald, R. (2002). Visualization of a Ran-GTP Gradient in Interphase and Mitotic Xenopus Egg Extracts. Science *295*, 2452-2456.

Kawajiri, A., Yasui, Y., Goto, H., Tatsuka, M., Takahashi, M., Nagata, K.-i., and Inagaki, M. (2003). Functional Significance of the Specific Sites Phosphorylated in Desmin at Cleavage Furrow: Aurora-B May Phosphorylate and Regulate Type III Intermediate Filaments during Cytokinesis

Coordinatedly with Rho-kinase. Molecular Biology of the Cell 14, 1489-1500.

Kelly, A.E., Sampath, S.C., Maniar, T.A., Woo, E.M., Chait, B.T., and Funabiki, H. (2007). Chromosomal Enrichment and Activation of the Aurora B Pathway Are Coupled to Spatially Regulate Spindle Assembly. Developmental Cell 12, 31-43.

Kim, Y., Holland, A.J., Lan, W., and Cleveland, D.W. (2010). Aurora Kinases and Protein Phosphatase 1 Mediate Chromosome Congression through Regulation of CENP-E. Cell 142, 444-455.

Kholodenko, B.N., Hancock, J.F., and Kolch, W. Signalling ballet in space and time. Nat Rev Mol Cell Biol *11*, 414-426.

Kurasawa, Y., Earnshaw, W.C., Mochizuki, Y., Dohmae, N., and Todokoro, K. (2004). Essential roles of KIF4 and its binding partner PRC1 in organized central spindle midzone formation. EMBO J *23*, 3237-3248.

Lackner, L.L., Raskin, D.M., and de Boer, P.A.J. (2003). ATP-Dependent Interactions between Escherichia coli Min Proteins and the Phospholipid Membrane In Vitro. Journal of Bacteriology *185*, 735-749.

Lampson, M.A., and Cheeseman, I.M. (2010). Sensing centromere tension: Aurora B and the regulation of kinetochore function. Trends in cell biology *21*, 133-140.

Liu, D., Vader, G., Vromans, M.J.M., Lampson, M.A., and Lens, S.M.A. (2009). Sensing Chromosome Bi-Orientation by Spatial Separation of Aurora B Kinase from Kinetochore Substrates. Science *323*, 1350-1353.

Lingwood, D., and Simons, K. (2010). Lipid Rafts As a Membrane-Organizing Principle. Science 327, 46-50.

Loose, M., Fischer-Friedrich, E., Ries, J., Kruse, K., and Schwille, P. (2008). Spatial Regulators for Bacterial Cell Division Self-Organize into Surface Waves in Vitro. Science *320*, 789-792.

Loose, M., Kruse, K., and Schwille, P. (2011). Protein Self-Organization: Lessons from the Min System. Annual Review of Biophysics *40*, 315-336.

Lovy-Wheeler, A., CÃ¡rdenas, L., Kunkel, J.G., and Hepler, P.K. (2007). Differential organelle movement on the actin cytoskeleton in lily pollen tubes. Cell Motility and the Cytoskeleton *64*, 217-232.

Loïodice, I., Staub, J., Setty, T.G., Nguyen, N.-P.T., Paoletti, A., and Tran, P.T. (2005). Ase1p Organizes Antiparallel Microtubule Arrays during Interphase and Mitosis in Fission Yeast. Molecular Biology of the Cell *16*, 1756-1768.

Ma, L.-Y., King, G., and Rothfield, L. (2003). Mapping the MinE Site Involved in Interaction with the MinD Division Site Selection Protein of Escherichia coli. Journal of Bacteriology *185*, 4948-4955.

Ma, L., King, G.F., and Rothfield, L. (2004). Positioning of the MinE binding site on the MinD surface suggests a plausible mechanism for activation of the Escherichia coli MinD ATPase during division site selection. Molecular Microbiology *54*, 99-108.

Ma, W., Trusina, A., El-Samad, H., Lim, W.A., and Tang, C. (2009). Defining Network Topologies that Can Achieve Biochemical Adaptation. Cell *138*, 760-773.

Macurek, L., Lindqvist, A., Lim, D., Lampson, M.A., Klompmaker, R., Freire, R., Clouin, C., Taylor, S.S., Yaffe, M.B., and Medema, R.H. (2008). Polo-like kinase-1 is activated by aurora A to promote checkpoint recovery. Nature *455*, 119-123.

Maeder, C.I., Hink, M.A., Kinkhabwala, A., Mayr, R., Bastiaens, P.I.H., and Knop, M. (2007). Spatial regulation of Fus3 MAP kinase activity through a reaction-diffusion mechanism in yeast pheromone signalling. Nat Cell Biol *9*, 1319-1326.

Malhó, R., Read, N.D., Trewavaqb, A.J., and Pais, M.S. (1995). Calcium Channel Activity during Pollen Tube Growth and Reorientation. The Plant Cell *7*, 1173-1184.

Martin, S.G., and Berthelot-Grosjean, M. (2009). Polar gradients of the DYRK-family kinase Pom1 couple cell length with the cell cycle. Nature *459*, 852-856.

Masuda, H., and Cande, W.Z. (1987). The role of tubulin polymerization during spindle elongation in vitro. Cell 49, 193-202.

Meinhardt, H., and de Boer, P.A.J. (2001). Pattern formation in Escherichia coli: A model for the pole-to-pole oscillations of Min proteins and the localization of the division site. Proceedings of the National Academy of Sciences *98*, 14202-14207.

Minoshima, Y., Kawashima, T., Hirose, K., Tonozuka, Y., Kawajiri, A., Bao, Y.C., Deng, X., Tatsuka, M., Narumiya, S., May Jr, W.S., et al. (2003). Phosphorylation by Aurora B Converts MgcRacGAP to a RhoGAP during Cytokinesis. Developmental Cell 4, 549-560.

Mishima, M., Kaitna, S., and Glotzer, M. (2002). Central Spindle Assembly and Cytokinesis Require a Kinesin-like Protein/RhoGAP Complex with Microtubule Bundling Activity. Dev Cell *2*, 41-54.

Mochida, S., and Hunt, T. (2007). Calcineurin is required to release Xenopus egg extracts from meiotic M phase. Nature *449*, 336-340.

Mollinari, C., Kleman, J.-P., Jiang, W., Schoehn, G., Hunter, T., and Margolis, R.L. (2002). PRC1 is a microtubule binding and bundling protein essential to maintain the mitotic spindle midzone. The Journal of Cell Biology *157*, 1175-1186.

Mora-Bermudez, F., Gerlich, D., and Ellenberg, J. (2007). Maximal chromosome compaction occurs by axial shortening in anaphase and depends on Aurora kinase. Nat Cell Biol *9*, 822-831.

Moseley, J.B., Mayeux, A., Paoletti, A., and Nurse, P. (2009). A spatial gradient coordinates cell size and mitotic entry in fission yeast. Nature *459*, 857-860.

Nachury, M.V., Maresca, T.J., Salmon, W.C., Waterman-Storer, C.M., Heald, R., and Weis, K. (2001). Importin-b Is a Mitotic Target of the Small GTPase Ran in Spindle Assembly. Cell *104*, 95-106.

Nakazawa, N., Mehrotra, R., Ebe, M., and Yanagida, M. (2011). Condensin phosphorylated by the Aurora-B-like

kinase Ark1 is continuously required until telophase in a mode distinct from Top2. Journal of Cell Science *124*, 1795-1807.

Nédélec, F., Surrey, T., and Karsenti, E. (2003). Self-organisation and forces in the microtubule cytoskeleton. Curr Opin Cell Biol *15*, 118-124.

Neef, R.d., Preisinger, C., Sutcliffe, J., Kopajtich, R., Nigg, E.A., Mayer, T.U., and Barr, F.A. (2003). Phosphorylation of mitotic kinesin-like protein 2 by polo-like kinase 1 is required for cytokinesis. The Journal of Cell Biology 162, 863-876.

Neef, R., Gruneberg, U., Kopajtich, R., Li, X., Nigg, E.A., Sillje, H., and Barr, F.A. (2007). Choice of Plk1 docking partners during mitosis and cytokinesis is controlled by the activation state of Cdk1. Nat Cell Biol *9*, 436-444.

Neurohr, G., Naegeli, A., Titos, I., Theler, D., Greber, B., Daez, J., Gabaldan, T., Mendoza, M., and Barral, Y. (2011). A Midzone-Based Ruler Adjusts Chromosome Compaction to Anaphase Spindle Length. Science *332*, 465-468.

Niethammer, P., Bastiaens, P., and Karsenti, E. (2004). Stathmin-Tubulin Interaction Gradients in Motile and Mitotic Cells. Science *303*, 1862-1866.

Nislow, C., Lombillo, V.A., Kuriyama, R., and McLntosh, J.R. (1992). A plus-end-directed motor enzyme that moves antiparallel microtubules in vitro localizes to the interzone of mitotic spindles. Nature *359*, 543-547.

Niethammer, P., Bastiaens, P., and Karsenti, E. (2004). Stathmin-Tubulin Interaction Gradients in Motile and Mitotic Cells. Science *303*, 1862-1866.

Niethammer, P., Grabher, C., Look, A.T., and Mitchison, T.J. (2009). A tissue-scale gradient of hydrogen peroxide mediates rapid wound detection in zebrafish. Nature *459*, 996-999.

Norden, C., Mendoza, M., Dobbelaere, J., Kotwaliwale, C.V., Biggins, S., and Barral, Y. (2006). The NoCut Pathway Links Completion of Cytokinesis to Spindle Midzone Function to Prevent Chromosome Breakage. Cell *125*, 85-98.

Peisajovich, S.G., Garbarino, J.E., Wei, P., and Lim, W.A. Rapid Diversification of Cell Signaling Phenotypes by Modular Domain Recombination. Science *328*, 368-372.

Petronczki, M., Glotzer, M., Kraut, N., and Peters, J.-M. (2007). Polo-like Kinase 1 Triggers the Initiation of Cytokinesis in Human Cells by Promoting Recruitment of the RhoGEF Ect2 to the Central Spindle. Dev Cell *12*, 713-725.

Pichoff, S., Vollrath, B., Touriol, C., and Bouché, J.-P. (1995). Deletion analysis of gene minE which encodes the topological specificity factor of cell division in Escherichia coli. Molecular Microbiology *18*, 321-329.

Piekny, A.J., and Glotzer, M. (2008). Anillin Is a Scaffold Protein That Links RhoA, Actin, and Myosin during Cytokinesis. Curr Biol *18*, 30-36.

Raskin, D.M., and de Boer, P.A.J. (1997). The MinE Ring: An FtsZ-Independent Cell Structure Required for Selection of the Correct Division Site in E. coli. Cell *91*, 685-694.

Raskin, D.M., and de Boer, P.A.J. (1999a). MinDE-Dependent Pole-to-Pole Oscillation of Division Inhibitor MinC in Escherichia coli. Journal of Bacteriology *181*, 6419-6424.

Raskin, D.M., and de Boer, P.A.J. (1999b). Rapid pole-to-pole oscillation of a protein required for directing division to the middle of Escherichia coli. Proceedings of the National Academy of Sciences *96*, 4971-4976.

Rathore, K.S., Cork, R.J., and Robinson, K.R. (1991). A cytoplasmic gradient of Ca2+ is correlated with the growth of lily pollen tubes. Developmental Biology *148*, 612-619.

Roberts, P.J., Mitin, N., Keller, P.J., Chenette, E.J., Madigan, J.P., Currin, R.O., Cox, A.D., Wilson, O., Kirschmeier, P., and Der, C.J. (2008). Rho Family GTPase Modification and Dependence on CAAX Motif-signaled Posttranslational Modification. J Biol Chem *283*, 25150-25163.

Ruchaud, S., Carmena, M., and Earnshaw, W.C. (2007). Chromosomal passengers: conducting cell division. Nat Rev Mol Cell Biol *8*, 798-812.

Schiøtt, M., Romanowsky, S.M., Bækgaard, L., Jakobsen, M.K., Palmgren, M.G., and Harper, J.F. (2004). A plant plasma membrane Ca2+ pump is required for normal pollen tube growth and fertilization. Proceedings of the National Academy of Sciences of the United States of America *101*, 9502-9507.

Shang, Z.-l., Ma, L.-g., Zhang, H.-l., He, R.-r., Wang, X.-c., Cui, S.-j., and Sun, D.-y. (2005). Ca2+ Influx into Lily Pollen Grains Through a Hyperpolarization-activated Ca2+-permeable Channel Which Can be Regulated by Extracellular CaM. Plant and Cell Physiology *46*, 598-608.

Shimamoto, Y., Maeda, Yusuke T., Ishiwata, S.i., Libchaber, Albert J., and Kapoor, Tarun M. (2011). Insights into the Micromechanical Properties of the Metaphase Spindle. Cell *145*, 1062-1074.

Speliotes, E.K., Uren, A., Vaux, D., and Horvitz, H.R. (2000). The Survivin-like C. elegans BIR-1 Protein Acts with the Aurora-like Kinase AIR-2 to Affect Chromosomes and the Spindle Midzone. Mol Cell *6*, 211-223.

Steegmaier, M., Hoffmann, M., Baum, A., LÃ©nÃ¡rt, P.t., Petronczki, M., KrÅ¡Å¡Ã¡k, M., GÃ¼rtler, U., Garin-Chesa, P., Lieb, S., Quant, J., *et al.* (2007). BI 2536, a Potent and Selective Inhibitor of Polo-like Kinase 1, Inhibits Tumor Growth In Vivo. Current Biology *17*, 316-322.

Steigemann, P., Wurzenberger, C., Schmitz, M.H.A., Held, M., Guizetti, J., Maar, S., and Gerlich, D.W. (2009). Aurora B-Mediated Abscission Checkpoint Protects against Tetraploidization. Cell *136*, 473-484.

Straight, A.F., Cheung, A., Limouze, J., Chen, I., Westwood, N.J., Sellers, J.R., and Mitchison, T.J. (2003). Dissecting Temporal and Spatial Control of Cytokinesis with a Myosin II Inhibitor. Science *299*, 1743-1747.

Subramanian, R., Wilson-Kubalek, E.M., Arthur, C.P., Bick, M.J., Campbell, E.A., Darst, S.A., Milligan, R.A., and Kapoor, T.M. (2010). Insights into Antiparallel Microtubule Crosslinking by PRC1, a Conserved Nonmotor Microtubule Binding Protein. Cell *142*, 433-443.

Sze, H., Frietsch, S., Li, X., Bock, K.W., and Harper, J.F. (2006). Genomic and molecular analyses of transporters in the male gametophyte. In Plant Cell Monographs, pp. 71-93.
Trueba, F.J. (1982). On the precision and accuracy achieved by <i>Escherichia coli</i> cells at fission about their middle. Archives of Microbiology *131*, 55-59.

Tanenbaum, M., and Medema, R. (2011). Localized Aurora B activity spatially controls non-kinetochore microtubules during spindle assembly. Chromosoma 120, 599-607.

Tirnauer, J.S., Grego, S., Salmon, E.D., and Mitchison, T.J. (2002). EB1-Microtubule Interactions in Xenopus Egg Extracts: Role of EB1 in Microtubule Stabilization and Mechanisms of Targeting to Microtubules. Molecular Biology of the Cell *13*, 3614-3626.

Tseng, B.S., Tan, L., Kapoor, T.M., and Funabiki, H. (2010). Dual Detection of Chromosomes and Microtubules by the Chromosomal Passenger Complex Drives Spindle Assembly. Developmental Cell 18, 903-912.

Vader, G., Kauw, J.J.W., Medema, R.H., and Lens, S.M.A. (2006). Survivin mediates targeting of the chromosomal passenger complex to the centromere and midbody. EMBO Rep 7, 85-92.

Walczak, C.E., Heald, R., and Kwang, W.J. (2008). Mechanisms of Mitotic Spindle Assembly and Function. In Int Rev Cytol (Academic Press), pp. 111-158.

Wan, X., O'Quinn, R.P., Pierce, H.L., Joglekar, A.P., Gall, W.E., DeLuca, J.G., Carroll, C.W., Liu, S.-T., Yen, T.J., McEwen, B.F., *et al.* (2009). Protein Architecture of the Human Kinetochore Microtubule Attachment Site. Cell *137*, 672-684.

Welburn, J.P.I., Vleugel, M., Liu, D., Yates, J.R., Lampson, M.A., Fukagawa, T., and Cheeseman, I.M. (2010). Aurora B Phosphorylates Spatially Distinct Targets to Differentially Regulate the Kinetochore-Microtubule Interface. Molecular cell *38*, 383-392.

Welburn, J.P.I., Vleugel, M., Liu, D., Yates Iii, J.R., Lampson, M.A., Fukagawa, T., and Cheeseman, I.M. (2011). Aurora B Phosphorylates Spatially Distinct Targets to

Differentially Regulate the Kinetochore-Microtubule Interface. Molecular cell 38, 383-392.

Wheatley, S.P., Henzing, A.J., Dodson, H., Khaled, W., and Earnshaw, W.C. (2004). Aurora-B Phosphorylation in Vitro Identifies a Residue of Survivin That Is Essential for Its Localization and Binding to Inner Centromere Protein (INCENP) in Vivo. Journal of Biological Chemistry 279, 5655-5660.

Wiese, C., Wilde, A., Moore, M.S., Adam, S.A., Merdes, A., and Zheng, Y. (2001). Role of Importin-b in Coupling Ran to Downstream Targets in Microtubule Assembly. Science *291*, 653-656.

Wilsen, K.L., and Hepler, P.K. (2007). Sperm Delivery in Flowering Plants: The Control of Pollen Tube Growth. BioScience *57*, 835-844.

Wu, J., Qu, H., Jin, C., Shang, Z., Wu, J., Xu, G., Gao, Y., and Zhang, S. (2011). cAMP activates hyperpolarization-activated Ca2+ channels in the pollen of Pyrus pyrifolia. Plant Cell Reports *30*, 1193-1200.

Wu, J., Shang, Z., Wu, J., Jiang, X., Moschou, P.N., Sun, W., Roubelakis-Angelakis, K.A., and Zhang, S. (2010a). Spermidine oxidase-derived H2O2 regulates pollen plasma membrane hyperpolarization-activated Ca2+-permeable channels and pollen tube growth. The Plant Journal *63*, 1042-1053.

Wu, W., Park, K.-T., Holyoak, T., and Lutkenhaus, J. (2010b). Determination of the structure of the MinD–ATP complex reveals the orientation of MinD on the membrane and the relative location of the binding sites for MinE and MinC. Molecular Microbiology *79*, 1515-1528.

Wu, Y., Xu, X., Li, S., Liu, T., Ma, L., and Shang, Z. (2007). Heterotrimeric G-protein participation in Arabidopsis pollen germination through modulation of a plasmamembrane hyperpolarization-activated Ca2+-permeable channel. New Phytologist *176*, 550-559.

Yudushkin, I.A., Schleifenbaum, A., Kinkhabwala, A., Neel, B.G., Schultz, C., and Bastiaens, P.I.H. (2007). Live-Cell Imaging of Enzyme-Substrate Interaction Reveals Spatial Regulation of PTP1B. Science *315*, 115-119.

Zeitlin, S.G., Shelby, R.D., and Sullivan, K.F. (2001). CENP-A is phosphorylated by Aurora B kinase and plays an unexpected role in completion of cytokinesis. The Journal of Cell Biology 155, 1147-1158.

Zhu, C., Lau, E., Schwarzenbacher, R., Bossy-Wetzel, E., and Jiang, W. (2006). Spatiotemporal control of spindle midzone formation by PRC1 in human cells. Proceedings of the National Academy of Sciences *103*, 6196-6201.